Connectivity Analysis of Human Cortical Networks for Mapping and Decoding

by

Heather L. Benz

A dissertation submitted to The Johns Hopkins University in conformity with the requirements for the degree of Doctor of Philosophy.

Baltimore, Maryland

September, 2014

Abstract

During cued speech and movement, information propagates from primary sensory areas, through association areas, to primary and supplementary motor and language areas. Traditionally, the neural activity in each region has been probed independently at the level of individual neurons or small neuronal populations. This approach suffers from a lack of information about how different neuronal populations interact to relay information through the cortical network, actuate movement or speech, and monitor feedback. Recently, however, advances in computational capacity have permitted the modeling of dynamic neural propagation with high spatial and temporal resolution. These dynamic network models may contain new information about processing that can inform cortical mapping for clinical and scientific purposes, or improve the ability to decode movement or speech from neural signals. Such decoded movement or speech may be used as a control signal for brain machine interfaces.

This dissertation explores the utility of time-varying neural connectivity features for mapping the neural correlates of movement and speech, and decoding movement and speech from neural signals. All neural data are recorded from human subjects

ABSTRACT

using electrocorticography, and the directional flow of neural activity is computed with multivariate autoregressive models. First, I characterize motor connectivity maps during hand movement, and demonstrate that connectivity computed from both temporal and spectral features varies with movement. Then I compare a grasp decoder based on traditional neural features to one based on connectivity features, and show that the connectivity-based decoder improves on the performance of the traditional decoder. Next, I characterize connectivity networks during speech, and use them to show that top-down modulation of neural processing may contribute to behavioral priming. Finally, I decode articulatory features during speech using traditional and connectivity features at multiple spatial scales (clinical ECoG and microECoG). I show that connectivity features within and between these spatial scales can improve speech decoding. This work demonstrates that effective connectivity models computed from human neurophysiological data are a rich source of features with the potential to improve both clinical and scientific mapping of the cortical activity underlying movement and speech, and brain machine interfaces that decode control signals from cortical activity.

Primary Reader: Dr. Nitish V. Thakor, Ph.D.

Secondary Reader: Dr. Nathan Crone, M.D.

Acknowledgments

I have received exceptional support from the Johns Hopkins community. My advisors, Nitish Thakor and Nathan Crone, have both demonstrated a tremendous commitment to my growth as a scientist and a professional.

My thesis committee has provided invaluable feedback throughout the development of this dissertation. Tassos Bezerianos not only helped developed the initial approach to connectivity-based motor decoding, but has continued to collaborate on speech decoding with his group of students in Greece. Dana Boatman provided extremely helpful feedback on priming and auditory processing.

A long list of fellow students in Thakor and Crone labs has made my experience at Hopkins not only educational, but enjoyable. Since we shared a room at a conference in Turkey, Rezina has been a friend and invaluable sounding board. In semi-chronological order, Soumya, Matt, Anna, Geoffrey, Guy, Yujing, Griff, and Max helped with ECoG data collection, analysis, and keeping things fun. Limitations of space make it impossible to do more than list all the other people with whom I enjoyed coffee hours, picnics, and talking shop: Vikram, Mohsen, Ryan, Elliott, Janaka,

ACKNOWLEDGMENTS

Xiaoxu, Matt T., Kyle, Akshay, Zach, Mike, Matt M., and many others.

A group of extraordinary students and Baltimore citizens has inspired me countless times with their spirit and compassion. I am grateful to everyone I have met through Thread for their energy and encouragement, including but certainly not limited to Sarah and Ryan, Tong and Alex, Helen, Mac, both Michelles, Barbara, Varun, Mariela, Mara, Sarah, Joanne, Debbie, Krishna, and Jan.

Erin, Scott, Chris, Sarah, Ben, and eventually Booker and Rosalind made sure I took some time off occasionally to think about something other than the brain. "Thanks" is not enough; I'll miss you all.

My best friend and husband, Derek, has been with me every step of the way through this Ph.D. I thank him for his understanding when I came home late, the listening ear he gave me every time I was frustrated with a manuscript draft, and the many (famously unique) lunches he packed. I thank my family, spread across Maryland, Florida, Virginia, Montana, and Ohio, for more support than I could ever ask for. Finally, I am grateful to my young son, Nicholas, who has kept me buoyant for the past two years.

Dedication

This thesis is dedicated to my father, who is my professional and personal role model, and my mother, who is always quietly and selflessly supportive.

Contents

List of Tables

List of Figures

Chapter 1

Background and Motivation

Recent technological advances in electrode recording capacity [1–3] and computing capability have led to the emergence of a new approach in understanding the relationship between cortical activity and behavior: cortical connectivity analysis, or the modeling of the propagation of information through the brain. Traditionally, the activity of single neurons or small neuronal populations have been correlated with primitives of movement or speech, such as position and velocity [4–6], or articulated phoneme [7–10]. However, the propagation of information through input sensory areas to association cortex and output motor areas is as relevant to understanding cortical processing as the activity of local processing units. To fully map cortical activity to behavioral parameters, large- and small-scale cortical interactions must be considered.

Accurately characterizing the relationship between cortical activity and task per-

formance is a neuroscientific and medical goal with wide-ranging clinical applications. The approach to analysis is context-dependent. Different techniques are required for mapping cortical activity to behavioral activity and decoding behavioral activity from cortical activity. In the following sections, I describe the state of the art in mapping and decoding motor and speech cortical activity, outline the hypothesized pathways of information propagation during motor and language tasks, briefly discuss the approach used to characterize neural signals, and conclude with a summary of the specific aims of this work and remaining chapters.

1.1 Cortical Mapping

Mapping the relationship between cortical activity and behavioral activity is an invaluable tool in planning surgical resections for the treatment of epilepsy or tumor [11–14], in addition to relevance for neuroscientific investigation such as understanding motor tuning [15] and the widespread cortical activation underlying speech production [16]. Such surgical resections are sometimes recommended when epilepsy is refractory to medication, which occurs in up to 30% of patients [17]. Prior to the resection, clinicians localize the site of seizure origination and "eloquent cortex", or cortical sites that are deemed necessary for the performance of motor, sensory, language, and other activities that are relevant to the patient's quality of life. Identification of the site of seizure origination is performed by neurologists reading intracranial EEG (iEEG

[18], electrical signals recorded from penetrating electrodes [19] and electrodes placed subdurally [20] or epidurally [21] on the surface of the brain (electrocorticography, or ECoG). Identification of eloquent cortex is typically performed using electrocortical stimulation mapping (ESM [22–24]), in which current is delivered through the ECoG electrodes, and the resulting disruption of task performance or initiation of movement or sensation is documented.

ESM is by nature time-consuming, due to the need to individually stimulate sites of interest, and in some cases causes pain, discomfort, after-discharges, or seizures [25, 26]. Such seizures are not useful in determining the site of seizure origination. Additionally, there have been reports of short-term and persistent language deficits following resections guided by ESM [14]. An alternative approach to cortical mapping based solely on cortical recordings could complement or even replace ESM. Such functional mapping has been demonstrated using fMRI [27] and the iEEG signal [28], an area of recent interest due to the possibility for signal decoding as well as real-time functional mapping. One feature of the iEEG, the high gamma power, or the power in iEEG oscillations with a frequency greater than 70 Hz, is particularly promising, as it has been shown to reflect local population firing rates [29,30]. However, the sensitivity and specificity of these functional mapping approaches in identifying eloquent cortex, as compared to ESM, are too low to rely upon them alone. An ability to map the propagation of information through the cortex during sensory processing and integration; motor planning and execution; and lexical retrieval, phonological code

retrieval, syllabification, and articulation could improve clinicians' understanding of the most relevant cortical sites for these tasks in individual patients.

1.2 Cortical Decoding

Brain-machine interfaces (BMI) or brain-computer interfaces (BCI) decode movement or communication intent from neural activity for rehabilitation and assistive devices for patients with paralysis, limb loss, stroke, and locked-in syndrome [31]. Paralysis affects over 5.5 million people in the United States [32], and limb loss has become a recent priority for defense funding due to the occurrence of amputations related to military conflicts [33]. Stroke is a leading cause of severe disability [34], and locked-in syndrome, which can result from ALS, stroke, or a variety of other causes, leads to complete paralysis. In some cases, limited communication via eye movement or blink is possible [35].

A variety of measures of neural activity have been used in BMIs, including signals from noninvasive methods such as electroencephalography (EEG [36, 37]), magnetoencphalography (MEG [38]), functional magnetic resonance imaging (fMRI [39,40]), and functional near-infrared spectroscopy (fNIRS [41]); and invasive methods such as individual units recorded with microelectrodes [42], the local field potential (LFP) recorded with penetrating microelectrodes [43], and iEEG [44]. Generally speaking, noninvasive approaches either permit decoding of limited one- or two-dimensional

outputs (EEG and fNIRS), or require equipment that is too cumbersome to be used outside a hospital or laboratory setting (MEG and fMRI). For example, EEG during motor imagery has been used to control a cursor [45], wheelchair [46], and four degrees of freedom of a robotic prosthetic limb [47]. FNIRS has been used to detect a binary decision (yes/no) by decoding prefrontal cortical processing compared to rest [48]. Therefore, measures of neural activity recorded from implanted electrodes are likely necessary to decode multiple-dimensional outputs to control a motor or speech prosthesis for use outside a laboratory setting.

Recent advances have brought implanted motor prosthetics to humans with paralysis. In 2006, a group demonstrated a pilot BMI controlled by the firing of individual neurons recorded with a penetrating microelectrode array in a human with quadriplegia [42]. Most notably, the subject was able to control a computer cursor and open and close a prosthetic hand. More recently, seven degree-of-freedom control of a prosthetic limb was achieved in a human with quadriplegia using single- and multi-unit activity recorded with 192 microelectrodes [49]. However, questions have been raised about the long-term stability of signal recordings and tissue response when using penetrating microelectrodes [50, 51], so some groups have complemented neural spiking signals with LFP or ECoG signals. The first demonstration of an ECoG-based BMI was published in 2004 [44]. One-dimensional cursor control was achieved with binary classification of motor or speech imagery. By 2013, a human with quadriplegia was able to control a three-dimensional cursor using the neural signals underlying

attempted arm movements, recorded with a very high-density ECoG array over the hand and arm area of sensorimotor cortex [52]. In spite of these advances, limitations to these approaches remain. Significant training, on the order of days to weeks, is typically required before optimal user control is obtained, and control may at first be unintuitive. Additionally, control is based on reach trajectory and grasp confirmation, rather than the more abstract control concepts typically used with a native limb. A large-scale cortical map of the propagation of information through areas related to sensory processing and motivation, in addition to primary sensorimotor areas, may ultimately provide additional information for motor decoding [53–55], leading to more intuitive and more precise control that incorporates higher-level motor goals.

A common approach to the development of a BMI for communication has been the use of the P300 event-related potential (ERP), recorded with EEG, to select individual letters from a grid [56, 57]. Letters, or subsets of letters, are highlighted or flashed sequentially, and the P300 is elicited when the user's intended letter is flashed. This approach, though appealing because it is noninvasive, suffers from a slow data transfer rate, on the order of one to ten selections per minute, and lack of intuitive control. Preliminary efforts to decode speech more directly have relied largely on the ECoG signal [8, 9, 58, 59], but a demonstration has also been made using a neurotrophic electrode [7]. Promising early results have achieved up to 36% accuracy in decoding classes of phonemes. It is possible that the propagation of information through neural populations will be informative for such speech BMIs, as

the selection of a word, phonological code retrieval, syllabification, and articulation require the coordination of a number of spatially distant cortical areas in the temporal, parietal, and frontal lobes [16]. In light of the detailed phonemic information detected with high density ECoG [60], an important consideration is the scale (clinical ECoG, high density ECoG, or both) at which this propagation of neural activity should be measured.

1.3 Neural Activity Propagation in Motor Systems

Although ESM largely finds motor effects near the central sulcus [61–63], and motor BMIs typically decode from primary sensorimotor areas [64], it has been demonstrated that a variety of cortical areas, including premotor cortex [65–68], supplementary motor area [69], and parietal areas near the intraparietal sulcus [70], contribute to motor planning and execution. Fig. 1.1 demonstrates the propagation of neural activity before and during visually-guided reach to grasp [65–79].

Parietal reach region (PRR) has been demonstrated to activate in relationship to motor goals and planning, particularly when spatial processing of reach is needed, and encodes information in gaze-centered coordinates [74, 76, 79]. It has been found that anterior intraparietal area (AIP) encodes complementary information about fine finger movements and grasp during goal-directed, visually guided reach-to-grasp [73,78].

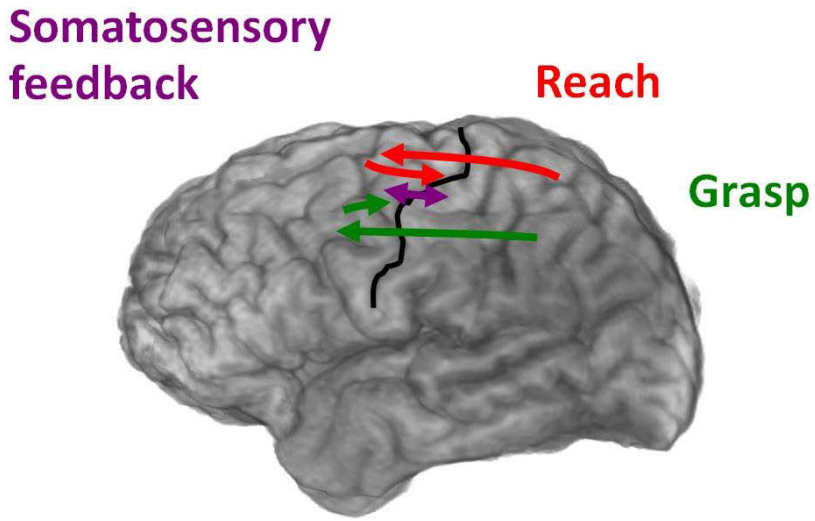

Figure 1.1: Schematic of hypothesized functional connectivity in motor cortical areas during visually-guided reach to grasp. The central sulcus is marked with a black line. Visual information is propagated from occipital cortex to parietal reach region (red reach pathway) and anterior intraparietal area (green grasp pathway), which are involved in postural planning. Parietal areas project to motor areas in the frontal lobe, including premotor and primary motor cortex. Primary motor cortex integrates information from parietal reach region and dorsal premotor cortex (reach), and anterior intraparietal area, ventral premotor cortex, and supplementary motor area (grasp). Interplay between primary motor cortex and primary somatosensory cortex (purple) monitors expected and actual somatosensory feedback.

Premotor cortex has been shown to be important for planning and coordinating movement dorsally (reach) and ventrally (grasp) [68]. Supplementary motor area (SMA) is active during a variety of movement types, including bimanual and sequential movements, and has corticospinal outputs, leading to hypotheses that it is involved in the coordination of dexterous hand movements [75] or sequential movements [69, 72]. Primary motor cortex integrates inputs from these upstream areas [77], in addition to feedback from primary somatosensory cortex [71], and has large corticospinal outputs [80]. Its neural activity is related to a number of movement parameters, including muscle movement and position [81], velocity [82], joint angle [83, 84], muscle synergies [85], and postures [86, 87].

1.4 Neural Activity Propagation in Language Systems

Speech preparation and articulation requires a coordinated cascade of information propagation through a number of cortical areas. Fig. 1.2 shows a simplified schematic of hypothesized cortical propagation preceding and during speech production, in this case during a visually cued task [16]. (For a more detailed figure with the relevant cortical areas highlighted, see Fig. 5.10.) Following early visual processing of the stimulus, fusiform gyrus is involved in word or category identification [88]. This information is passed to middle temporal gyrus, which is active during lexical

retrieval [89], or the identification of the word to be spoken. Posterior superior temporal gyrus (Wernicke's area) transforms the lexical concept to phonological code [90], following which Broca's area participates in syllabification and additional articulatory preparation [91]. Cortical processing converges in inferior primary motor cortex, which is responsible for articulation of the vocal tract [92]. Finally, somatosensory feedback from primary somatosensory cortex in parietal cortex and auditory feedback from the superior temporal lobe and other auditory areas monitor articulation through interactions with primary motor cortex [93, 94].

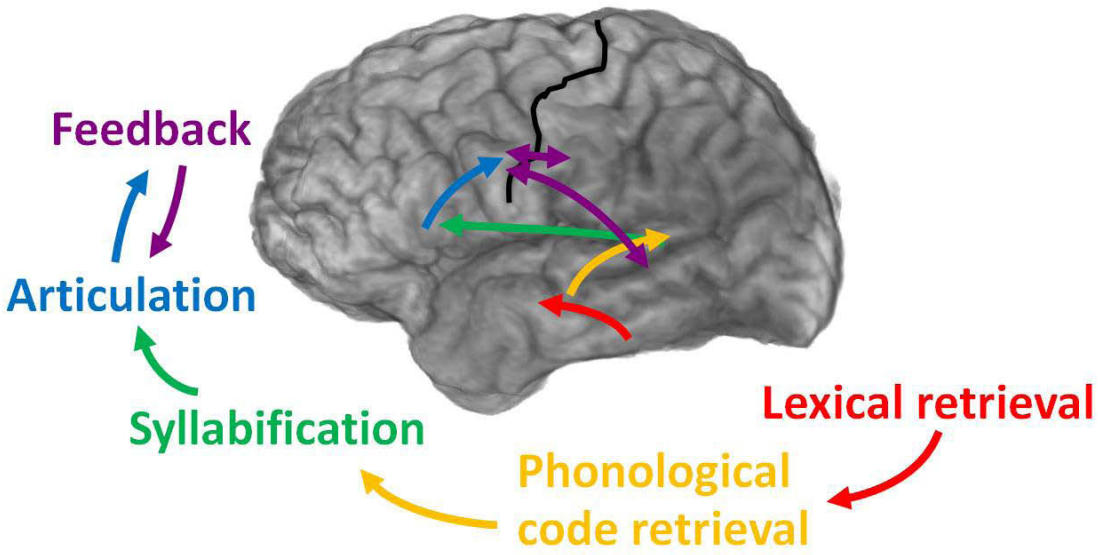

Figure 1.2: Simplified schematic of hypothesized functional connectivity in cortical areas involved in speech production. The central sulcus is marked with a black line. Middle temporal gyrus is involved in lexical retrieval; superior temporal gyrus is involved in phonological code retrieval; inferior frontal cortex is involved in phonological code retrieval, syllabification, and articulatory planning; primary motor cortex is involved in articulation; and somatosensory and auditory cortex provide feedback during articulation.

1.5 Measurements of Neural Activity and Propagation

Processing information propagation through widespread cortical areas during movement and speech is likely to be informative for mapping how cortical activity leads to movement and speech, and decoding movement and speech parameters from cortical signals. In this dissertation, I will therefore model the connectivity, or propagation of neural activity, between cortical areas relevant to movement and speech. ECoG, an indicator of cortical activity recorded with electrodes implanted on the surface of the brain [95], is a promising modality for measuring cortical connectivity, due to wide coverage of the brain, millisecond-scale temporal resolution, and centimeter- to millimeter-scale spatial resolution. As discussed above, the ECoG signal has recently become a modality of interest for use in brain-machine interfaces (BMI) [44, 96–105]. ECoG's utility as a control signal for a BMI was demonstrated in 2004 on a one- and two-directional cursor control task [44]. It has since been used in cursor control tasks [96, 97], [99, 100], [103, 104], reach decoding [98], and grasp and individual finger decoding [101, 102, 105]. High-density ECoG arrays have also shown promise in mapping neural correlates of speech [60].

1.6 Summary and Dissertation Organization

In this dissertation, my objective is to map the dynamics of interactions between cortical areas during movement and speech, and to use these dynamics for decoding hand movements and spoken syllables. My specific aims are:

Aim 1 Use a connectivity-based approach to map cortical network dynamics during dexterous motor tasks.

I hypothesize that cortical network dynamics will encode information about the kinematics of dexterous motor tasks. Discovering consistent task-related changes in motor network dynamics will indicate that connectivity features may be informative for motor decoding, a significant result.

Aim 2 Use a connectivity-based approach to decode grasp aperture from human neural signals.

I hypothesize that features will be present in connectivity networks that encode palmar grasps. This work will be the first to apply time-varying directed connectivity information to kinematic decoding.

Aim 3 Use a connectivity-based approach to map cortical network dynamics during object naming.

I hypothesize that cortical networks involved in object naming will demonstrate consistent changes across subjects between initial and repeated exposure to object

stimuli. This finding would establish the presence of reliable speech networks that may be informative for speech decoding. This analysis will also demonstrate the utility of connectivity mapping for testing the predictions of models of cortical mechanisms.

Aim 4 Use a connectivity-based approach to decode spoken syllables.

I hypothesize that features will be present in connectivity networks that encode place of articulation and vowel formant frequency. This work will be the first to apply time-varying directed connectivity information to speech decoding, and will determine for the first time the relevance of microECoG connectivity for decoding speech components such as syllables.

Chapter 2 provides an overview of approaches for measuring cortical connectivity: coherence, phase estimation, and multivariate models. Chapter 2 includes a discussion of the relative merits of the methods used in this dissertation. Chapters 3-6 will each detail the motivation, research, and results for individual specific aims. Chapter 3 explores changes in cortical connectivity during palmar grasp and individuated finger movement, establishing that connectivity features vary consistently with movement. Chapter 4 demonstrates that such changes in cortical connectivity can be used to decode grasp aperture during palmar grasp from human neural signals with a high degree of accuracy. Chapter 5 maps cortical connectivity during object naming, leading to observations that support a model in the literature of the cortical mechanism underlying implicit memory. Chapter 6 demonstrates that cortical connectivity

at clinical ECoG and microECoG scales can improve decoding accuracy of spoken syllables. Chapter 7 summarizes the overall conclusions from Chapters 3-6, discusses the impact of the results, and proposes future directions for additional investigation.

Chapter 2

Cortical Connectivity Models and Proposed Approach

A number of approaches exist to estimate task-related cortical connectivity. While the underlying anatomical connectivity may provide a foundation for understanding the relationships between cortical areas, for the purposes of mapping task-related connectivity and decoding movement or speech parameters from connectivity information, functional or effective connectivity are more relevant measures of cortical interactions. Functional connectivity measures the correlated activity of different cortical regions [106, 107]. It does not establish a causal link between the related cortical regions, but does find interrelated locations of cortical processing. Functional connectivity is often useful in analyzing fMRI data, because the wide-area spatial coverage permits the investigation of the relationships between many cortical regions [107].

Effective connectivity, in contrast, includes an inherent element of directional information propagation [108], and is therefore a highly informative, information dense measure. High temporal resolution at the scale of propagation of neural activity, on the order of tens of milliseconds, is useful in measuring effective connectivity [109]; however, effective connectivity may also be measured using fMRI [110]. In this chapter, I review common approaches to measuring functional and effective connectivity in neurophysiological signals such as EEG and ECoG. I then outline the proposed approach for mapping effective connectivity in motor and speech networks for the purpose of this work, and conclude with a summary of the main contributions of the work presented in this dissertation and their relevance to the scientific community.

2.1 Functional Connectivity: Coherence and Phase Estimation

Coherence is one of the simplest measures of functional connectivity, and has a straightforward interpretation: it is the linear correlation between two signals as a function of frequency. It is is normalized to take values from 0 to 1, aiding in interpretability. Under the correct assumptions, it is a simple measure of causality. However, because neurophysiological signals violate the required assumptions, in a practical implementation for cortical data, it is best interpreted as functional connec-

tivity. Its definition at a given frequency f is given by [111]:

$$C_{xy}(f) = \frac{|S_{xy}(f)|}{[S_{xx}(f)S_{yy}(f)]^{1/2}} \tag{2.1}$$

where $S_{xy}(f)$ is the cross-spectral density between signals x and y, normalized by the autospectral densities $S_{xx}(f)$ and $S_{yy}(f)$. The cross-spectral density is the Fourier transform of the cross-correlation function, $R_{xy}(\tau)$, which is the expected value of the input and time-shifted output:

$$R_{xy}(\tau) = E\left(x(t)y(t-\tau)\right) \tag{2.2}$$

The cross-spectra cannot be computed from finite data, but may be estimated by multiplying the discrete Fourier coefficient of $x(t)$ with the complex conjugate of the discrete Fourier coefficient of $y(t)$. This approach leads to highly variable results [112], so smoothing is useful to improve interpretability.

Coherence has been used extensively, and for several decades, to explore the relationships between cortical regions as represented by EEG and ECoG [113–122]. In fact, some groups have proposed that coherence is a fundamental mechanism by which the brain achieves sensorimotor integration, attention [118], and conscious perception [119]. Coherence has been used to measure functional connectivity related to movement [114, 115], associative learning [116], executive function [120], and intelligence [121]. It may even be useful as a measure to predict autism [122] or identify tumors or epileptic cortical tissue [117] where there is a localized increase in coherence.

However, there are several drawbacks to using coherence to measure cortical con-

nectivity, which make it nonideal for the purposes of mapping functional networks and decoding intended movement or speech. First, it is inherently not a method applicable to real-time or even single-trial analysis. Although some modifications could permit variants of coherence to be used on a single-trial basis [111], the high variability of coherence estimates limits its value for decoding. Additionally, as a measure of functional connectivity, it does not provide information about the directionality of neural propagation. Finally, because it is a pairwise measure, it is limited in its ability to detect cortical network activity with a high degree of statistical significance and power due to corrections for multiple statistical tests when considering a network with several sites (electrodes) and the need to correct for the detection of indirect neural propagation. For example, if neural activity propagates from site A through site B to site C, coherence may incorrectly detect connections between sites A and C.

Phase synchrony is a nonlinear approach to modeling functional connectivity in neurophysiological signals [123], and may be used by fundamental cortical processes such as perceptual binding [124] and working memory [125]. Phase locking occurs in ideal signals when the following condition is met:

$$\psi(t) = |\phi_x(t) - \phi_y(t)| \leq b \tag{2.3}$$

where ϕ_x and ϕ_y are the phases of the signals x and y, and the magnitude of their difference should be less than some constant [126]. In neurophysiological signals, a statistical approach must be used, so that phase locking is inferred when, for a given time period, the phase difference has a statistical tendency to remain constant over

time, even when the phases of the signals in question are varying [127]. There are a number of ways to estimate a signal's phase, including the Hilbert Transform and wavelet transform, of which the Hilbert Transform is the most popular [126]. The Hilbert Transform, $x_H(t)$, of signal $x(t)$ is defined as:

$$x_H(t) = f(\tau) = \frac{1}{\pi}\text{p.v.}\int_{-\infty}^{\infty}\frac{x(\tau)}{t-\tau}\text{d}\tau \tag{2.4}$$

where p.v. represents the Cauchy principal value. Then the analytic signal is given by:

$$\zeta(t) = x(t) + ix_H(t) \tag{2.5}$$

and the instantaneous phase is found with the arctangent of the Hilbert Transform divided by the original signal:

$$\phi_x(t) = \arctan\left(\frac{x(t)}{x_H(t)}\right) \tag{2.6}$$

Phase synchronization has been observed during perception [128, 129], and has been proposed as a cortical mechanism of sensory binding [130] and segmenting cortical processing epochs [131]. Investigation into phase synchrony and phase locking in rabbits in the theta (4-8 Hz) and gamma (20-80 Hz) bands, and humans in the theta (4-8 Hz) and high gamma (greater than 70 Hz) bands has found that theta synchrony with gamma and high gamma bands plays an important role in coordinating communication across brain regions in cortical processing [127, 132]. Phase synchronization has been demonstrated to change significantly during early development, consistent with the structural changes ongoing in the brain during that period [133]; changes in a

predictable way preceding seizures in epilepsy [134–136]; and is decreased in patients with Alzheimer's disease [136].

The disadvantages to mapping and decoding cortical state with the phase synchrony approach are similar to those with the coherence approach. Because it is a bivariate and directionless measure, statistical corrections for multiple comparisons become unwieldy with a large network, and there is inherently less information about the propagation of neural activity than in a model that incorporates directionality. Additionally, it has been shown that in 96% of EEG epochs, patterns of phase coherence can be described by purely linear methods, and do not require a nonlinear approach such as phase synchrony [137].

2.2 Effective Connectivity: Multivariate Connectivity Models

Two similar methods, the partial directed coherence (PDC [138, 139]) and the directed transfer function (DTF [140]) have used the concept of Granger causality to introduce directionality into the modeling of neural activity propagation and overcome limitations of pairwise approaches to connectivity [141]. There is Granger causality from signal $x(t)$ to signal $y(t)$ if information from the past and present of $x(t)$ improves the ability to predict the future of $y(t)$, compared to predictions made only with past and present information of $y(t)$.

Multivariate models have improved the ability to model the direct propagation, instead of indirect propagation, of neural activity through a network. Both PDC and DTF construct a multivariate autoregressive (MVAR) model of the form:

$$X(t) = \sum_{j=1}^{p} A_j X(t-j) + \varepsilon(t) \tag{2.7}$$

where $X(t)$ is a vector of the preprocessed neural activity measured at an arbitrary number of sites n at time t, A_j is an n by n matrix with information about the directional propagation of activity, the MVAR model order is p, and $\varepsilon(t)$ is independent Gaussian white noise. In the frequency domain, with frequency f and sampling interval Δt, this model is transformed to:

$$X(f) = H(f)E(f) \tag{2.8}$$

where $E(f)$ is the transformed error term and $H(f)$ is the transfer function, given by:

$$H(f) = \left(\sum_{j=0}^{p} A_j e^{-i2\pi j f \Delta t} \right)^{-1} \tag{2.9}$$

The PDC and DTF are derived from these formulae. The PDC is computed from the Fourier transform of A. If $\bar{A}(f) = I - A(f)$ and $H(f) = \bar{A}^{-1}(f)$, then each coefficient of the PDC is found with:

$$\pi_{ij}(f) = \frac{\bar{a}_{ij}(f)}{\sqrt{\bar{a}_j^H(f)\bar{a}_j(f)}} \tag{2.10}$$

The superscript ^{H} represents the conjugate transpose. Each element of the PDC is therefore normalized with respect to the outflows from a given site. No matrix

inversion is required to compute the PDC, making it a relatively computationally efficient measure; however, it has been shown that due to the normalization approach, weak flows from a channel with few outflows may be inflated [141]. The DTF, in contrast, is found using the transfer matrix and is normalized with respect to the inflows to a site:

$$\delta_{ij}(f) = \frac{H_{ij}(f)}{\sqrt{h_i^H(f)h_i(f)}} \tag{2.11}$$

Two modifications to the DTF have made it a suitable measure for detecting time-varying directed neural propagation at a time scale relevant to cortical processing. When the full frequency DTF (computed by summing the denominator of the DTF over all relevant frequencies) is multiplied by the partial coherence, only direct flows between channels are represented. This measure is called the direct DTF, or dDTF [142]. If multiple trials are available, it is possible to compute the short-time DTF, or SDTF, with ensemble averaging, so that the window length can be as small as p, the model order for the MVAR model [143]. These approaches have been combined in the SdDTF [144], which can be applied to neurophysiological signals obtained during standard cognitive experiments to model direct flows in windows on the order of 100-200 ms. This development permits the modeling of temporally cascaded neural propagation involved in all stages of cortical processing.

Granger causality and MVAR models have been used in a variety of neurocognitive contexts, and have identified novel feedback flows during face discrimination [145], probed the role of communication between the anterior cingulate cortex and dorso-

lateral prefrontal cortex [146] and temporal, parietal, and frontal cortex [147] when responding to familiar vs. unfamiliar stimuli, and tested hypotheses about the direction of interhemispheric information flow during wakefulness and varying sleep states [148]. The SdDTF measure specifically has been used to discriminate between auditory processing, response preparation, and verbal response in an auditory word repetition task [144], and it has been demonstrated to vary predictably with verbalized and signed language [149].

These models have also been used extensively to characterize ictal sources [150–156] and have been employed in a number of other disease contexts. These include testing a model of mild cognitive impairment [157], demonstrating a difference in parieto-to-frontal flows in patients with mild cognitive impairment and Alzheimer's disease compared with normal elderly subjects [158], detecting a difference in interhemispheric flows in adolescents with Down syndrome compared with normal adolescents [159], and quantifying differences in cortical connectivity in Parkinson's disease [160].

2.3 Proposed Approach

When using connectivity measures to map cortical interactions and decode movement and speech from these interactions, there are three key considerations. First, the methods used must be information dense, generating a sizable number of fea-

tures that are highly correlated with the intended movement or speech. For this reason, effective connectivity measures, which include a directional component, are more suitable for these applications than functional connectivity measures. Second, the methods must be time-varying with a temporal scale relevant to the scale at which activity propagates through the cortex, on the order of hundreds of milliseconds. The short-time modification to the dDTF (SdDTF, discussed above) is useful in capturing these temporally volatile task-related networks. A statistical testing framework is needed to apply the SdDTF within a mapping context to discover event-related changes in these networks. Here event-related causality (ERC) [144] is used as this statistical framework when mapping speech networks. Third, in a decoding context, the methods must be computationally tractable, so that features can be generated in near real time and used to predict intent immediately. The DTF and its variants are not ideally suited to this context because they are computationally intensive. Here a simplified conceptualization of the SdDTF, a time-varying dynamic Bayesian network (TV-DBN) [161], is used to generate features for decoding to capture similar time-varying directional connectivity information to that found with SdDTF, with less parameter optimization required and increased computational simplicity.

2.3.1 Event-Related Causality

ERC is a statistical testing framework to find network propagation related to a perceptual or behavioral event. The SdDTF is first calculated in sliding overlap-

ping windows, yielding smoothed connectivity estimates. The method of penalized thin-plate splines [162] is used to create a 95% joint confidence interval to compare connectivity estimates during a trial to connectivity estimates during the baseline period preceding the trial. Those connectivity estimates that are significantly different from baseline connectivity are considered a part of the ERC network.

2.3.2 Time-Varying Dynamic Bayesian Networks

TV-DBN uses a similar framework to that used by MVAR effective connectivity measures such as the PDC and DTF, However, two constraints on the model decrease computational complexity, making TV-DBN a highly favorable connectivity measure for decoding purposes. Essentially, the MVAR model relating signals at time t to past signals (Eqn. 2.7) is reduced to a model order of 1:

$$X(t) = AX(t-1) + \varepsilon(t) \tag{2.12}$$

The asymmetric matrix A contains the TV-DBN connectivity coefficients. To find A, an additional assumption is made that the adjacency matrix is smooth over time. Multiple observations in time are therefore weighted with a Gaussian RBF kernel when estimating A, so that observations close to time t contribute most to the estimation of A. The model is solved using regularized least squares.

2.4 Main Contributions of This Work

The work described in this dissertation makes four significant novel contributions to the literature. The first is the finding that time-varying directed neural connectivity varies consistently with dexterous movement. The second is the demonstration that information contained in the connectivity improves the ability to decode dexterous movement from neural signals. These results suggest a future role for time-varying directed neural connectivity in BMI, particularly for the purpose of enhancing decoding accuracy and permitting a more complex BMI based on large-scale neural signals that integrates multiple sensorimotor processing streams. The third is the discovery, via the application of time-varying directed connectivity mapping to a repetitive language task, of a refined model for implicit memory based upon changes in cortical networks. The fourth is the demonstration that connectivity features improve the decoding of elements of speech, and the finding that sub-millimeter scale cortical connectivity and cross-scale cortical connectivity contain features that are informative for speech decoding.

2.5 Relevance of the Results to the Scientific Community

Taken together, these results serve as a series of case studies that validate the hypothesis that cortical connectivity is a useful feature in both mapping the dynamically changing cortical state during behavior and decoding for BMIs. In addition to the immediate relevance to design considerations in the BMI field, these findings also suggest a role for mapping cortical connectivity in scientific contexts, beyond the clinical motivation for mapping described in Chapter 1.

Directed, time-varying connectivity mapping based on neurophysiological signals may be extended to other areas of active research about cortical processing that involves a flow of information, such as the perceptual binding problem [163], attentional modulation [164], the integration of information leading to decision making [165], and the brain states underlying consciousness [166]. Many studies have highlighted the importance of low frequency oscillations in memory [167], binding [168], and coordinating processing [169, 170]. It is likely that exploring effective connectivity in these contexts may yield additional information about the flows of information through cortical networks, and how it is gated or bound via low frequency oscillations.

Chapter 3

Directed Causality of the Human Electrocorticogram During Dexterous Movement

3.1 Abstract

While significant strides have been made in designing brain-machine interfaces for use in humans, efforts to decode truly dexterous movements in real time have been hindered by difficulty extracting detailed movement-related information from the most practical human neural interface, the electrocorticogram (ECoG). In this chapter, we explore a potentially valuable, largely untapped source of movement-related information in the form of cortical connectivity computed with time-varying

dynamic Bayesian networks (TV-DBN). We find that, on average, TV-DBN connectivity decreases from baseline preceding grasp and then becames negative, indicating an alteration in the phase relationship between electrode pairs. In some subjects, this change occurs preceding and during movement, before changes in low or high frequency power. In dexterous individuated finger movement, we demonstrate that measures of connectivity derived from the local motor potential varies with dexterous movement in 65% of movement-related electrode pairs tested, and measures of connectivity derived from spectral features vary with dexterous movement in 76%. Due to the large number of features generated with connectivity methods, the TV-DBN is a promising tool for decoding.

3.2 Introduction

ECoG decoding algorithms largely mirror similar algorithms used in EEG-based BMIs. Frequency-domain features are extracted, often using an autoregressive model [171], and low-frequency and/or high-frequency band power variations are typically used in a linear model as predictors for a conditioned task or the kinematics of movement. An additional slow temporal feature, the local motor potential (LMP), has also been shown to vary with slow reaching and grasping motions and is included as a feature in recent BMI decoding models [98, 105].

We aim to find movement-related information in the electrocorticogram (ECoG)

to aid in studying and decoding highly dexterous movements. We have demonstrated previously that directional connectivity, a description of directed connections between cortical areas, provides grasp-related information beyond what is present in standard decoding features [172]. Here, we apply a dynamic directional connectivity technique, time-varying dynamic Bayesian networks (TV-DBN) [161], to ECoG data collected during grap individual finger flexion and extension. We hypothesize that cortical connectivity maps contain movement-related variation that may be relevant for dexterous decoding. We seek evidence that movement-related variation in TV-DBN coefficients occur on a different time scale compared to movement-related variation in spectral features.

We choose to investigate rapid changes in connectivity using the recently described method of time-varying dynamic Bayesian networks (TV-DBN) [161, 172]. The dynamic nature of the method permits the extraction of data at several time points throughout a movement trial. The method also takes advantage of graph theory to achieve efficient computation. TV-DBN is applicable to the estimation of directed, constantly time-varying networks, and avoids pitfalls such as fixed node dependencies [173], the use of a priori static networks that may fail to detect rapid connectivity changes [174], and piece-wise stationary models that do not vary constantly in time [175]. We choose this method over coherency and phase-based methods [135, 176–181], first because it produces directional results, potentially doubling the amount of data extracted from a single connectivity map over undirected ap-

proaches; and second because we seek to create a map of information flow at known time delays. Dynamic Bayesian networks have also been shown to outperform a Granger causality-based approach in the case of short data windows [182]. Moreover, SdDTF, a Granger causality-based approach that is applicable to short time windows, is calculated using a multivariate autoregressive model, an algorithm that is prohibitively computationally expensive in the context of BMI [144]. We have further compared TV-DBN and alternative methods in Discussion and Conclusions, below (page 57).

3.3 Methods

3.3.1 Study Participants and Data Collection

Five patients with epilepsy undergoing monitoring in preparation for surgery participated in motor experiments. During the experiments clinical ECoG data were collected. The experimental protocol was approved by the Johns Hopkins Institutional Review Board and all subjects gave informed consent. The study participants were three males and two females, aged 12-58 years. Table 3.1 summarizes additional subject details. Subjects A-D participated in the grasp study, and subjects A, B, and E participated in the individual finger movements study.

The ECoG signal was recorded using subdurally implanted grids with 88 to 114 platinum electrodes of diameter 4 mm imbedded in a silastic sheet and spaced 10

mm apart (Adtech Medical Instrument Corp., Racine, WI). The electrode locations were determined with Curry software (Neuroscan Inc.) by co-registration of pre-implantation MRI with post implantation CT using anatomical fiducials. In all subjects there was coverage of motor, premotor, and/or supplementary motor cortex, shown in Fig. 3.1. Clinical electrocortical stimulation mapping data, also depicted in Fig. 3.1, was used to assist in identifying sensorimotor areas. The ECoG signal was recorded using a 128-channel amplifier (Stellate Systems Inc., Montreal), digitized at 1000 Hz per channel, and referenced to an inactive intracranial electrode. The ECoG data were filtered between 0.15-300 Hz, with a second-order Butterworth filter. A notch filter was used at 60 Hz. The signals were re-referenced with a common average reference (CAR) filter [183] to remove sources of noise common to all channels.

During the motor experiments, 18 joint angles of the hand contralateral to the hemisphere of the implanted ECoG grid were recorded and digitized at 25 Hz using a data glove (CyberGlove, CyberGlove Systems LLC, San Jose, CA). These joint angles were metacarpal phalangeal, interphalangeal, and distal phalangeal joints and abduction/adduction of all five fingers. These hand motor data were synchronized to the ECoG signal by writing simultaneous time stamps and event markers to both data streams.

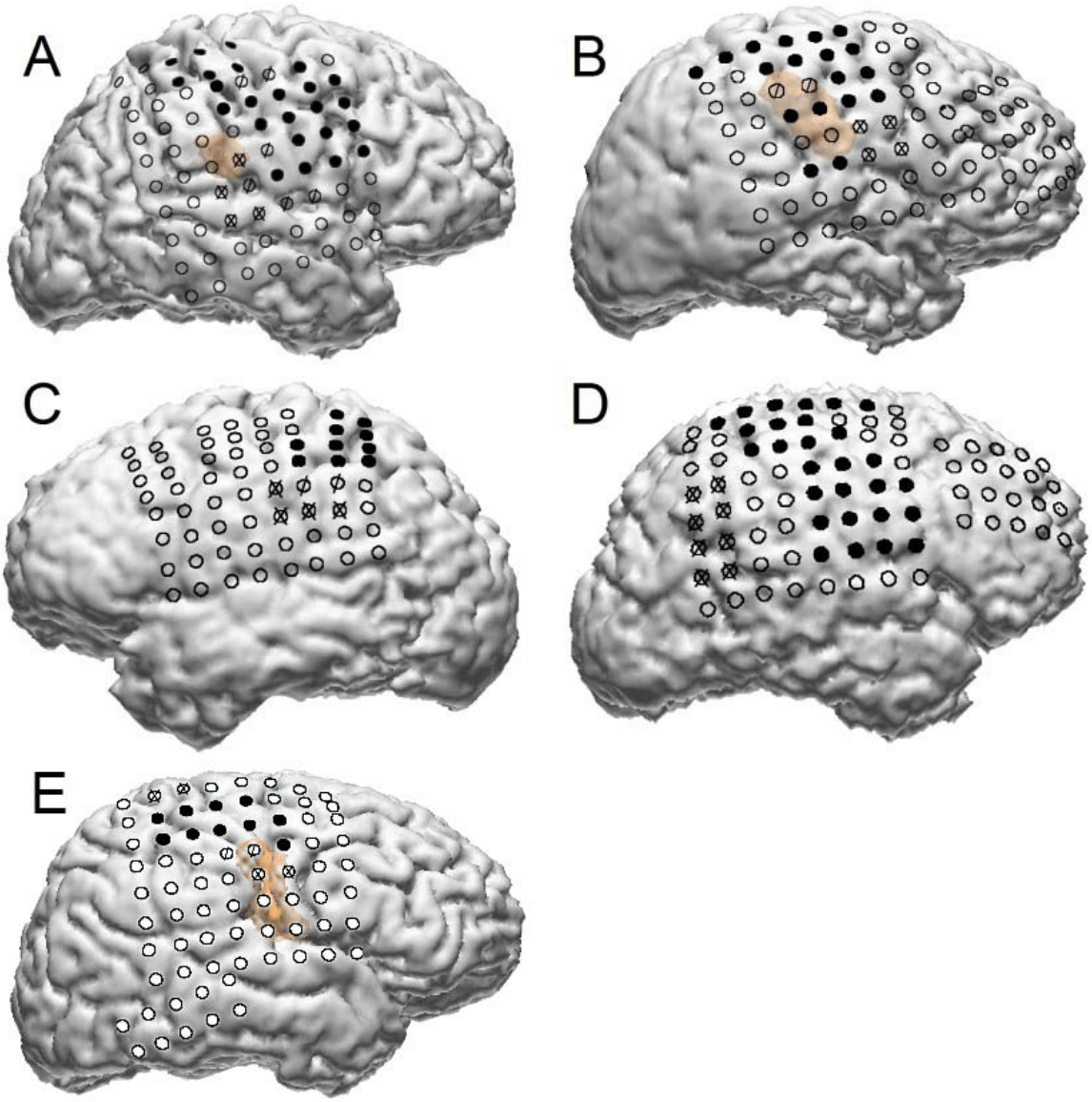

Figure 3.1: Grid of ECoG electrode locations in each of the five studied subjects. Portions of motor, supplementary motor, and premotor cortex are covered by the grids in all subjects. Solid black electrodes are those for which electrical stimulation mapping (ESM) elicited a motor response, electrodes marked with an "X" are those for which ESM elicited a sensory response, and electrodes marked with a "/" are those for which ESM elicited both motor and sensory responses. The light brown regions in the figures for subjects A, B, and E are locations of cortical dysplasia.

Subject	ECoG coverage	Seizure focus / pathology	CyberGlove hand
A	Right frontal-parietal-temporal grid	Right parietal operculum / cortical dysplasia	Left
B	Right frontal-parietal-temporal grid	Right frontal-parietal operculum / cortical dysplasia	Left
C	Left frontal-parietal grids, left temporal strips	Left posterior superior frontal gyrus / post-traumatic encephalomalacia	Right
D	Right frontal-parietal grid	Right superior frontal sulcus / cortical dysplasia	Left
E	Right frontal-parietal-grid	Right ventral peri-central encephalomalacia	Left

Table 3.1: Experimental Subject Summary

3.3.2 Experimental Protocol

Experimental sessions lasted approximately one to three hours in length, during which a battery of several hand motor tasks was performed. For this work, only palmar grasp and individual finger movement trials were analyzed. Each subject performed 10-25 palmar grasps over the course of 128-378 s, across all trials. Subject A was tested on two successive days; all other subjects were tested in only a single session. Individual trials lasted between approximately one and five minutes. Session and trial length accommodated subject fatigue and interest. A neurologist monitored all experimental sessions and subjects were permitted to rest between trials.

The experiment was designed to collect data that could be used to build a decod-

ing model to control a hand prosthesis. During ECoG recording, joint angles were recorded with the arm in a comfortable position, somatosensory feedback was limited, and a typical prosthesis movement was repeated a number of times. Each subject sat in a hospital bed, with the arm of the hand wearing the data glove to record joint angles resting on a pillow to permit it to rest in a comfortable position between trials. The elbow joint was usually partially flexed in this position, and the hand partially prone. To limit unusual somatosensory feedback, the hand did not touch the pillow or any other surfaces during experimental recording.

In the grasp study, the subjects performed repeated slow-paced palmar grasps, opening and closing all fingers on the hand contralateral to the implanted ECoG grid. A slow-paced palmar grasp was chosen to mimic the most typical use of a hand prosthesis. These grasps were either self-paced or verbally cued depending on patient compliance with the task.

In the individual finger movement study, subjects flexed and extended each finger several times before moving to the next, in a random order. They repeated these multiple flexion and extensions between 10 and 35 times per trial. Subjects were either self-paced, vocally cued, or visually cued. In some cases, subjects viewed a virtual representation of a prosthetic hand in the MSMS virtual environment [184] moving in synchrony with their own hand on a computer screen.

3.3.3 Local Motor Potential

The LMP, a smoothed amplitude feature of the ECoG in the temporal domain, was used as an ECoG feature in conjunction with high frequency and low frequency power information for analysis. The LMP on sensorimotor electrodes has been shown to vary with slow-paced grasping motions like those used in this study, and is a commonly-used feature in ECoG BMI algorithms [98]. We have shown that the LMP alone can be used to decode these slow grasps with high accuracy, even when very few electrodes are used in the decoding model [105].

We computed the LMP with a moving average window T of 2 s duration:

$$LMP(t)_n = \frac{1}{T} \int_{t-T/2}^{t+T/2} X(\tau)_n^{CAR} \tag{3.1}$$

Here $X(\tau)_n^{CAR}$ is the time signal from the nth ECoG electrode after filtering, where τ is the time. The LMP was used in screening for electrodes whose activity was related to movement.

3.3.4 ECoG Electrode Activation Index

To restrict initial TV-DBN analysis to sensorimotor electrodes, we first screened electrodes for motor-related activity using the electrode activation index (AI), described below. The AI is a measure of the average extent of change in ECoG features between baseline and movement. It is calculated using both the power in low frequency bands and power in high frequency bands, ECoG features that are known to

vary in sensorimotor areas preceding and during hand movement [44, 98, 185, 186].

It has been suggested that changes in broadly-defined low and high frequency power bands are sufficient to quantify motor activity [104]. In the grasp study, we therefore calculated log power in low (12-30 Hz) and high (75-150 Hz) frequency bands. To ensure compatibility of the algorithm with eventual clinical applications needing computationally efficient implementations, the fast Fourier transform (FFT) [187], which has been used in many recent online ECoG BMI implementations [99, 188], was used rather than autoregressive modeling [171]. The FFT was implemented with standard MATLAB (MathWorks, Natick, MA) toolboxes. The window size for the low frequency band (LFB) was 512 ms, and the window size for the high frequency band (HFB) was 256 ms.

In the individual finger movement study, in order to maximize potentially useful features, we considered spectral features in standard frequency bands: delta (0-4 Hz), theta (4-8 Hz), mu (8-13 Hz), beta (14-30 Hz), low gamma (31-50 Hz), and high gamma (70-110 Hz). Spectral power was calculated in 1 Hz bins with an autoregressive model using the Burg method of order 20 on windows of 1 s.

We compared each of the three grasp features (LMP, LFB, and HFB) or seven individual finger features (LMP and six spectral bands), between the baseline state (rest, r) and active state (hand movement, m). We used a well-accepted statistic, the

cross-correlation coefficient [189]:

$$F = \left| \frac{(m-r)^3}{|m-r|\,\sigma^2_{m\cup r}} \frac{N_m N_r}{N^2_{m\cup r}} \right| \tag{3.2}$$

Here r denotes the average feature value during rest, m denotes the average feature value across all hand movements, σ denotes the feature variance across all hand states, and N denotes the total number of incidences of each state.

The AI was then determined for each electrode by the feature with the largest normalized change between rest and movement states for all hand movements; e.g., in the case of grasp:

$$AI = \max\{LMP, LFP, HFP\} \tag{3.3}$$

In the grasp study, the five electrodes with the highest AI values were considered to represent hand movement-related locations for the purposes of connectivity analysis. Five electrodes were chosen because for all subjects except Subject C, previous work has shown that within five electrodes, decoding accuracy (r, correlation between actual and predicted hand movements) reached approximately 95% of maximum decoding accuracy [105]. Furthermore, preliminary networks of five electrodes contained sufficient connections to probe with maps of cortical connectivity. In the individual finger movement study, the ten electrodes with the highest AI values were included in connectivity analysis, in order to more fully probe the connectivity feature space.

3.3.5 Time-Varying Dynamic Bayesian Networks

The TV-DBN framework was used to model connectivity and directionality between pairs of ECoG electrodes. Under this framework we considered the connectivity coefficient from electrode i to electrode j to be high at time t if information about activity at electrode i at time $t-1$ could be used to predict activity at electrode j at time t. The N ECoG channels recorded from each patient were represented as a vector at time t:

$$X^t = \left(x_1^t, x_2^t, ..., x_N^t\right) \in \mathbb{R} \tag{3.4}$$

The time steps $t = 1, ..., T$ were used to express a time series of ECoG data with length T. A first order Markov model was used, meaning that the state of each ECoG signal, X, at time t depended only on the previous state of all ECoG channel signals at time $t-1$, 200 ms before time t. In this case the conditional probability of observing a given set of ECoG amplitudes at time t given amplitudes at previous time $t-1$ was $P\left(X^t|X^(t-1)\right)$.

The distribution of temporal ECoG transitions was modeled with linear regression:

$$X^t = A^t X^{t-1} + \varepsilon \tag{3.5}$$

The term $A^t \in \mathbb{R}^{N \times N}$ was then a connectivity coefficient matrix, in which A_{ij}^t was the connectivity weight from the ith to the jth channel from time $t-1$ to time t. The A^t term was estimated at time t by minimizing the criterion:

$$\hat{A}_i^t = \text{argmax}_{A_i^t \in R^{1 \times N}} \frac{1}{T} \sum_{t^*=1}^{T} w^t(t^*) x_i^{t^*} - A_i^t X^{t^*-1} + \lambda ||A_i^t|| \tag{3.6}$$

The parameter λ was a regularization term that shrank the connectivity terms of the connectivity matrix A. Previous work led us to use a value of 100 for this parameter [161]. The weight of an observation at time t^* was given by $w^t(t^*)$, defined using a Gaussian RBF kernel:

$$w^t(t^*) = \frac{K_h(t^* - t)}{\sum_{t^*=1}^{T} K_h(t^* - t)} \tag{3.7}$$

$$K_h(\cdot) = e^{-t^2/h} \tag{3.8}$$

The kernel bandwidth was given by the parameter h, which controls the scattering of the kernel. We used a value of 5 for h [161]. The Gaussian RBF kernel was used in estimating A^t to reduce noise and provide a more stable estimate. It was summed only over points up to t, maintaining causality. The low variance ensured that only data near time t was used in estimating A^t.

The connectivity coefficient matrix A was estimated by decomposing the matrix into two orthogonal axes. The first axis was defined at each time point by the weight term, which weights the signal heavily near time t. The second axis was defined by each channel, as in Eqn. 3.6. Through this decomposition simplification, the network can be solved as a weighted regression problem by least squares.

3.4 Results: Connectivity during Grasp

This section presents results obtained from subjects A-D participating in the grasp study.

3.4.1 Selection of Movement-Related Electrodes

Motor-related electrodes were selected using the metric AI representing the average change in ECoG features between baseline and movement. Maps of normalized absolute AI are shown for each subject in Fig. 3.2. A subset of the five electrodes from each subject with highest absolute AI values was chosen for subsequent analysis of movement-related changes in connectivity. Details on the electrodes selected for analysis, including approximate electrode location and clinical electrocortical stimulation mapping (ESM) results are given in Table 3.2. Electrodes with high absolute AI were largely located over peri-Rolandic sensorimotor areas (75%). In three of four subjects (A, B, and D) the activity on a few electrodes was well correlated with movement. Subject C had generally very low correlation between motor activity and ECoG features.

3.4.2 Peri-Movement TV-DBN Connectivity Coefficients

TV-DBN connectivity coefficients were computed between all possible pairs from the five most movement-related electrodes for each subject. A representative plot of the evolution of TV-DBN connectivity coefficients for subject A is shown in Fig. 3.3. On average, movement-related TV-DBN connectivity coefficients decreased preceding movement, entering a period during which the average influence was negative, and

Subject	Electrodes selected	Approximate cortical region	ESM result
A	2	Temporal lobe	No sensory or motor result
	4	Parietal lobe	No sensory or motor result
	39	Peri-Rolandic area	Motor result
	55	Peri-Rolandic area	Motor result
	68	Peri-Rolandic area	No sensory or motor result*
B	5	Peri-Rolandic area	Motor result
	11	Peri-Rolandic area	Motor result
	12	Peri-Rolandic area	Motor result
	26	Peri-Rolandic area	Motor result
	36	Peri-Rolandic area	Sensory result
C	18	Peri-Rolandic area	No sensory or motor resultX
	23	Peri-Rolandic area	No sensory or motor resultX
	27	Parietal lobe	Motor result
	50	Frontal area	No sensory or motor result
	55	Peri-Rolandic area	No sensory or motor result/
D	42	Peri-Rolandic area	Motor result
	43	Peri-Rolandic area	Motor result
	45	Parietal lobe	No sensory or motor result/
	50	Peri-Rolandic area	Motor result
	51	Peri-Rolandic area	Motor result

*Adjacent to electrodes with a motor ESM result
XAdjacent to electrodes with a sensory ESM result
/Adjacent to electrodes with motor and sensory ESM results

Table 3.2: AI-Based Electrode Selection

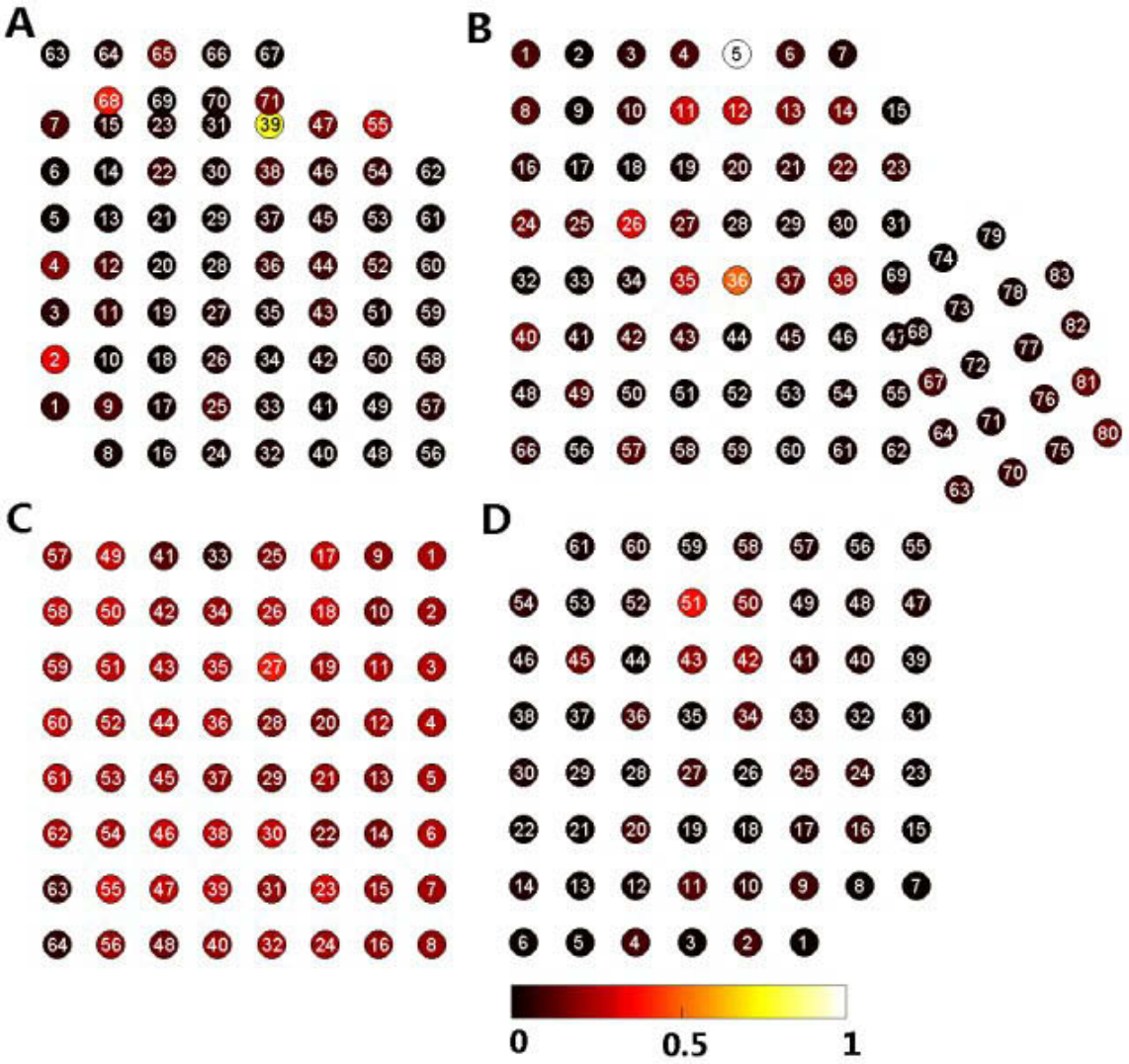

Figure 3.2: Normalized absolute AI on all electrodes for each subject. High AI indicates that the LMP or spectral features recorded on an electrode were more correlated with hand movements than those with low AI. For each subject the five electrodes with highest absolute AI values were used for subsequent analysis (see Table 3.2). ©2012 IEEE

recovered gradually over the time course of movement. Negative values in TV-DBN connectivity coefficients may indicate a change in the phase difference between signals, or more simply that an increase in activity at one electrode precedes a decrease in the activity at another.

In three subjects the TV-DBN connectivity coefficients between at least two pairs of movement-related electrodes showed a statistically significant change from baseline during movement (p <0.05, Kruskal-Wallis test). For subject A, 6 electrode pairs exhibited statistically significant changes in TV-DBN connectivity coefficients; for subject B, 13 electrode pairs; and for subject D, two electrode pairs. For subject C no electrode pairs exhibited a statistically significant change in TV-DBN connectivity coefficients. Fig. 3.4 depicts TV-DBN connectivity coefficients between all movement-related electrodes for all subjects averaged over hand movement trials. Movement onset is indicated with a vertical line.

3.4.3 TV-DBN Connectivity Coefficient Evolution in Time

In order to better visualize the evolution of the cortical connectivity network preceding and during movement, TV-DBN connectivity coefficients between movement-related electrodes with a statistically significant change from baseline (p <0.05, Kruskal-Wallis test) were overlaid on cortical reconstructions. An example set of cortical con-

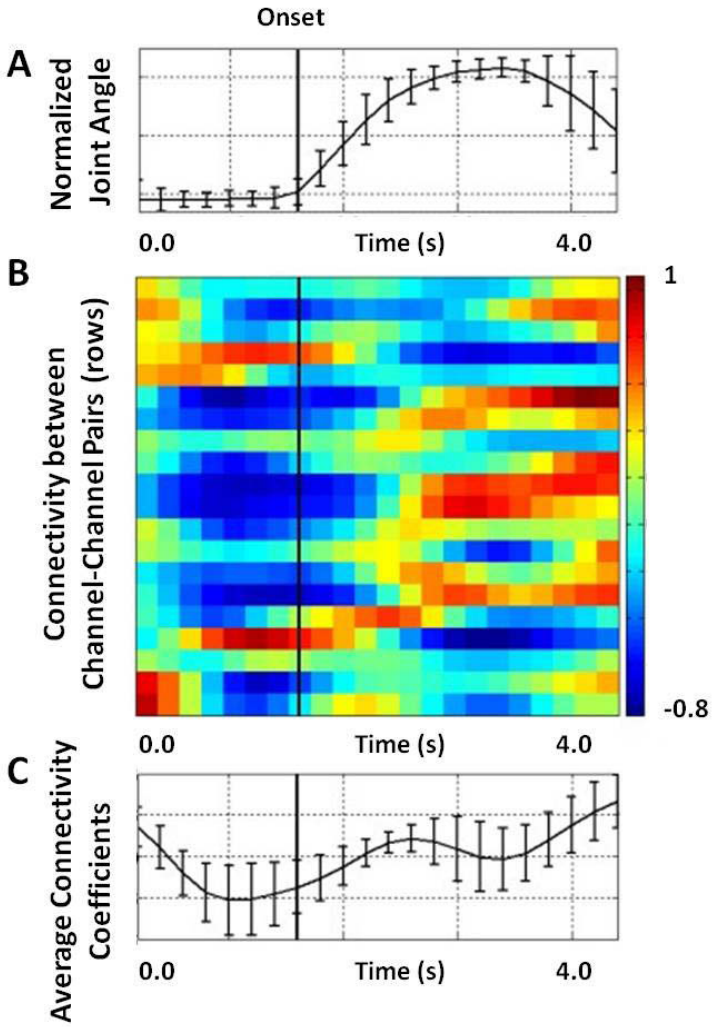

Figure 3.3: TV-DBN connectivity coefficients between ECoG electrodes during hand movement for subject A. Movement onset is marked with a vertical black line. (a) Time course of normalized joint angle averaged across trials. Movement onset occurs at 0.8 s from the beginning of the trial. (b) TV-DBN connectivity coefficients between all pairs of movement-related electrodes before and during movement. Values were averaged across all trials. In most channel pairs connectivity varied with movement. (c) TV-DBN connectivity coefficients averaged across movement-related electrode pairs. A change in connectivity coefficients begins prior to movement and recovers gradually over the time course of the movement.

nectivity networks is shown in Fig. 3.5 for subject A for pre-movement (-0.6 to -0.2 s), movement onset (0 to 0.2 s), and during movement (0.4 to 1.4 s) conditions. In subject A the pre-movement connectivity network was widespread with strong projections between motor-related electrodes. Connectivity at movement onset was more limited. As the movement continued, the connectivity network incorporated several electrodes and may have represented sensorimotor integration.

We observed what appeared to be an early onset of TV-DBN connectivity coefficient changes, relative to the onset of movement and the onset of movement-related changes in other ECoG features. As an example, the average time courses of spectral features and TV-DBN connectivity coefficients for subjects A and B are shown in Fig. 3.6.

We used principal component analysis to explore whether the changes in connectivity coefficients preceding and following movement onset could be grouped in a meaningful way. Principal components (PCs) of TV-DBN connectivity coefficients for all four subjects did tend to separate into those that were most activated pre-movement, near movement onset, and during movement (see Fig. 3.7). A representation of the connectivity coefficients that most contributed to the first four PCs for Subject A is shown in Fig. 3.8. The PC whose largest change occurred pre-movement is the only one to include significant connections to and from a frontal electrode, while the PC with large post-movement change includes primarily connections to and from peri-Rolandic areas.

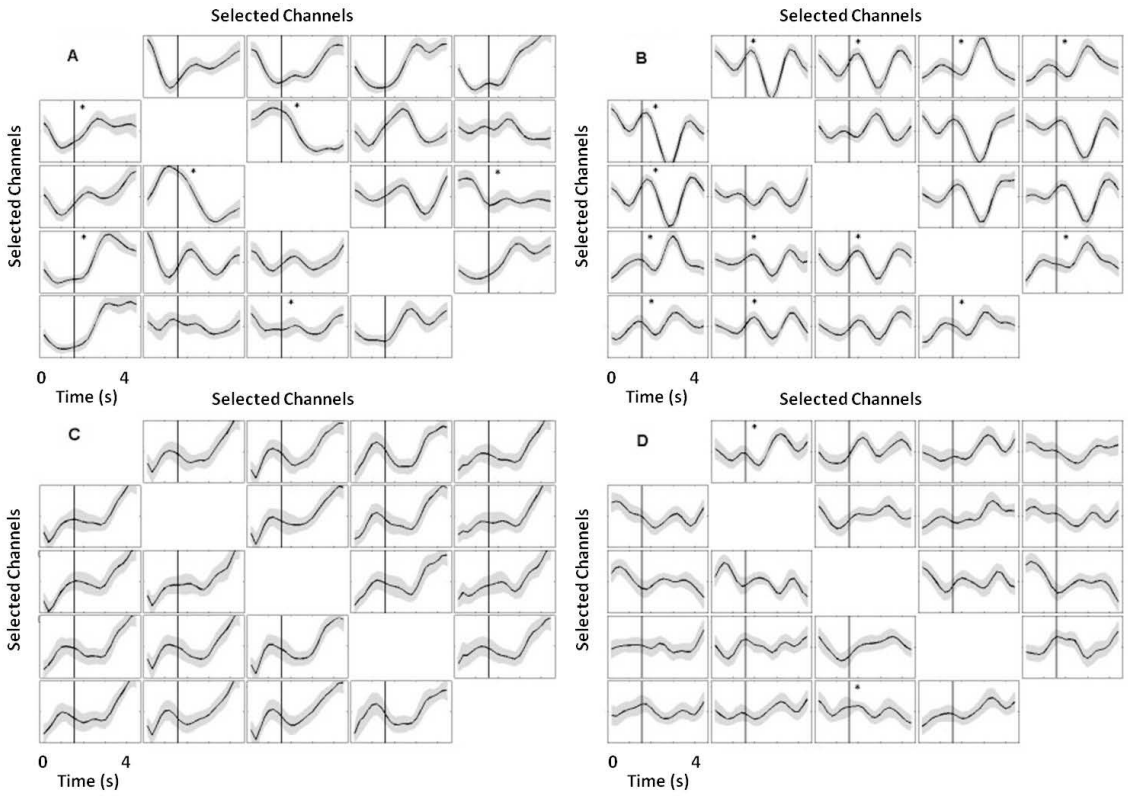

Figure 3.4: TV-DBN connectivity coefficients between movement-related electrodes changing in time, averaged across all hand movements. Standard error is shown above and below the mean, and plots with statistically significant changes in movement coefficients compared to baseline are marked with an asterisk. A) Six electrode pairs show statistically significant changes in connectivity coefficients. B) Thirteen electrode pairs show statistically significant changes in connectivity coefficients. C) No electrode pairs show statistically significant changes in connectivity coefficients. D) Two electrode pairs shows a statistically significant change in connectivity coefficient.

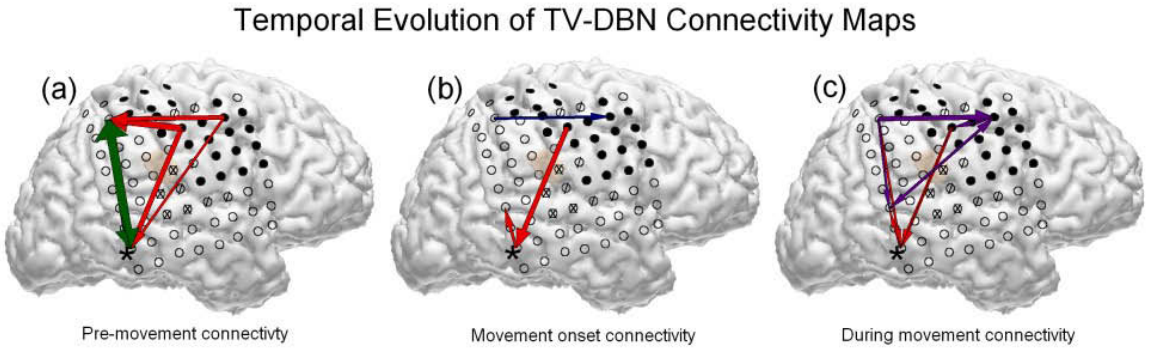

Figure 3.5: Depiction of statistically significant absolute TV-DBN connectivity coefficients between movement-related electrodes on reconstructed brain surfaces. Positive TV-DBN values, indicating direct relationships between the source and sink electrodes, are shown in green (pre-movement), blue (movement onset), and purple (during movement). Negative TV-DBN values, indicating inverse relationships between the source and sink electrodes, are shown in red. Arrow width indicates the magnitude of the TV-DBN coefficient. (a) Large pre-movement (0.6 to 0.2 s before movement onset) TV-DBN connectivity coefficients projected within peri-Rolandic regions and between electrode 2 (starred) and peri-Rolandic regions. (b) At movement onset, a limited connectivity network was observed between motor electrodes and from a motor electrode that was highly correlated with movement to electrode 2. (c) During movement (0.4 to 1.2 s after movement onset) sustained and distributed connectivity was observed, potentially integrating sensory and motor processing.

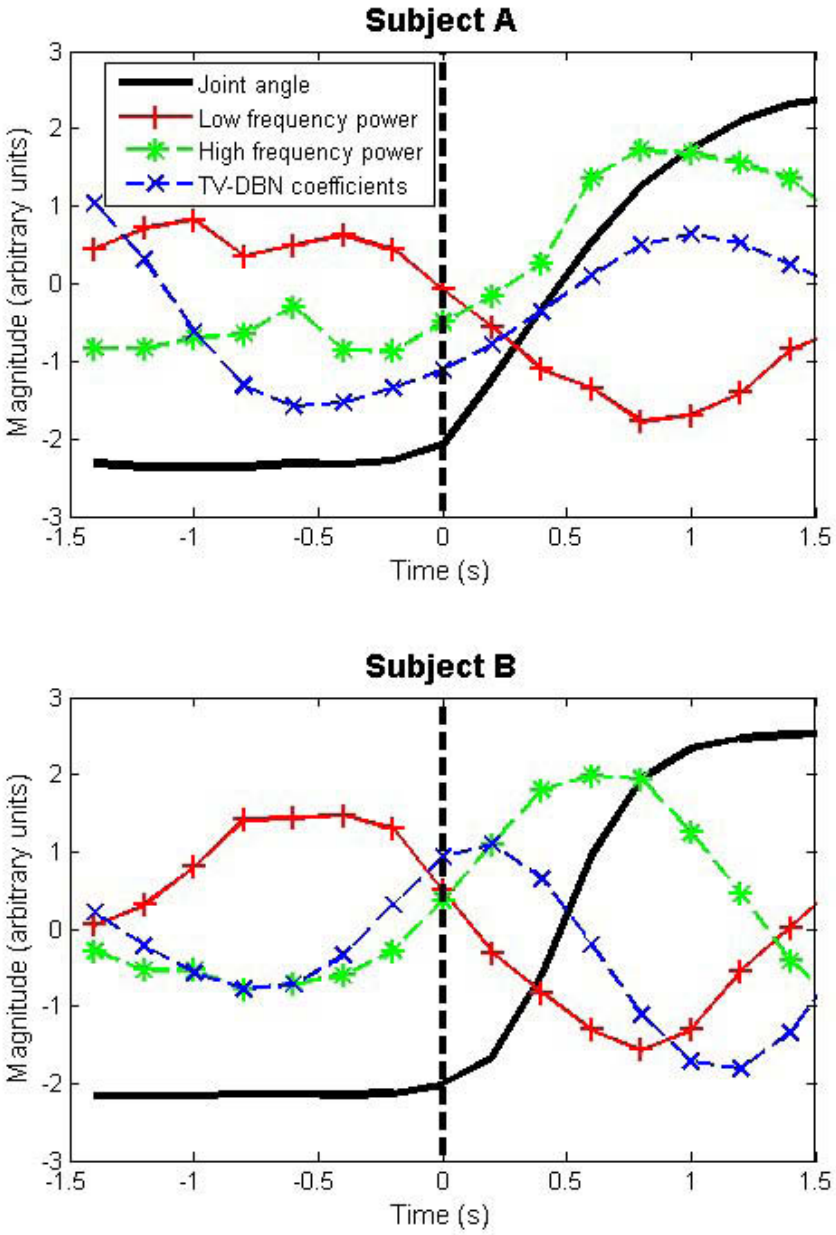

Figure 3.6: The average time course of spectral features and TV-DBN connectivity coefficients preceding movement onset (time 0 s) and during movement for subject A (upper) and subject B (lower). The early onset of movement-related change in TV-DBN connectivity coefficients may be a useful feature for movement decoders, for which change in kinematic predictions usually lags actual kinematic change. ©2012 IEEE

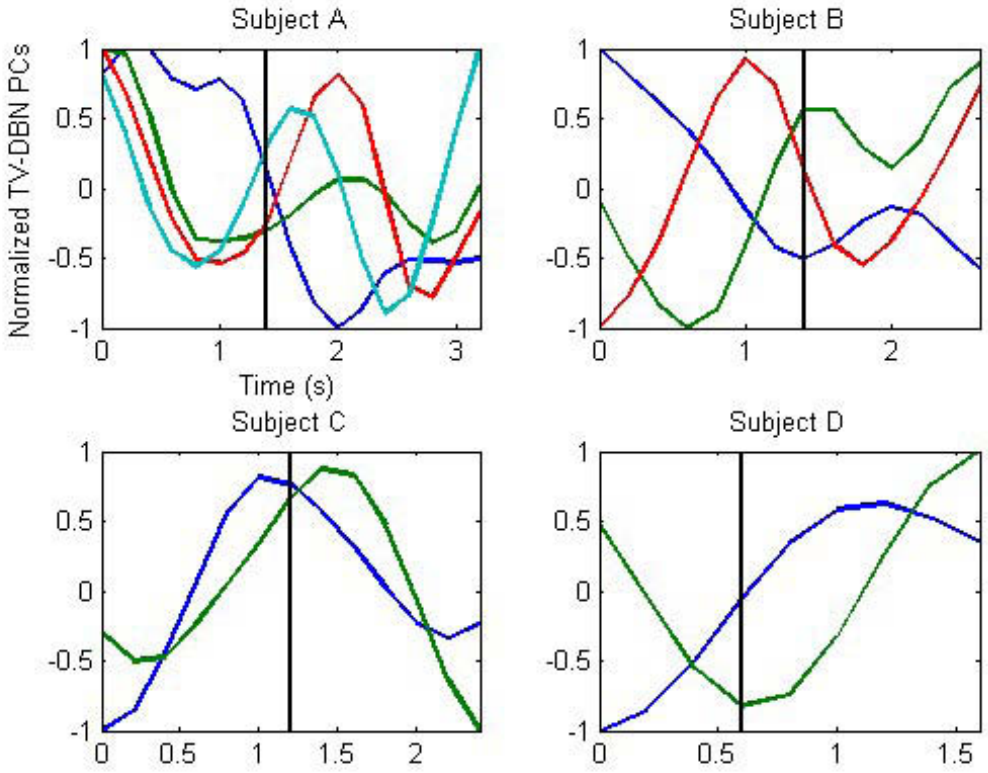

Figure 3.7: Trial-averaged PCs of TV-DBN connectivity coefficients varying in time. PCs shown account for 95% of TV-DBN connectivity coefficient variance for each subject (four PCs for subject A, three for subject B, and two for subjects C and D). The first PC is blue, second is green, third is red, and fourth is cyan. The vertical black line marks movement onset. Components emerge for most subjects that reach extrema both pre-movement onset and post-movement onset, possibly representing ensembles of cortical processing areas engaged in pre-movement and movement activities, respectively.

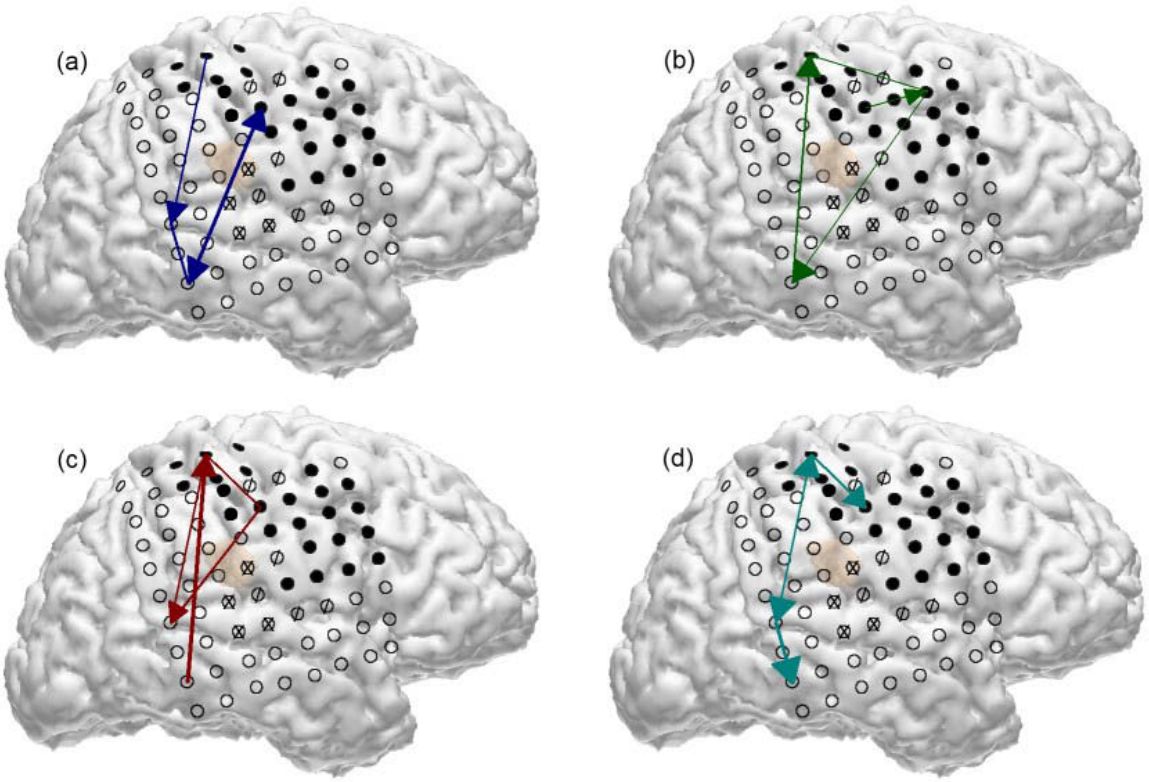

Figure 3.8: Depiction of largest contributors (top 20% of electrode pairs) to each of the four PCs for Subject A. (a) The first PC (blue) changed largely during the movement, and includes projections to and from the peri-Rolandic area. (b) The second PC (green) changed preceding movement but very little during movement, and is the only grouping to contain connections to and from the frontal electrode. (c) The third PC (red). (d) The fourth PC (cyan).

3.5 Results: Connectivity during Individual Finger Movements

This section presents results obtained from subjects A, B, and E participating in the individual finger movement study.

3.5.1 Local Motor Potential and Connectivity

Following the demonstration of a relationship between LMP-based connectivity and grasp during the slow hand open and close task, we probed connectivity during individual finger movements. Fig. 3.9 demonstrates that LMP-based connectivity also changes with more rapid individual finger flexions and extensions. In two subjects the TV-DBN connectivity fluctuated in an oscillatory pattern. Across the three subjects, the LMP distribution changed statistically significantly between movement and baseline (Wilcoxon rank sum test with Bonferroni correction, $p < 0.05$) in 126 electrodes, or 54% of all electrodes, whereas the LMP-based TV-DBN connectivity changed statistically significantly from baseline in 176 channel-channel connectivity pairs, or 65% of the 270 channel pairs tested. This large number of movement-related features may help to inform a decoder for dexterous movement. This is a small fraction of the 53,130 total channel pairs that could have been explored with TV-DBN across all three subjects; we limited our selection to ensure we obtained results that are relevant to real-time decoding, which will require rapid computation that is

only possible when analyzing a few channels with TV-DBN.

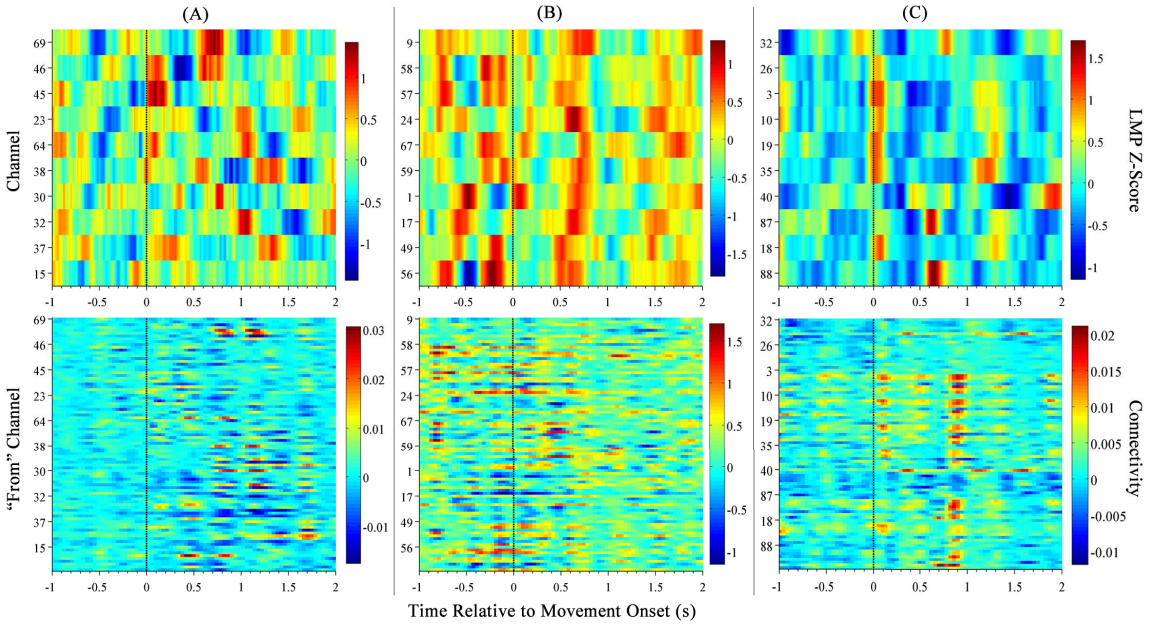

Figure 3.9: Trial-averaged LMP (upper row) and trial-averaged TV-DBN calculated from LMP (lower row) for one trial each for subjects A, B, and E. Plots are channels vs. time. Movement onset occurs at 0 s and is indicated with a dashed line. Movement-related LMP changes are difficult to distinguish, with the exception of subject E. Movement-related changes in TV-DBN coefficients, however, are evident in all subjects. ©2012 IEEE

3.5.2 Spectral Features and Connectivity

One group has previously studied the response of TV-DBN connectivity coefficients constructed from activity in the alpha band of EEG activity during movement imagery [161]. TV-DBN connectivity has not been explored in other frequency bands. Fig. 3.10 shows the average spectrograms for subjects A and B, who had robust movement-related changes in spectral connectivity, as well as plots of average

connectivity changes in the delta bands (A and B) and gamma band (A). Eighty-two percent of all spectral features on all channels included in the analysis changed from baseline to movement (Wilcoxon rank sum test with Bonferroni correction, $p < 0.05$). The number of channel-channel connectivity pairs whose connectivity changed statistically significantly relative to baseline ranged from 69-82% for individual features. Beta, low gamma, and high gamma-based connectivity features changed relative to baseline more often than lower frequency features. While the ratio of TV-DBN features changing was not higher than that of spectral features, with only ten electrodes we found between 357 and 494 modulating TV-DBN features per subject.

3.6 Discussion and Conclusions

We have described the application of a new method for determining directional connectivity of brain functional regions using the ECoG signal. The benefits of the TV-DBN method are the abilities to detect early changes in connectivity, handle short data windows, and vary constantly in time. This method was applied to human ECoG data to identify cortical connectivity preceding and during hand movement.

We have also described changes in cortical connectivity related to dexterous individual finger movement. In connectivity computed from the LMP, oscillatory movement-related activity was observed. Connectivity computed from spectral features varied, and included both peri-movement increases in delta and high gamma

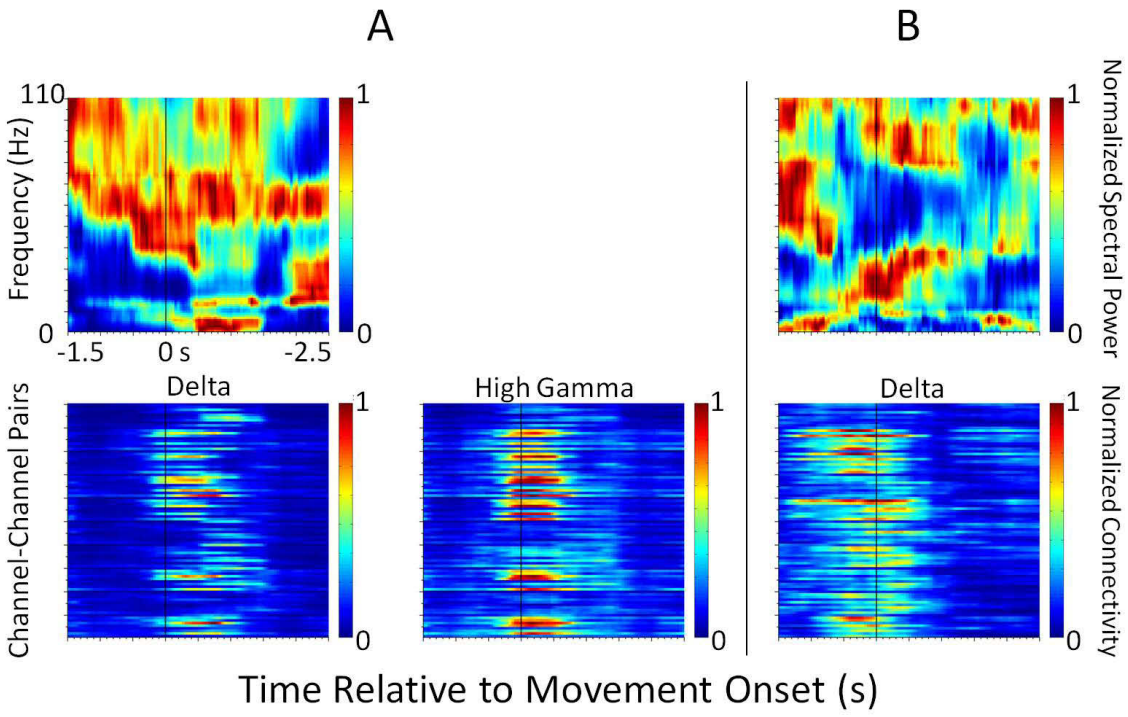

Figure 3.10: Selected average spectral (upper row) and spectral connectivity (lower row) features. Spectrograms are frequency vs. time for channel with the highest AI. Connectivity plots are channels vs. time. Movement onset occurs at 0 s and is indicated with a dashed line. (A) For Subject A, spectral-based connectivity in both the delta band (bottom left) and high gamma band (bottom right) changed visibly in many channel pairs before and during movement. (B) For Subject B, spectral-based connectivity in the delta band (bottom) dropped following movement onset, a phenomenon observed in the results for the grasp task. ©2012 IEEE

connectivity in one subject, and decreases in delta connectivity following movement in a separate subject.

We explored only ten electrodes per subject during individual finger movement in order to draw conclusions relevant for online motor decoding, which is feasible with TV-DBN calculations for ten electrode pairs but not for an entire ECoG grid. However with only these ten electrode pairs per subject we discovered hundreds of movement-related connectivity features. Future work will probe the correlation of information contained in these features, with an aim to identify large feature sets with highly independent information content. Such information-rich feature sets may permit dexterous decoding to advance beyond simple grasps to individual finger movements.

3.6.1 Interpretation of Connectivity Coefficients

From literature, it is expected that immediately preceding hand movement there may be activity from supplementary motor [69,190,191] and premotor areas [192,193]. This activity informs the primary motor cortex, which is directly responsible for movement control [194]. It is possible that this early activity created the change in TV-DBN connectivity coefficients that we observed preceding movement. During movement, somatosensory information provides feedback to motor areas [195], updating the projected motor model. Statistically significant changes in TV-DBN connectivity coefficients from baseline support this model, with connectivity between a variety of motor areas preceding hand movement. At grasp onset, a limited directed connec-

tivity network develops involving the motor electrode most highly correlated with hand movement. As grasp continues, there are once again more spatially widespread statistically significant connectivity coefficients. This connectivity network present during grasp may be a reflection of the fact that the motor areas are receiving sensory feedback to update the projected motor model.

3.6.2 Comparison to Alternative Techniques

A handful of approaches exist to map influences or similarities between time-varying signals, including coherency and phase-based methods [177, 178, 181] and Granger causality-based methods [140–142, 144, 196–198]. These approaches can be applied to the problem of discovering connectedness between areas of cortex covered by ECoG electrodes.

Coherency is a baseline measure of interactivity between cortical areas [177, 178]. The imaginary part of coherency has been used in EEG to find directionality of information flow [181]. Similar phase-based methods [135, 176, 179, 180] can indicate EEG and ECoG signal flow and in some cases directionality. However, due to the nature of the phase, it is not possible to create a precise temporal map of information flow at known time delays. Moreover, there is a problem of high correlation in multichannel data, causing pair-wise interactivity algorithms to incorrectly estimate overriding common influences across multiple channels [141, 197].

The directed transfer function (DTF), an extension of the Granger causality con-

cept to multivariate signals [140], addresses the problem of pair-wise connectivity algorithms. The DTF has been further refined in the direct DTF (dDTF), which exhibits improved ability to differentiate direct causality from cascaded causality [142], and the short-time DTF (SDTF), which is applicable to short signal windows [196, 198]. The dDTF and SDTF have been combined in the SdDTF [144], which is well suited to exploring rapid changes in direct connectivity. However, the SdDTF requires multiple trials and is calculated using a multivariate autoregressive model, an algorithm that is computationally expensive.

Because the TV-DBN results demonstrated here are independent of ECoG frequency band, unlike techniques such as the imaginary part of coherency [181] or SDTF [198] and SdDTF [144], we are able to investigate causality outside the constraints of frequency. The TV-DBN, like Granger causality-based methods, has a basis in causality. Connections discovered with the TV-DBN therefore reflect relationships more clearly than, for example, the imaginary part of coherency, which can only indicate that one element of an interacting pair preceded another. Compared to the SdDTF, a measure of causality that can be applied to short time windows [144], the TV-DBN has decreased computational complexity but is applicable to similarly short time windows (200 ms in this study compared to 360 ms in the 2008 SdDTF study).

3.6.3 Limitations of the Method

The TV-DBN model used in this analysis was based on a first order Markov model, in which the state of an ECoG signal depended only on the previous state of all ECoG channels at a time 200 ms earlier. It is unlikely that this offset effectively probes all causal relationships between cortical regions, and a more comprehensive model would consider the effects of channel states at multiple time lags. We chose to study the model at a single time lag to preserve computational efficiency of the TV-DBN and to enable implementation in a real-time BMI.

The method did not incorporate explicit models of physiological mechanisms of connectivity. For example, we did not probe phase synchronization or specific frequency bands, such as theta oscillations, that have been shown to synchronize during a variety of tasks, potentially guiding the synchronization of cortical processing [132, 169, 170, 199, 200]. However, physiological mechanisms for connectivity may be incorporated into the model in a "black box" way, without being explicitly defined, because the TV-DBN finds signal connectivity.

Chapter 4

Connectivity Analysis as a Novel Approach to Motor Decoding for Prosthesis Control

4.1 Abstract

The use of neural signals for prosthesis control is an emerging frontier of research to restore lost function to amputees and the paralyzed. Electrocorticography (ECoG) brain-machine interfaces (BMI) are an alternative to EEG, neural spiking, and local field potential BMI approaches. Conventional ECoG BMIs rely on spectral analysis at specific electrode sites to extract signals for controlling prostheses. We compare traditional features with information about the connectivity of an ECoG electrode

network. We use time-varying dynamic Bayesian networks (TV-DBN) to determine connectivity between ECoG channels in humans during a motor task. We test TV-DBN output in a hand kinematic decoder in four subjects and obtain an average correlation coefficient (r^2) between actual and predicted joint angle of 0.40, and as high as 0.66 in one subject. This result compares favorably with spectral feature decoders, for which the average correlation coefficient in our study is 0.13. This work introduces a new BMI feature set based on connectivity and demonstrates its potential to improve ECoG BMI accuracy.

4.2 Introduction

While high decoding accuracy for classification of movement has been reported in the literature [96,97,102], trajectory prediction accuracy and online decoding latency has not improved significantly since ECoG's introduction as a BMI control signal [44], with an average of 90% of targets hit in a 1D control task using imagined movement and speech. It is unlikely that the target population for ECoG-based BMI use will accept accuracy significantly below that provided by a natural or cable-controlled arm in clinical use [201]; therefore, fundamental shifts in BMI features and decoding algorithms will be necessary to create a truly clinically relevant BMI.

Human ECoG-based decoding has progressed since its first demonstration in 2004 [44], with some forays into dexterous decoding, including grasps [105, 202, 203].

Classification of contralateral and ispsilateral individual finger movement [102] and decoding the time course of individual finger tapping [101] have been demonstrated. However these offline dexterous decoding achievements have not been replicated in a real-time ECoG BMI, in which the challenges of asynchronous decoding will require much more information-rich signals than are currently available.

A clinically relevant BMI would need to operate in real-time and derive sufficient information from the neural signal to achieve nearly 100% accurate control. In order to create a BMI with an operating speed approaching natural execution time and a level of accuracy that is acceptable to a patient population, new models of cortical communication and new techniques are required with rapid calculation speed and high information rate. Current BMIs use signals from individual electrodes and features based on changes in frequency band power, indicators only of localized processing. It is very likely, however, that most processing involves extended cortical circuits in parietal, temporal, frontal, and sensorimotor areas, which are better observed through the signals recorded over a wider span of the ECoG array. A better understanding of the flow of information through these circuits may improve BMI accuracy. One new and promising approach is connectivity mapping, the reconstruction of functional connections between cortical areas based on the signals present in those areas. Here we implement a high-throughput, dynamic, and computationally cheap method to map connectivity. We hypothesize that the connectivity coefficients of these directed connectivity maps will be informative in decoding joint angle during palmar grasp

from the ECoG signal.

Here we apply TV-DBN estimation of directed connectivity to multichannel ECoG data recorded during a simple motor grasping task. Then we use these connectivity coefficients to create an ECoG kinematic decoder and compare it to a standard spectral feature-based decoder. We expect the accuracy of the connectivity-based decoder to improve upon the accuracy of the standard decoder.

4.3 Methods

4.3.1 Experimental Protocol

The experimental protocol was that used for the grasp study described in Chapter 3. Four human subjects performed palmar grasps while kinematic and ECoG data were simultaneously recorded. Data preprocessing, standard feature extraction, connectivity feature extraction with TV-DBN, and channel selection using the activation index (AI) were performed according to the methods described in the previous chapter.

4.3.2 General Regression Neural Networks

We hypothesized that connectivity coefficients found with TV-DBN would improve decoding of kinematic information from neural data over using traditional features

alone. To test this hypothesis, we constructed two general regression neural networks (GRNN) per subject, which decoded continuous joint angle for one angle that was chosen to be representative of the trajectory of hand opening and closing [204]. The GRNN was chosen to maintain rapid computational speed. It is a fast learning, non-iterative algorithm. The first GRNN decoded joint angle from standard BMI features (the "spectral feature GRNN"), and the second used TV-DBN connectivity coefficients (the "TV-DBN GRNN").

The spectral feature GRNN used as inputs the LMP and the log power of low (12 to 30 Hz) and high (75 to 150 Hz) frequency bands for all electrodes (3 types of features, between 264 and 342 total features). The TV-DBN GRNN used the connectivity coefficient matrix A. To maximize decoding accuracy, we computed TV-DBN connectivity coefficients for all electrodes, and chose as decoding features the 5% of connectivity coefficients most highly correlated with the time course of the hand joint angle (between 387 and 650 total features).

For both GRNN decoders, the states of hand movement were defined as $y_t(t - 1, ..., T)$, in T time steps. The spectral feature matrix S and the connectivity coefficient matrix A at time t were reshaped as a vector. For the TV-DBN decoder, this vector was $C(A^t_{1,1}, ..., A^t_{1,N}, ..., A^t_{N,1}, ..., A^t_{N,N})$. Then y was a function of C and y, and was estimated by its expected value:

$$E[y|A] = \frac{\int_{-\infty}^{\infty} y f(C, y) \mathrm{d}y}{\int_{-\infty}^{\infty} f(C, y) \mathrm{d}y} \tag{4.1}$$

The probability distribution function $f(C, y)$ was estimated with:

$$\hat{f}(C, y) = \frac{1}{(2\pi)^{(p+1)/2}\phi^{p+1}} \frac{1}{n} \sum_{i=1}^{n} e^{-D_i^2/2\phi^2} e^{-(y-y_i)/2\phi^2} \tag{4.2}$$

Here n was the number of sample observations, p was the dimension of the connectivity coefficient matrix A, ϕ was a smoothing parameter, and D_i^2 was the distance between C and the ith observation C_i. Substituting Eqn. 4.2 into Eqn. 4.1, we estimated the movement state with:

$$\hat{y}(C) = \frac{\sum_{i=1}^{n} y_i e^{-D_i^2/2\phi^2}}{\sum_{i=1}^{n} e^{-D_i^2/2\phi^2}} \tag{4.3}$$

The GRNNs used were four-layer networks with input vector C. Each unit of the pattern layer output the distance D_i^2 to the summation layer, which performed the numerator and denominator operations in Eqn. 4.3. The output layer computed the ratio between the numerator and denominator. Initial models were trained on 30% of the data and tested on 70%. Five-fold cross-validation was used to construct comparison spectral feature and TV-DBN models.

4.4 Results: Motor Decoding with TV-DBN Connectivity Coefficients

To investigate whether TV-DBN connectivity coefficients could improve upon neural decoding based on spectral and LMP ECoG features, we constructed two GRNNs with five-fold cross-validation for each subject to decode joint angle from neural data.

The first set of GRNNs used spectral features in a low frequency bin (12 to 30 Hz) and a high frequency bin (75 to 150 Hz) and the LMP for all electrodes, a total of 264-342 features. The second set of GRNNs used the top 5% of TV-DBN connectivity coefficients most correlated with joint angle, a total of 387-650 features. Decoding accuracy is shown for each subject in Table 4.1, and TV-DBN decoding results for one trial for each subject are shown in Fig. 4.1. For subject A, the optimal decoding accuracy (correlation coefficient, r^2, between actual and predicted joint angle) with the spectral feature set of GRNNs was 0.31, and with the connectivity feature set of GRNNs was 0.66, more than double. For subject B, the spectral feature accuracy was 0.18, and the connectivity feature accuracy was 0.40, also more than double. Decoding accuracy was near zero with both feature sets for subject C. For subject D, decoding accuracy was very poor with the spectral feature set at 0.02, but much higher with the connectivity feature set at 0.52. Although the spectral feature GRNN's decoding accuracy is below the average reported in a recent study of decoding individual finger movement from ECoG (0.27 [101]), the TV-DBN decoding results are on average higher.

It is likely that at least some of the improved accuracy in the TV-DBN GRNN may be attributed to the increased number of features included in the decoder. For LMP, LFP, and HFP, the maximum number of features that can be used in decoding is 3N, where N is the number of ECoG channels, whereas the maximum number of directed connectivity-based features is $N^2 - N$. The large feature set available through this

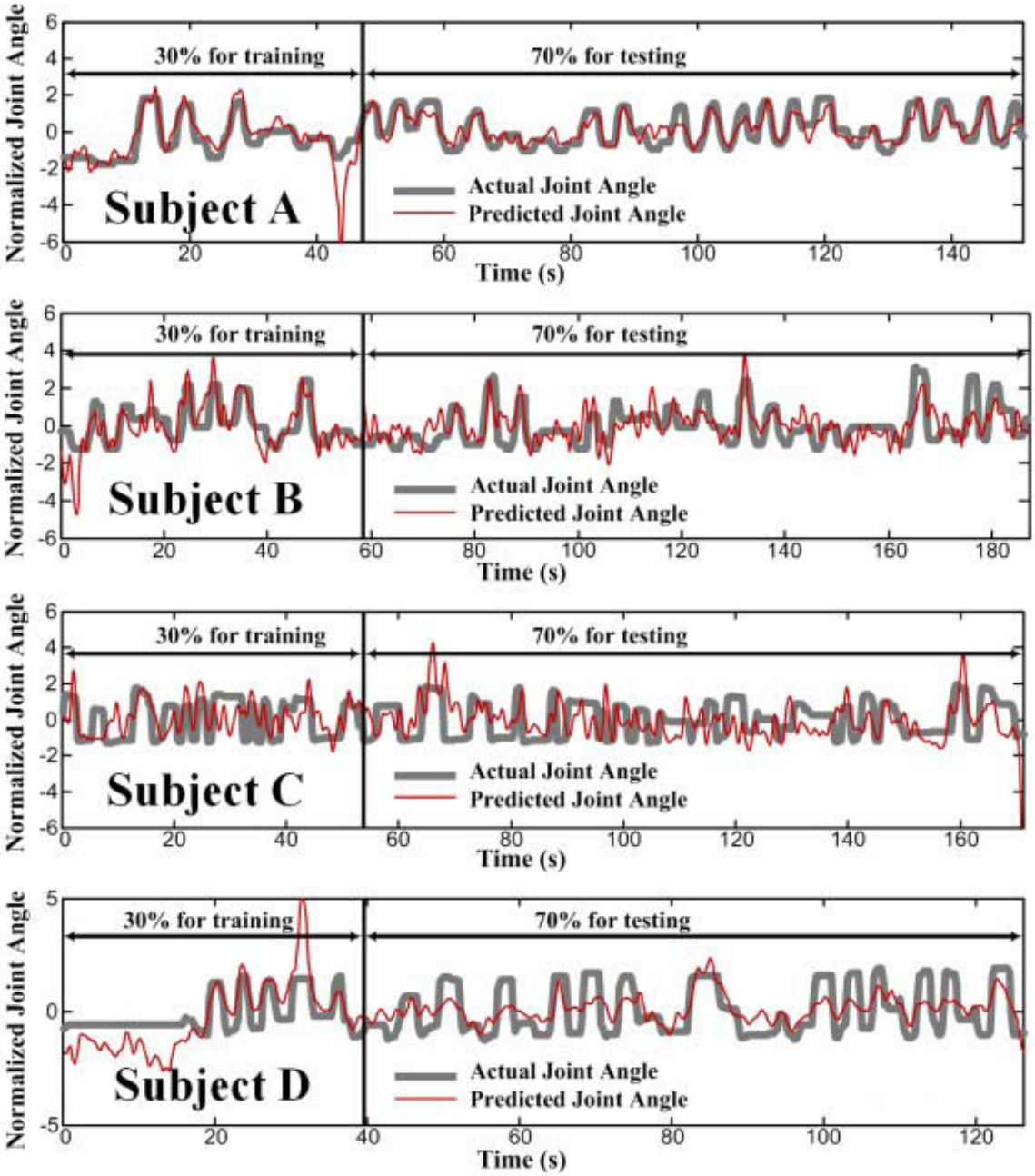

Figure 4.1: TV-DBN GRNN joint angle decoding results for all subjects. Thick gray trace represents actual normalized joint angle, and thin red trace represents normalized predicted joint angle. One joint angle from a data glove was chosen to be representative of the opening and closing of the hand. GRNN decoders were trained on 30% of data and tested on 70%, and cross-validation was not used. Correlation coefficient (r^2) between actual and predicted joint angle was 0.66 for subject A, 0.40 for subject B, 0.01 for subject C, and 0.52 for subject D. ©2012 IEEE

Subject	Spectral and LMP GRNN decoder	TV-DBN GRNN decoder
A	0.31	0.66
B	0.18	0.40
C	0	0.01
D	0.02	0.52

Table 4.1: Average Maximum Decoding Accuracy by Subject (Correlation Coefficient, r^2)

method may lead to improved decoding capabilities.

Using MATLAB 2011b on an Intel(R) Core(TM)2 Duo 2.53 GHz processor, the approximate computation time for extracting TV-DBN features for five electrodes was 4 ms for each 200 ms time step. With five fold cross-validation, GRNN training time was 110 ms, and the computation time of each GRNN output for testing was negligible. Using only 5 electrodes, this system would be applicable to real-time BMI. However, as implemented, calculating TV-DBN coefficients for all electrodes required approximately 580 ms per time step, meaning that pre-selecting a subset of electrodes is necessary for real-time neuroprosthetic control.

4.5 Discussion and Conclusions

We have used TV-DBN connectivity coefficients to decode joint angle during grasp, which improved upon a decoder constructed with standard spectral and LMP ECoG features. This approach has potential applications in ECoG-based BMI, not only as

a method for extracting additional information, but also for probing pre-movement and movement cortical circuits. Results suggest that further investigation into signatures of pre-movement activity may yield early movement prediction and improved decoding.

4.5.1 Limitations of the Method

Clinical ECoG currently offers coverage dictated by clinical need, and electrodes spaced millimeters to centimeters apart. It is likely that for a practical ECoG-based BMI, more localized and spatially dense coverage will be most practically feasible and provide the best signals for BMI control [188]. However, because $N^2 - N$ features are extracted with directed connectivity methods, compared to the number extracted with spectral analysis (proportional to N), this may be a more information rich method of signal analysis for ECoG-based BMI.

In this experiment subjects received somatosensory, proprioceptive, and visual feedback as they moved the hand and observed their own movements. In the operation of a prosthesis, somatosensory and proprioceptive feedback would be absent, and visual feedback may be different from what the subject expects. Directed connectivity mapping provides a unique tool to model the interactions between proprioceptive, somatosensory, visual, and motor areas. The models may then be adapted to account for the absence of normal activity in these areas.

4.5.2 Future Directions

In order to verify the utility of connectivity features for BMI, a connectivity-based decoder should be implemented in a real-time decoding paradigm in which subjects control a prosthetic limb using overt or covert (imagined) movement. Connectivity features could be used in conjunction with power spectral features to optimize decoding accuracy. This paradigm would also be an ideal method to test the early prediction of movement with connectivity features. Connectivity features could be used, as in this chapter, directly as features for a kinematic decoder, together with power spectral features. Alternatively, connectivity features could be used to control a gating classifier, which would initiate kinematic decoding only when relevant cortical flows, such as flows from parietal or premotor areas to primary motor ares, were detected.

Additionally, connectivity decoding should be tested with more complex motor tasks that require bimanual coordination or explicitly integrate sensory information. Bimanual tasks may lead to neural propagation through supplementary motor area or both hemispheres [69, 75], and sensory processing may lead to neural propagation through somatosensory, visual, or auditory areas, depending on the sensory stimuli used during the task.

Chapter 5

Top-Down Neural Propagation Regulates Neural Activity during Behavioral Priming

5.1 Abstract

We have demonstrated that effective connectivity features, generated from models of neural propagation, contain information about movement. Moreover, this information can be used to inform motor decoding from neural signals. While mapping the propagation of neural activity during speech could have similar applications to speech prosthetics, such connectivity models would also be of significant use in testing models of the cortical activity underlying speech production. Here we provide one example

of the utility of effective connectivity, computed from neurophysiological signals, for testing and refining models of cortical activity. Repeated exposure to a perceptual stimulus is known to result in decreased neuronal activation (repetition suppression) and more rapid behavioral responses (behavioral priming), but the cortical mechanisms underlying these observations remain unresolved. To clarify these mechanisms at the level of neural populations, we used subdural electrocorticography in six subjects performing a picture naming task and studied the effects of stimulus repetition on activation at individual sites and on effective connectivity between sites with repetition effects. We verified behavioral priming in all subjects, with a mean reduction of 149 ms in verbal latencies for repeated vs. novel stimuli. We observed repetition suppression most consistently at sites in ventral occipital-temporal cortex (VOTC) and inferior prefrontal cortex. In addition, we observed repetition enhancement (increased neural responses) at sites in frontal, parietal, and temporal regions. At early latencies (90-270 ms) repeated stimuli were associated with an increase in top-down propagation of neural activity (relative to novel stimuli) from perisylvian frontal, parietal, and temporal cortices into VOTC. Subsequently (350-620 ms), bottom-up propagation from VOTC sites with repetition suppression was decreased (repeated vs. novel). Repeated stimuli were also associated with an increase in top-down propagation from sites with repetition enhancement to sites in lateral frontal-temporal cortex with repetition suppression, and a decrease in bottom-up flows in the reverse direction. These results suggest that during repeated stimulus exposure, early top-down network con-

nectivity is strengthened, resulting in less activation (repetition suppression) and less bottom-up network propagation. Connectivity mapping therefore supports a role for top-down regulation of neural activity in repetition suppression and behavioral priming, consistent with predictive coding in large-scale cortical network dynamics.

5.2 Introduction

Repetition suppression, a decrease in cortical activation upon repeated stimulus exposure, has been widely observed under a variety of experimental conditions [205–207] and has been extensively exploited as an experimental tool in fMRI studies [208]. Repeated stimulus exposure is also associated with faster behavioral responses, i.e. behavioral priming, believed to result from more efficient large-scale network dynamics [209–211]. However, the neural mechanisms by which faster responses occur in spite of less neural activity remain a mystery [212]. These mechanisms have great practical significance for functional neuroimaging research, but are also of fundamental importance for understanding cortical mechanisms of learning and implicit memory [213].

Several models of the neurophysiological mechanisms relating repetition suppression to behavioral priming have been proposed; for a review, see [210]. These models can be distinguished in large part by their predictions for the temporal dynamics of task-related neural population activity. However, the low temporal resolution of the

BOLD response does not allow for explicit testing of these predictions. The electrocorticogram (ECoG), which records local field potentials from the surface of the brain with excellent temporal resolution, is an ideal modality for testing key predictions of these models. Compared to EEG, ECoG has far higher spatial resolution and superior signal quality, especially for high gamma (HG) responses that reflect overall firing rates in neural populations [29, 30]. Because models of repetition suppression also make predictions about relative changes in top-down and bottom-up propagation of neural activity, we used a recently developed technique, based on Granger causality, to measure the timing, magnitude and directionality of task-related changes in neural propagation across activated cortical networks [144, 149].

5.3 Methods

5.3.1 Subjects

Six human subjects gave informed consent to participate in experimental testing while electrocorticogram (ECoG) signals were recorded under a Johns Hopkins University School of Medicine Institutional Review Board approved protocol. Subdural implantation of ECoG electrodes was done solely according to clinical needs. Localization of these electrodes was performed using the BioImage Suite [214] with pre-implant MRI and post-implant CT. For details on the MNI electrode registration, see [215].

5.3.2 Experimental Paradigm

E-Prime (Psychology Software Tools, Sharpsburg, PA, USA) was used to present stimuli, which consisted of color images of objects on a white background displayed on a computer monitor 1 meter from the subject. Each stimulus was displayed for 1 second and then replaced by a fixation cross. The inter-trial interval was jittered randomly in four 250-ms increments around 4 seconds. Two hundred and fifty images were displayed in pseudo-randomized order, including 50 stimuli that were repeated identically, either consecutively (no intervening stimulus) or with one different stimulus intervening between them. The remaining 150 trials were not analyzed for this study. The object names were matched for word frequency. Pairs of novel/repeated trials with artifacts in the ECoG signals and trials in which the subject did not promptly and correctly name the picture were excluded from analysis, leaving 26-45 trials in our subjects.

5.3.3 Signal Acquisition and Preprocessing

ECoG signals were recorded subdurally with 2.3 mm diameter platinum-iridium electrodes (Ad-Tech Medical Instrument Corporation, Racine, WI, USA) spaced 10 mm apart center-to-center. A Stellate (Stellate Systems Inc., Montreal, Canada), Nihon Kohden (Nihon Kohden Corporation, Tokyo, Japan), or NeuroPort (Blackrock Microsystems, Salt Lake City, UT, USA) amplifier was used to record neural data,

which was referenced to an inactive intracranial electrode. Signals were digitized at 1000 Hz.

ECoG channels with artifacts or excessive noise were manually excluded from analysis. The remaining ECoG channels were re-referenced using a common average reference (CAR) and digitally band-pass filtered using a 490 order FIR filter in a HG frequency band (70-118 Hz).

5.3.4 Identification of Event-Related Activation and Repetition Effects

Spectral power was extracted from the ECoG signals in the 16 to 200 Hz range using 128 ms long overlapping windows of the band-pass filtered data with a 16 ms shifting overlap using a multi-taper algorithm from the Chronux toolbox [216]. Signal power was extracted from each window using 5 orthogonal tapers with a time-bandwidth product of 3. The power in each window after cue onset were normalized to the baseline power in the corresponding channel and frequency bin from the 1 second prior to cue onset from all trials for each subject. An estimate of the high gamma (HG) power at each time point in each trial was obtained by averaging the power in each bin between 70 and 120 Hz.

Event-related activation was tested with a nonparametric sign test for each subject at every channel and time point, for both novel and repeated trials, with cue-aligned

data and response-aligned data. A channel exhibited event-related activation if the normalized power was significantly greater than one, representing an increase over baseline (p <0.05, one-sided test with FDR correction [217]).

Event-related repetition effects were tested with a paired sign test for each subject at every channel and time point between windows from novel and repeated trials. The effect of priming was marked as significant if activation of either novel or repeated trials in windows with a fixed relationship to the cue or response was both: 1) significantly greater than one, representing an increase over baseline (p <0.05, one-sided test with FDR correction), and 2) significantly greater than that in either repeated or novel trials, respectively (p <0.05, two-sided test with FDR correction).

5.3.5 Event-Related Causality and Repetition Effects

Event-related causality (ERC, implemented in custom analysis interface (ANIN) software [218]) finds statistically significant, event-related, effective connectivity between cortical areas using multivariate autoregressive models of ECoG activity in a selection of recorded signals. We chose to use this method rather than TV-DBN due to the thorough statistical testing that has been developed for it. The method is discussed in sections 2.2 and 2.3.1, and in [144]. Briefly, between 15 and 21 electrodes were selected for inclusion in the ERC analysis to ensure there was sufficient data to fit

model parameters. For most subjects, all electrodes exhibiting repetition effects were included (details on subject B, the exception, below). Then in order of the magnitude of task-related activation, up to a total of 20 electrodes were selected for inclusion. Electrodes were then excluded if more than three electrodes were adjacent. Finally, if stimulation mapping identified sites for naming in VOTC (ventral occipital-temporal cortex, responsible for object identification), these sites were included. Because subject B had 25 electrodes exhibiting repetition effects, we limited the number of sites for this subject to 19 (of which 15 exhibited repetition effects) to ensure the MVAR model for this subject was comparable to that of other subjects.

The selected ECoG signals were CAR referenced to subtract non-specific activity such as volume conduction and digitally band-pass filtered backward and forward to avoid phase shifts in the 70-120 Hz frequency band. A multivariate autoregressive (MVAR) model was fitted to the ECoG signals in the selected electrodes:

$$x(t) = -\sum_{j=1}^{p} A_j x(t-j) + e(t) \tag{5.1}$$

Here $x(t)$ represents a vector of ECoG signals of zero mean and variance equal to 1 from the selected channels at time t and consecutive time shifts $j = 1, 2, ..., p$, and $e(t)$ is zero mean uncorrelated residual noise. The model order p was determined using the Akaike Information Criterion (AIC [219]). The coefficients in each A_j were calculated by solving the Yule-Walker equations [220, 221]. To follow the temporal course of brief changes in signal propagation between different brain regions, an algorithm introduced by Ding et al. [143], using the property that multiple repetitions of the

same task can be treated as multiple realizations of a stochastic process with locally stationary segments, was applied for MVAR coefficient estimation. We used data from 100 trials for each subject (50 each for the novel and repeated conditions), excluding trials with artifacts or trials that the subject did not perform correctly.

In the frequency domain, the MVAR model is given by:

$$X(f) = H(f)E(f) \tag{5.2}$$

$$H(f) = \left(\sum_{j=0}^{p} A_j e^{-i2\pi j f \Delta t} \right)^{-1} \tag{5.3}$$

Here f is frequency, Δt is the sampling interval, $X(f)$ is the transformed ECoG signals, and $E(f)$ is the transformed residual noise. To map only direct connections, we multiplied the elements of the transfer matrix H with elements of the partial coherence matrix:

$$\chi_{kl}(f) = \frac{c_{kl}(f)}{\sqrt{c_{kk}(f)c_{ll}(f)}} \tag{5.4}$$

where c is an element of the inverse of the spectral matrix S, found with:

$$S(f) = H(f)VH^*(f) \tag{5.5}$$

The asterisk indicates transposition and complex conjugation, and V is the residual noise covariance matrix, which can be estimated by summing the products of the estimated MVAR coefficients and the estimate of the covariance matrix.

The short-time direct directed function (SdDTF) is given by:

$$\zeta_{kl}(f) = \frac{|h_{kl}(f)|\,|\chi_{kl}(f)|}{\sqrt{\sum_f \sum_{kl} |h_{kl}(f)|^2 \,|\chi_{kl}(f)|^2}} \tag{5.6}$$

This equation describes the SdDTF from the kth channel to the lth channel, where $h_{kl}(f)$ is an element of the transfer function H and $\chi_{kl}(f)$ is partial coherence.

We calculated the SdDTF with a 140 ms overlapping window to investigate the dynamics of priming processes. Consecutive windows had a 96% overlap to smooth the connectivity estimates. ERC values were then obtained using statistical testing (penalized thin-plate spline [162]) to compare the estimates of connectivity during post-stimulus intervals to baseline connectivity estimates. The one second preceding the stimulus presentation in each trial was used as a baseline. A 95% joint confidence interval was constructed for the difference between the estimates of connectivity during trials and the baseline estimate of connectivity. Only positive values of ERC were considered for this analysis because decreases in connectivity, as compared to baseline, are less likely to be related to task performance.

The effect of priming on connectivity strength was tested with a one-sided sign test for each subject at every channel-channel pair and time-frequency point in anatomical regions of interest between sliding 50% overlapping cue-aligned windows from novel and repeated trials. Window lengths were varied from the length of the SdDTF sliding window (140 ms) to twice this length (280 ms) in 40 ms increments, to decrease the effect of multiple statistical tests. The early (0-310 ms following cue, or half the fastest response time) effect of priming was marked as significant if average connectivity in a region of interest for repeated trials was significantly greater than connectivity in the region of interest for novel trials (p <0.05, one-sided t-test with Bonferroni

correction). The late (310-620 ms following cue, or half the fastest average response time to the fastest average response time) effect of priming was marked as significant if average connectivity in a region of interest for repeated trials was significantly less than connectivity in the region of interest for unpaired trials (p <0.05, one-sided t-test with Bonferroni correction). The windows showing significant change were then combined into a single window, which was again tested for significance.

5.4 Results

5.4.1 Behavioral Priming

For all subjects, we observed a statistically significant decrease in response time for repeated trials (average decrease in median response time of 0.15 s, p <0.05, one-sided paired Wilcoxon signed rank test). Median response time and median absolute deviation for each subject for successful novel and repeated trials are shown in Table 5.1.

5.4.2 Repetition Suppression and Repetition Enhancement

At least three recording sites in each subject (maximum of 15) demonstrated statistically significant repetition suppression (Fig. 5.1a left), i.e. less activation (HG

Subject	Novel Median RT ± MAD RT (s)	Repeated Median RT ± MAD RT (s)
A	1.09 ± 0.26	1.01 ± 0.17
B	0.89 ± 0.10	0.72 ± 0.05
C	1.17 ± 0.27	0.94 ± 0.24
D	0.90 ± 0.13	0.67 ± 0.10
E	0.87 ± 0.10	0.81 ± 0.08
F	0.69 ± 0.07	0.60 ± 0.10

Table 5.1: Reaction Time (RT) by Subject

augmentation) for repeated vs. novel stimuli (p <0.05, sign test with FDR correction). At least two sites for each subject (maximum of 7) also demonstrated repetition enhancement (Fig. 5.1a center), i.e. greater activation with repeated stimuli. On average, activation was greater at sites with repetition suppression than at sites with repetition enhancement (compare left and center plots in Fig. 5.1a). Studies in the fMRI literature report repetition suppression much more commonly than repetition enhancement [222]. Our findings raise the possibility that this is due to the occurrence of repetition enhancement at fewer sites and at sites with less robust activation. A small number of cortical sites (8 in three subjects) had no difference in the magnitude of activation for repeated vs. novel stimuli, but did demonstrate a temporal shift (Fig. 5.1a) in the peak of activation relative to stimulus onset. However, this shift was no longer apparent when the cortical signals were aligned to response onset (Fig. 5.2),

indicating that activation at these sites was linked to response processing and that the temporal shift was due to shorter latencies to respond to repeated stimuli.

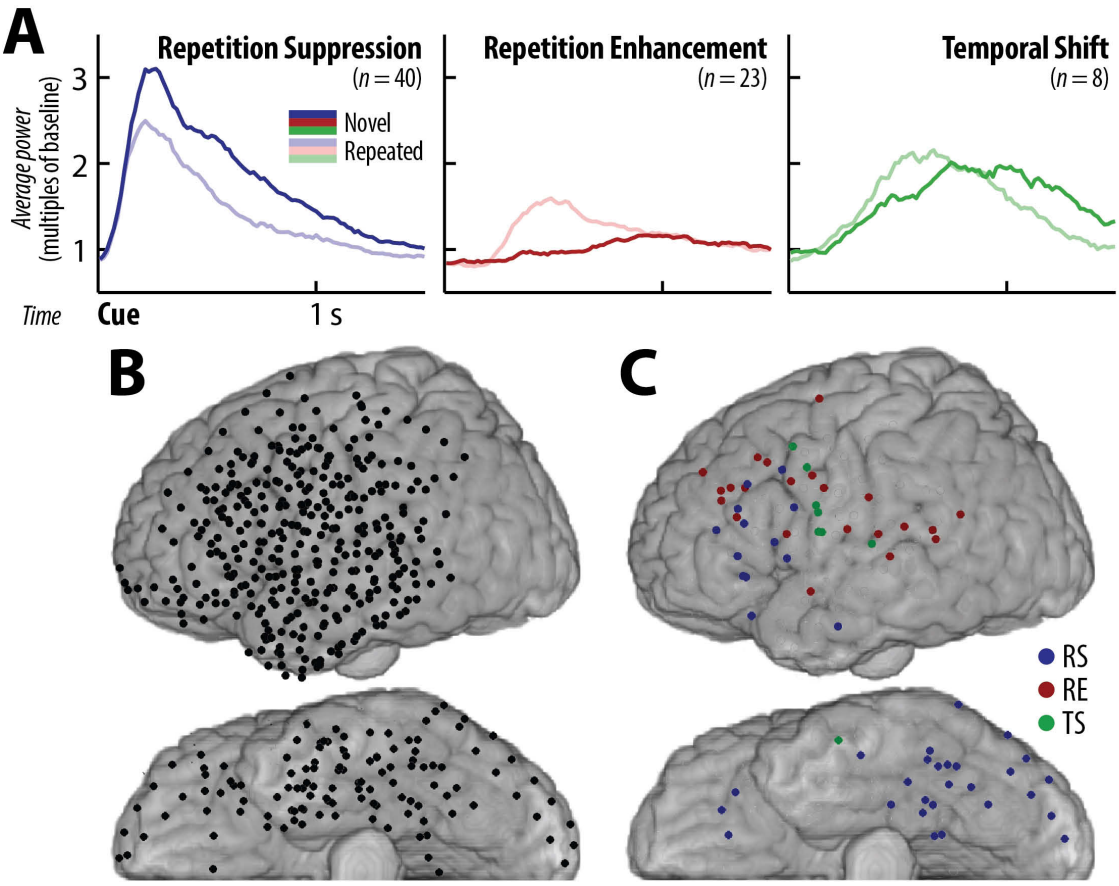

Figure 5.1: (a) Mean power in the 70-120 Hz band, aligned to stimulus onset, relative to baseline power, for novel trials (darkened lines) and repeated trials (light lines) across all sites for all subjects displaying statistically significant (left) repetition suppression, (middle) repetition enhancement, or (right) a temporal shift in peak activation. (b) All sites recorded and analyzed in 6 subjects, projected onto an MNI brain atlas. (c) Sites for all subjects with repetition suppression (blue, RS), repetition enhancement (red, RE), or a temporal shift in peak activation (green, TS).

The anatomical distribution of repetition effects was sampled with a total of 444 sites recorded across all 6 subjects (Fig. 5.1b). We observed repetition suppression at 40 of these sites (Fig. 5.1c, blue sites). The majority of these sites were in VOTC

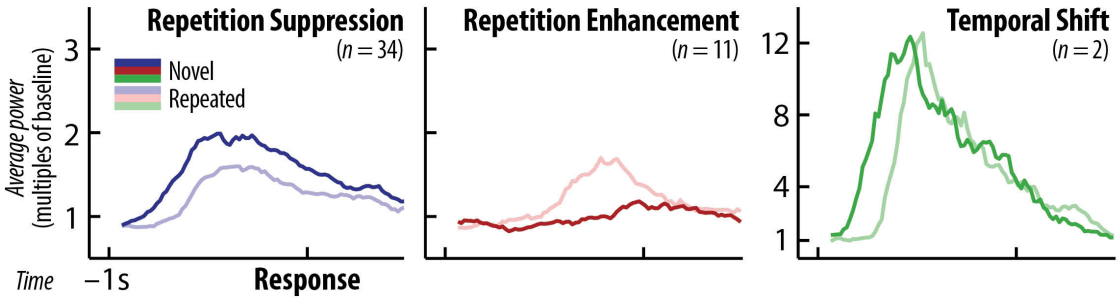

Figure 5.2: Mean power in the 70-120 Hz band, aligned to response time and scaled to mean baseline power. Compared with stimulus-aligned responses (Fig. 5.1), repetition suppression was still observed in nearly as many sites as it was with stimulus-aligned data, and repetition enhancement was observed at approximately half as many sites. A temporal shift, observed at 8 sites in stimulus-aligned responses (Fig. 5.1a), however, was seen at only two sites with neural responses aligned to behavioral responses. The shape of these latter responses was nearly identical for novel vs. repeated stimuli, but the onset of neural responses preceding speech onset was later for repeated stimuli, suggesting less activation in preparation for articulation.

(observed in all subjects) and in inferior prefrontal cortex (5 subjects). In two subjects, we also observed repetition suppression at a site in lateral temporal cortex. Repetition enhancement was observed in 23 sites (Fig. 5.1, red) in frontal, parietal, and temporal cortex. Electrode locations with repetition suppression, enhancement, and temporal shift are shown in Fig. 5.1c, projected onto an MNI brain atlas. Examples of repetition suppression, enhancement, and temporal shift at individual sites are shown in Fig. 5.3.

The timing of cortical activation and repetition effects depended on anatomy. The average peak in activation in VOTC sites with repetition suppression occurred 217 ms after stimulus onset in both novel and repeated trials (Fig. 5.4). This was consistent with previous reports of the timing of activation in this region during visual object

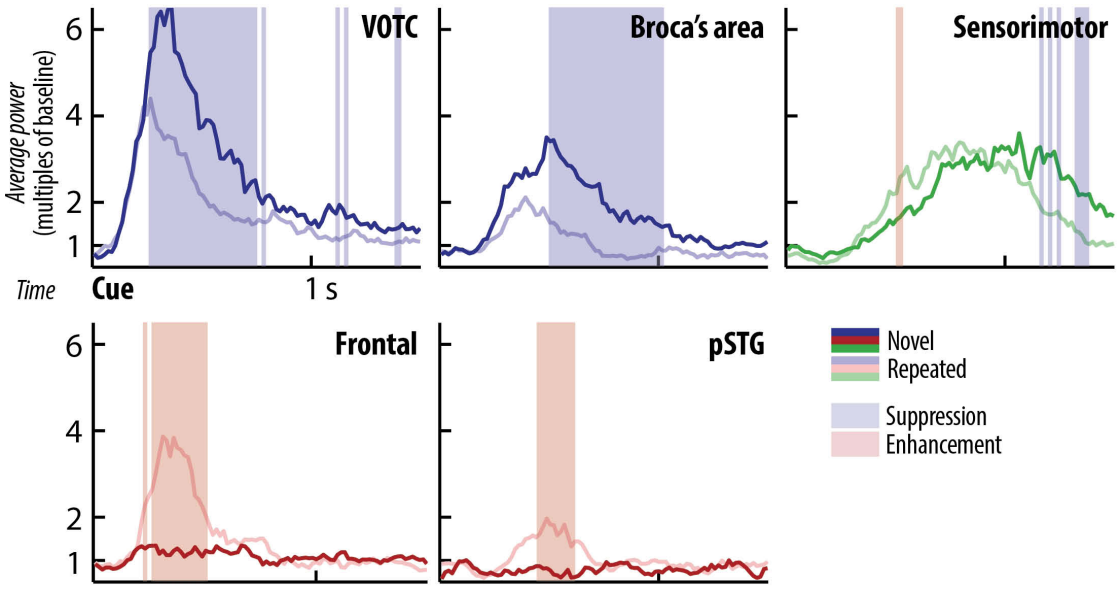

Figure 5.3: Examples of repetition suppression (blue), repetition enhancement (red), and a temporal shift in peak activation (green), aligned to stimulus onset, are shown for sites in the indicated cortical regions. Median power for each site was normalized to maximum power. Bars indicate windows in which power in novel (darkened lines) or repeated (light lines) trials is statistically significantly larger (p <0.05, sign test with FDR correction).

perception [223]. When we observed repetition suppression at sites other than VOTC, the average peak in activation occurred later for novel trials than for repeated trials (521 ms after stimulus onset in novel trials, 377 ms in repeated trials, Fig. 5.4). The average peak in activation at sites with repetition enhancement (489 ms after stimulus onset in repeated trials, Fig. 5.5) occurred after the average peak in activation at VOTC sites with repetition suppression, but before the average peak in activation at sites outside VOTC with repetition suppression.

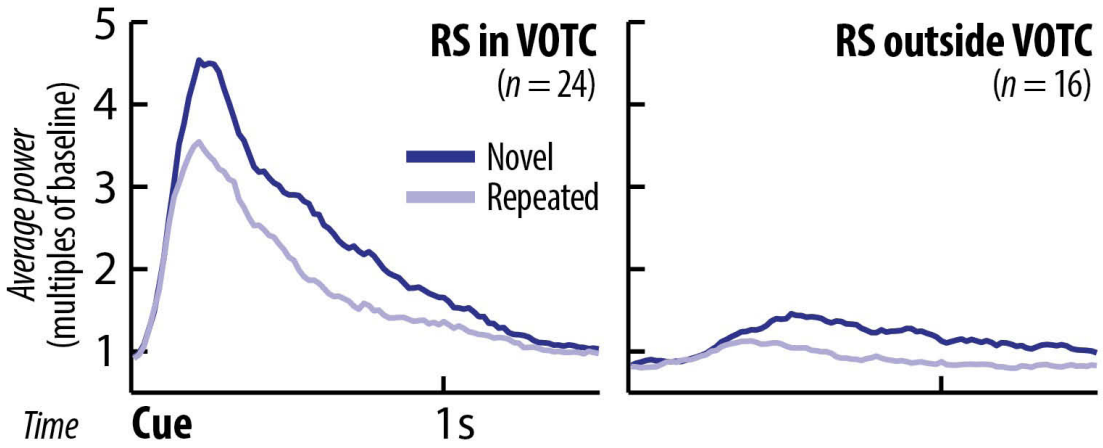

Figure 5.4: Mean power in the 70-120 Hz band, aligned to the time of stimulus presentation and scaled to mean baseline power. Average task-related activation and repetition suppression are larger and peak earlier in VOTC sites than in sites outside of VOTC with repetition suppression.

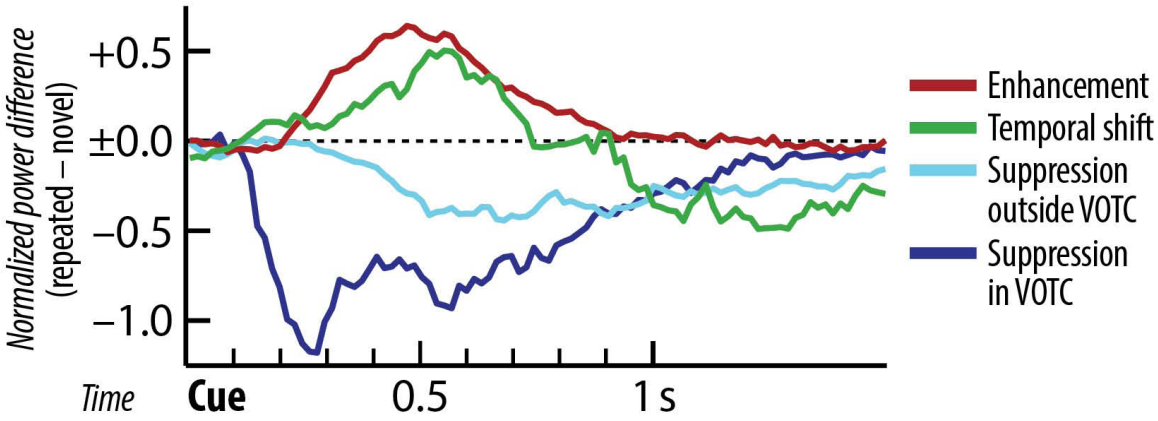

Figure 5.5: Mean difference in HG power for novel vs. repeated trials in sites with repetition suppression in VOTC (blue), repetition suppression outside of VOTC (cyan), repetition enhancement (red), and a temporal shift in activation (green).

5.4.3 Repetition-related Changes in Effective Connectivity

In five out of six subjects, sites in VOTC received stronger neural propagation (ERC inflows) from sources in frontal, parietal, and temporal lobe sites with repeated vs. novel stimuli. We observed this effect of stimulus repetition 90-270 ms after stimulus onset (p <0.05, one-sided t-test with Bonferroni correction). The sites used for ERC analyses in all subjects, projected onto an MNI brain atlas, are shown in Fig. 5.7a (left). The mean magnitude of propagation (ERC inflows) into all VOTC sites are compared in Fig. 5.7a (right) for novel vs. repeated stimuli. An example of increased top-down propagation is shown for one subject in Fig. 5.6.

In five out of six subjects we observed a repetition-related decrease in propagation from VOTC sites with repetition suppression (ERC outflows) to sites outside of

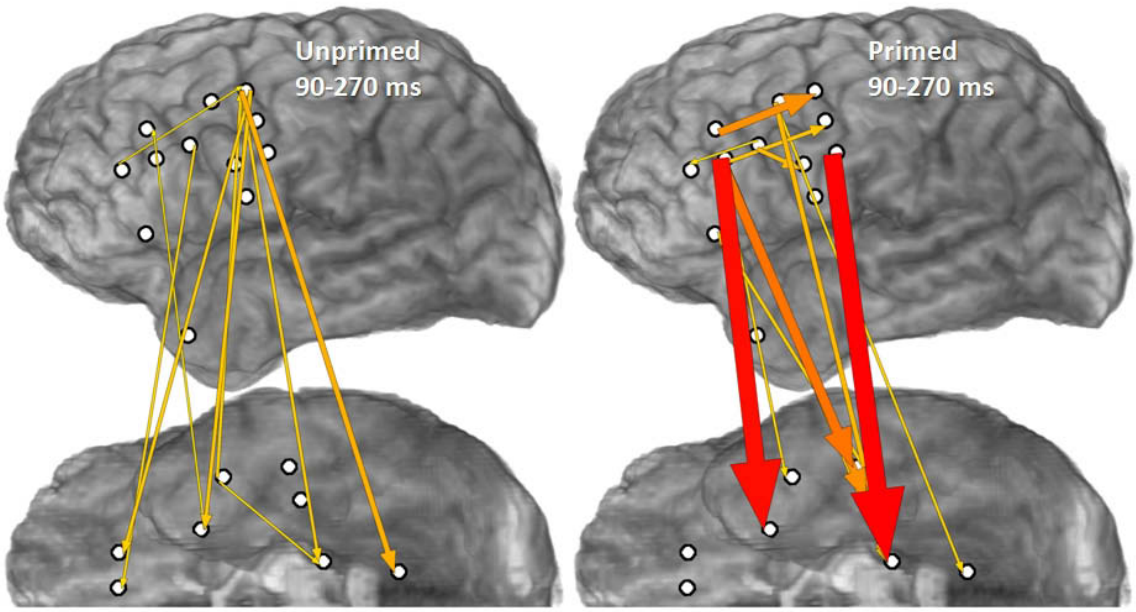

Figure 5.6: Neural propagation during novel (left) vs. repeated (right) task conditions in one representative subject (subject D) 90-270 ms after stimulus onset. Arrow width and color both correspond to the strength of estimated ERC flows. Only sites used for estimating ERC flows are shown. Top-down propagation into VOTC is stronger during repeated than during novel task conditions.

VOTC (p <0.05, one-sided t-test with Bonferroni correction). This effect of stimulus repetition occurred 350-620 ms after stimulus onset. The locations of VOTC sites with repetition suppression, and with weaker bottom-up propagation, during repeated trials are shown in Fig. 5.7b (left). The mean magnitude of propagation from VOTC sites with repetition suppression (ERC outflows) are compared in Fig. 5.7b (right) for novel vs. repeated stimuli. An example of the overall decrease in bottom-up propagation in one subject is shown in 5.8.

In Subject C, no sites outside of VOTC exhibited repetition suppression. In the remaining five subjects, we observed a repetition-related increase in propagation into prefrontal sites with repetition suppression from sites with repetition enhancement (excluding all sites in pre- and post-central gyri) (Fig. 5.9, top left). This effect was statistically significant in four subjects (p <0.05, one-sided t-test with Bonferroni correction, Fig. 5.9, top right) in a time period between stimulus onset and the earliest average response onset (620 ms). In the time period between 310 and 620 ms following stimulus onset, all subjects had a repetition-related decrease in propagation (ERC flows) from the prefrontal sites with repetition suppression to the sites with repetition enhancement (Fig. 5.9, bottom row, p <0.05, one-sided t-test with Bonferroni correction). In four subjects, these propagations disappeared completely with stimulus repetition.

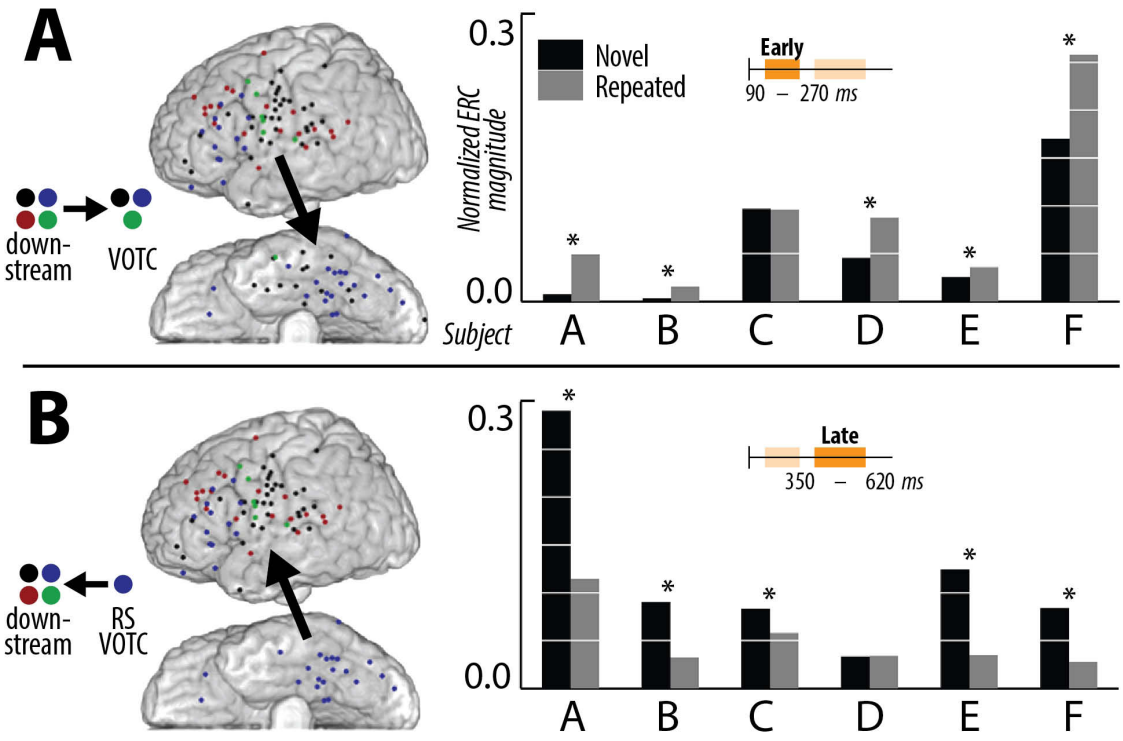

Figure 5.7: (a) Top-down propagation into VOTC sites (ERC inflows) from downstream areas is increased with stimulus repetition in the 90-270 ms window following stimulus onset. The MNI brain atlas shows sites used for ERC estimates in all subjects. Mean ERC inflows to the VOTC sites are shown for novel (black) vs. repeated (gray) conditions in the 90-270 ms window following stimulus onset. For five out of six subjects (marked with stars), top-down ERC inflows into VOTC were increased in the repeated condition compared to the novel condition (p <0.05, one-sided t-test with Bonferroni correction). (b) Bottom-up propagation from VOTC sites with repetition suppression (ERC outflows) to downstream cortical areas increased in the 350-620 ms window following stimulus onset. The MNI brain atlas shows sites considered for this comparison, i.e., VOTC sites with repetition suppression and all downstream non-VOTC sites. Mean ERC outflows from the VOTC sites with repetition suppression are shown for novel vs. repeated conditions in the 350-620 ms window following the stimulus presentation. For five out of six subjects (marked with stars) bottom-up ERC outflows were decreased in the repeated condition compared to the novel condition (p <0.05, one-sided t-test with Bonferroni correction).

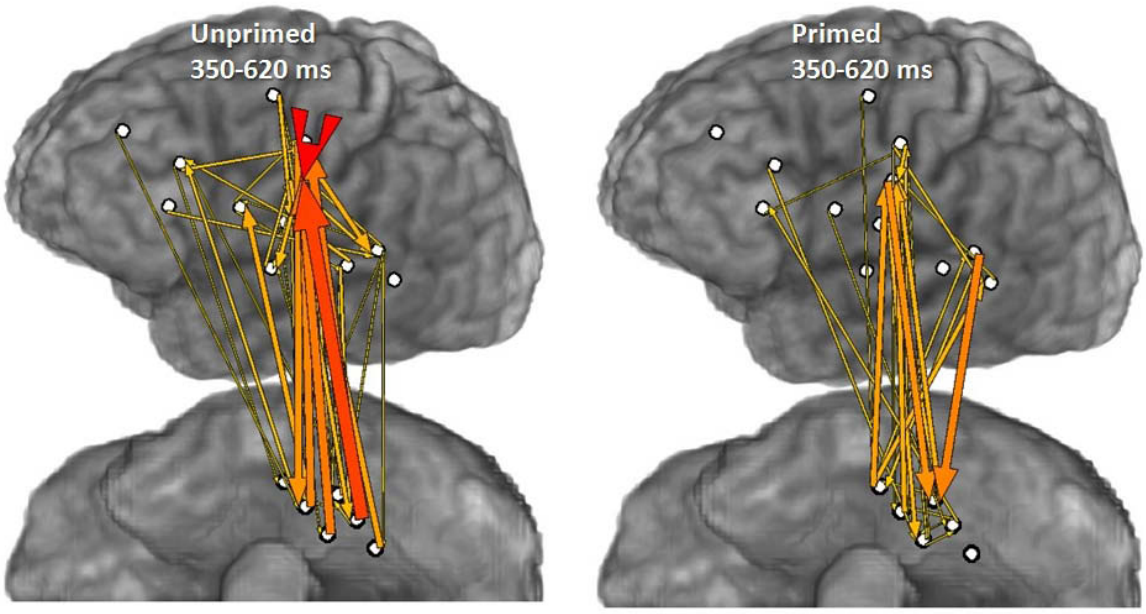

Figure 5.8: Neural propagation during novel (left) vs. repeated (right) task conditions in a representative subject (subject A) 350-620 ms after stimulus onset. Arrow width and color both correspond to the strength of estimated ERC flows. Only sites used for estimating ERC flows are shown. During the repeated task condition, bottom-up connectivity from VOTC is weaker than during the novel task condition.

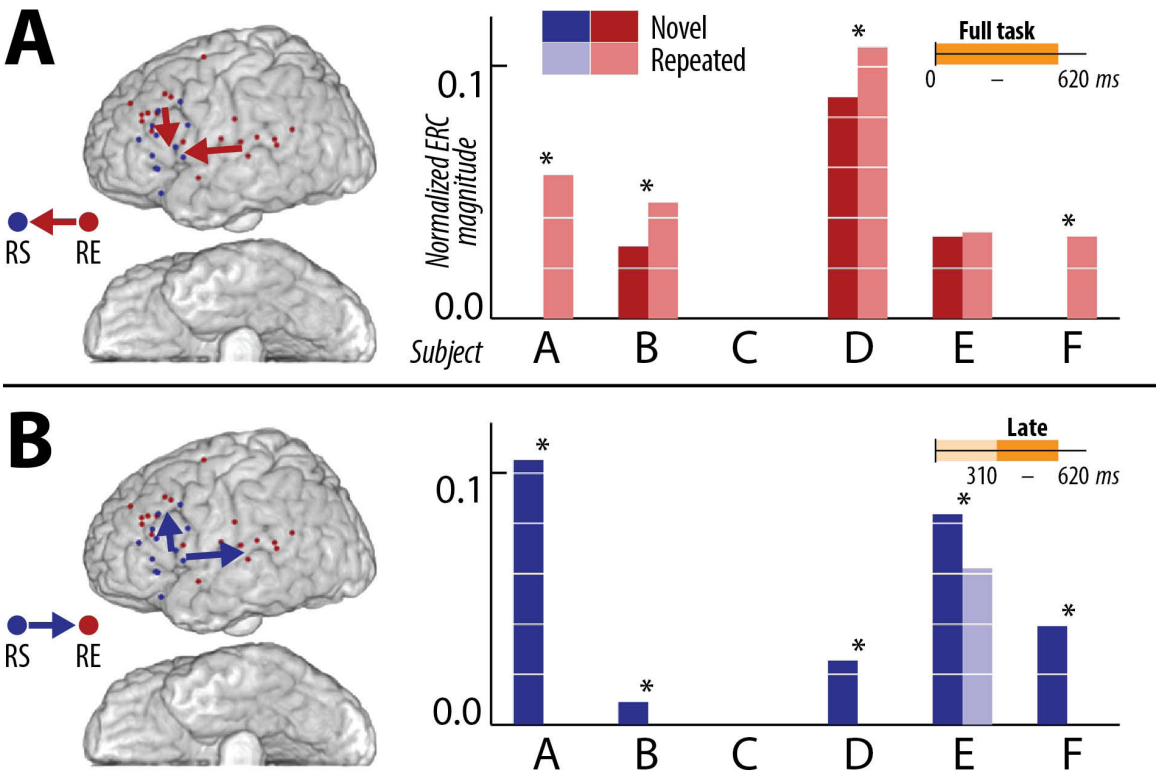

Figure 5.9: (a) Propagation (ERC inflows) into sites with repetition suppression in prefrontal cortex from sites with repetition enhancement increased with stimulus repetition. The MNI brain atlas shows sites used for ERC estimates in all subjects (sites in pre- and post-central gyri excluded). Mean ERC inflows into sites with repetition suppression are shown for novel (red) vs. repeated (pink) conditions in the 620 ms window following stimulus onset. (b) Propagation from prefrontal sites with repetition suppression to sites with repetition enhancement were increased with stimulus repetition in the 310-620 ms window following stimulus onset. This effect was statistically significant in all 5 subjects (significance marked with a star, p <0.05, one-sided t-test with Bonferroni correction).

5.5 Discussion and Conclusions

Behavioral priming is of great interest in cognitive neuroscience as a form of implicit learning that may involve activity-dependent learning in neocortex, rather than hippocampal learning [205]. Additionally, because repetition suppression has been widely used in fMRI paradigms to identify the behavioral selectivity of cortical activation [208], a model of the mechanisms underlying its occurrence and its relationship with behavioral priming are of great relevance to functional neuroimaging research. Current competing models for these mechanisms yield different predictions for the timing of population responses in large-scale cortical networks (Figs. 5.10 and 5.11). For example, a "facilitation model" emphasizes more efficient neural processing and predicts briefer, and at downstream sites, earlier neural activation with stimulus repetition [222]. In a "sharpening model", in contrast, neurons that are not essential to task completion drop out of the activated population with stimulus repetition, leading to an overall reduction in the magnitude of activation, without changing its temporal envelope [224]. To explain how a reduction in the activated population could nevertheless result in faster behavioral responses, a recent "synchrony model" suggests that the remaining pool of neurons fires more synchronously on repeated trials, resulting in a greater (and earlier) impact on downstream neurons [209]. Meanwhile, a "predictive coding model" posits that an interaction between bottom-up perceptual processing and top-down influences on perceptual processing [225] results in faster behavioral responses. This model also implies different temporal profiles of activation

at different stages of processing.

The fMRI BOLD signal indirectly measures firing rates in cortical neuronal populations, but is delayed and integrates these firing rates over long time scales (seconds). Because the ECoG signal has high temporal resolution, and ECoG high gamma responses are highly correlated with population firing rates [29, 30], it is well-suited to test features of the aforementioned models of repetition suppression that cannot be explicitly tested using fMRI. Not only can ECoG be used to measure the precise timing of cortical activation at each recording site, but measures of time-varying effective connectivity derived from the ECoG signal provide information about the propagation of neural activity to and from cortical areas undergoing repetition suppression. Such measures reveal another dimension in the dynamics of large-scale cortical networks that can be leveraged to discriminate among the predictions of different models.

To investigate the effects of stimulus repetition on any cognitive task, one needs a model of the large-scale cortical networks that will be engaged during the task. Picture naming is a task that is widely used to probe cortical activation and interaction in language networks [226]. Additionally, picture naming is particularly susceptible to neurological injury [227, 228] and is most commonly used for mapping language cortex prior to epilepsy surgery [229, 230]. Finally, this task employs a brief stimulus with well-defined timing and requires an overt response, which can be used to verify behavioral priming.

The temporal-spatial dynamics of cortical activation are not specified in most

models of picture naming, due to the lack of methods that can explicitly measure them. However, Indefrey and Levelt [16] have proposed a model of naming and other word production tasks that specify both the anatomy and timing of cortical regions responsible for the different cognitive operations necessary for task performance. This model incorporates information from a meta-analysis of psychophysics experiments on word production [16, 231]. A summary of the proposed propagation and timing of neural activity in this model is shown in Fig. 5.10. In our study, we used VOTC as a region of interest for processing the visual features of the picture stimulus and access to pre-lexical object representations [88]. This process is referred to as conceptual preparation by Indefrey and Levelt [16] and lasts 200 ms or more after visual stimulus onset. Middle temporal gyrus, most active in Indefrey and Levelt's model approximately 200-275 ms after stimulus onset, receives information from VOTC and retrieves a lexical representation of the object. Access to the corresponding phonological code likely occurs in posterior superior temporal gyrus (STG) and to some extent in adjacent portions of supramarginal and angular gyri, collectively known as Wernicke's area. This area is believed to be most active at approximately 275-355 ms. Broca's area, in the dominant posterior inferior frontal gyrus, is most active during syllabification, phonetic encoding, and articulatory planning, typically at 355-600 ms, with a variable duration depending on the number of phonemes and syllables to encode. Finally, articulation is processed by sensorimotor areas on either side of the ventral central sulcus, and has an onset around 600 ms following stimulus onset.

At all stages, feedback occurs from downstream areas, presumably to monitor and regulate temporally overlapped processing in upstream areas.

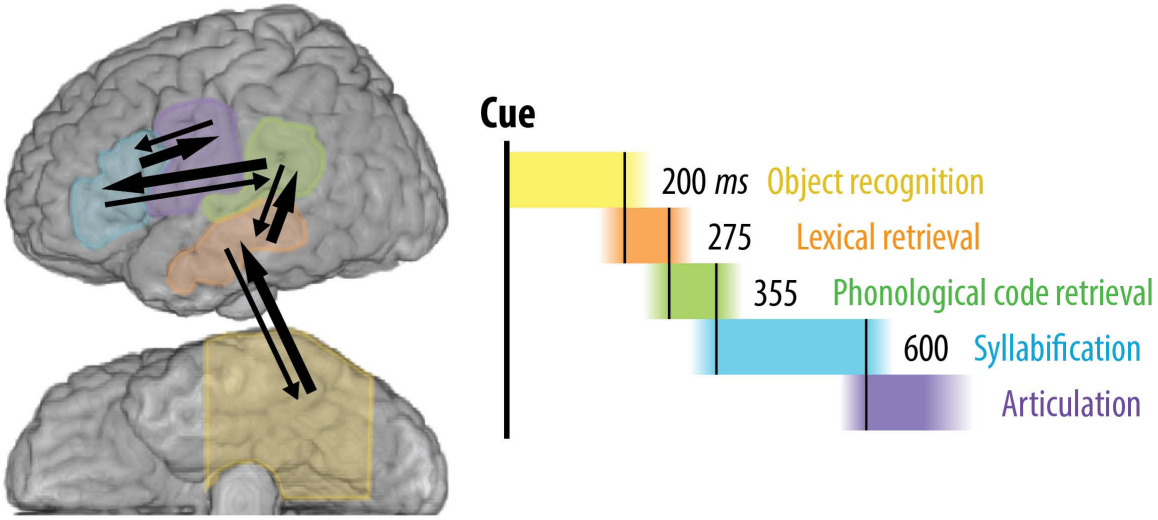

Figure 5.10: Proposed activation and propagation of neural activity during picture naming, from object recognition to articulation.

Our results for the timing of HG activation were approximately consistent with this model. In novel trials, VOTC activity in sites with repetition suppression peaked at 217 ms following stimulus onset, and activity in other sites with repetition suppression (primarily inferior frontal gyrus) peaked 512 ms following stimulus onset. The earliest median onset of articulation across subjects was 690 ms following stimulus onset, but occurred as late as 1170 ms following stimulus onset in one subject. Longer response latencies in some subjects may have been due to medications and other factors in the post-operative period. The general correspondence between these temporal dynamics and those observed in previous studies of picture naming, and word production in general, provided a framework for interpreting the effects of stimulus repetition on

both the timing of cortical activation in broadly defined regions of interest, and the propagation of activation between these regions. Furthermore, this allowed us to test key predictions of competing neurophysiological models of stimulus repetition and behavioral priming at the level of large-scale cortical networks.

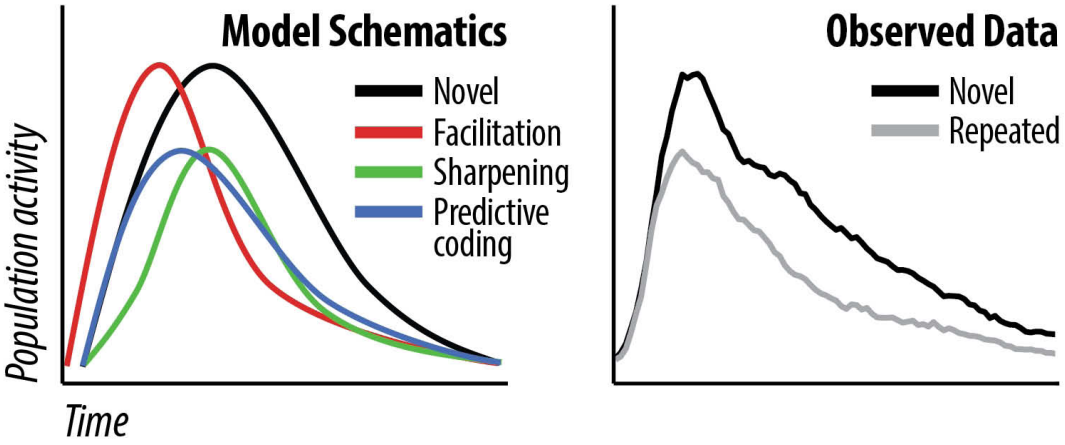

Figure 5.11: (Left) Predictions of population dynamics from models of repetition suppression for late-stage visual processing. In the facilitation model of repetition suppression (red) neural population activity occurs more efficiently, resulting in an overall shift of the population activity curve to the left. In the sharpening model (green) neurons that are less necessary decrease in activity, leading to a decrease in the peak and width of the population activity curve. In the predictive coding model (blue) following an initial flow of information through the visual system, top-down predictions lead to a decrease in error, resulting in an earlier, lower peak in population activity. (Right) Observed HG power augmentation in all sites with statistically significant repetition suppression. The waveform in sites with repetition suppression most closely matches that of the predictive coding model.

5.5.1 Facilitation

The facilitation model suggests that cortical processing of the stimulus and response preparation occur more efficiently in repeated trials. As a result, the temporal

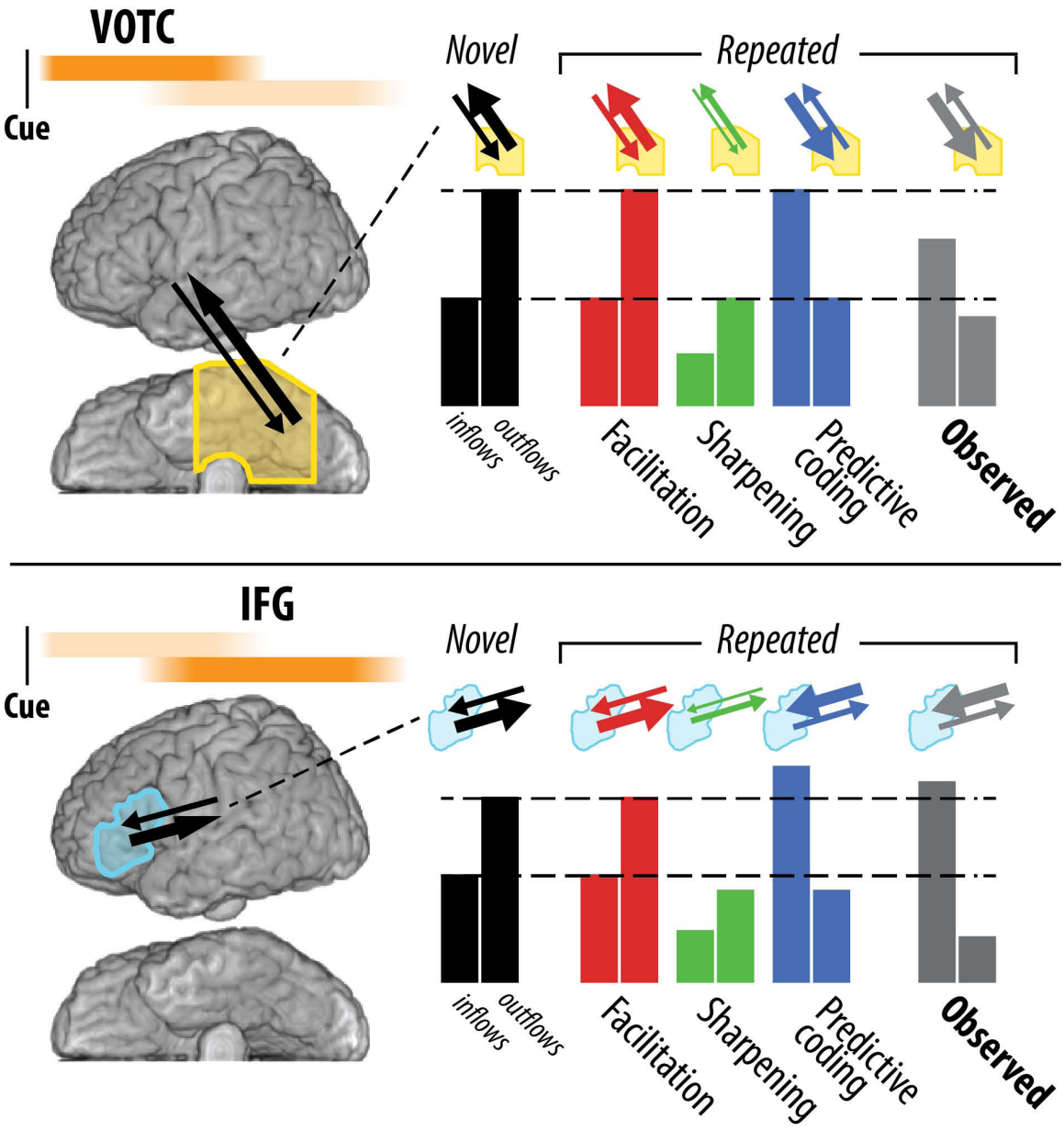

Figure 5.12: Model-based predictions of effective connectivity changes for three models of repetition suppression: facilitation (red), sharpening (green), and predictive coding (blue). In the facilitation model, flows in repeated trials should be briefer, and in downstream sites, occur earlier. In the sharpening model, there is a decrease in the strength of aggregated flows. In the predictive coding model, top-down predictive flows are stronger, leading to weaker late bottom-up flows. (Gray) Summary of observed changes in flows during repetition. Flows to VOTC from downstream cortical areas increased, and then reciprocal flows decreased. Additionally, flows from sites with repetition enhancement to sites with repetition suppression in lateral frontal areas increased, and reciprocal flows decreased.

envelope of population activity in activated sites should be briefer, peaking faster and ending sooner. In downstream sites, this change is expected to result in a shift to the left (earlier) in the peak of activation (Fig. 5.11 left, red). Because the temporal window of integration in fMRI is long, faster activation would result in a decrease in activity measured by fMRI. The high temporal resolution of ECoG HG activation permitted us to directly observe a shift in peak population activity. In our data only 8 sites from three subjects (out of a total of 444 sites across six subjects) displayed a temporal shift in peak activation in repeated trials, and these sites were largely located in sensorimotor areas. When the ECoG signal was aligned to the response onset instead of the stimulus presentation, these effects disappeared, indicating that the shift could be almost completely attributed to earlier response latencies with no change in the duration of processing. Repetition suppression was observed in 40 sites in VOTC (including BA 20, 37), anterior lateral temporal cortex (including BA 21, 22), and inferior frontal gyrus (including BA 44, 45), cortical areas known to be involved in object naming [16,232]. The peak activation in VOTC sites with repetition suppression occurred at the same time in novel and repeated trials, and the peak activation in sites with repetition suppression was lower in repeated compared to novel trials. These findings do not fulfill predictions of the facilitation model.

5.5.2 Sharpening

The sharpening model proposes that neurons that are not critical to the task are less activated in repeated trials than novel trials. This decrease in task-related activation would lead to weaker increases in population firing rates, as measured with ECoG HG power, and a decrease in the height and width of the population activity curve (Fig. 5.11 left, green). Because there would be interactions between fewer neurons on a large scale, we predicted that propagation of population activity between task-related ECoG sites should also decrease at all stages of processing (Fig. 5.12, green). Although we did observe a decrease in activation at many recording sites, we did not observe a global reduction in ERC flows. Instead, these flows increased from downstream cortical areas to VOTC sites and from sites with repetition enhancement to sites in left lateral frontal and temporal cortices with repetition suppression. These complex changes in large-scale network interactions are not present in the sharpening model.

5.5.3 Predictive Coding

According to the predictive coding model, cortical regions mediating behavioral responses receive input from early upstream sensory processing of the stimulus and generate a top-down prediction of subsequent sensory processing (Fig. 5.12, blue). With repeated stimulus exposure, to the degree that top-down predictions match

bottom-up perceptual inputs, additional sensory processing is extinguished, resulting in early completion of perceptual processing with decreased prediction error. At the level of population responses, this model would result in a lower peak and a shorter duration of overall activation (Fig. 5.11 left, blue). It is noteworthy that to date, this model has not been directly applied to picture naming.

The average HG activation we observed was consistent with the predictive coding model. In sites with repetition suppression, the ascending limb of activation was indistinguishable between novel and repeated trials (Fig. 5.11, right), but activation during repeated trials had a smaller peak and faster return to baseline. We observed sites in articulatory and auditory processing areas with repetition enhancement. These sites may have resulted from predictive processing of downstream lexical and phonological representations based on early and incomplete input from upstream processing. We also observed patterns of ERC flows that were consistent with the predictive coding model. In particular, top-down flows into VOTC were larger for repeated than for novel trials, in a window 90-270 ms after stimulus onset. This difference was observed before and during times that repetition suppression was observed in VOTC sites. This enhancement of flow would be consistent with greater input from enhanced predictive processing in downstream regions. Following these larger top-down "predictive" flows, we observed a repetition-related decrease in bottom-up flows from VOTC sites where we also observed repetition suppression (Fig. 5.12, top gray). Similarly, in downstream cortical areas, we observed a repetition-related

increase in flows from sites with repetition enhancement (possibly from enhanced predictions) to sites with repetition suppression (decreased prediction errors), which were primarily located in inferior frontal gyrus. This increase in top-down flows was followed by decreased reciprocal, bottom-up flows from sites with repetition suppression (Fig. 5.12, bottom gray). In both cases (VOTC and inferior frontal gyrus), we observed a repetition-related increase in propagation consistent with improved predictions of the object to be named (VOTC flows) and the phonetic code to be articulated (Wernicke's and Broca's). This increase in predictive propagation was followed by a repetition-related decrease in propagation from sites with repetition suppression, consistent with a reduction in prediction error.

5.5.4 Synchronization

The enhanced synchronization model proposed by Gotts, *et al.* [210], explicitly attempts to resolve the apparent inconsistency between reduced neural firing rates and faster behavioral responses. This model predicts that reductions in firing rates are accompanied by realignment of exact spike timing that enhances the synchrony of post-synaptic potentials in downstream neural populations, increasing the likelihood of action potential generation, ultimately resulting in faster propagation through the network to neural populations controlling behavioral effectors, for example articulation during naming. One potential experimental prediction of this model is that increased synchronization of post-synaptic potentials elicits LFPs that are phase-

locked with the stimulus or that are phase-locked across cortical sites activated by the task. Results supporting this prediction have to date consisted of enhanced event-related potentials at relatively low frequencies [209]. Although the methods we used in this study did not explicitly test this model, we do not believe that our results are necessarily inconsistent with it. Subthreshold oscillations in membrane potential can influence exact spike timing, thereby enhancing synchronization of firing in a neural population. Indeed, this mechanism may be responsible for the modulation of HG activity by low-frequency (theta) oscillations [132]. Furthermore, increased phase-amplitude modulation of HG activity could potentially enhance neural propagation, including propagation in bottom-up and top-down directions. Additional studies will be needed to determine the extent to which changes in neural propagation are dependent on phase-amplitude coupling between low and high frequency neural activity.

5.5.5 Limitations and Extensions

All study subjects were epilepsy patients undergoing ECoG monitoring for clinical purposes. Some task-relevant cortical areas may not have been recorded in some subjects due to clinical considerations. For example, only 5 of 6 subjects exhibited repetition suppression in the frontal lobe; more electrode coverage may have permitted the observation of repetition suppression in the frontal lobe in the sixth subject. Electrode placement may also have contributed to the subtlety of some of the observed repetition suppression or enhancement effects. In some electrodes very few samples

from the repeated spectral power time series met our statistical criteria for repetition effects. Although ERC finds effective connectivity in a Granger causal sense, there may have been flows of information that were not captured by our models.

The complexity of the repetition suppression and priming phenomena we and others have observed suggests that they may arise due to a combination of mechanisms. For example, it has been shown that the prefrontal cortex learns stimulus-response associations, whereas repetition suppression in posterior perceptual regions is independent of such associations [233]. In lateral prefrontal cortex, evidence has been found for changes in both cortical tuning and stimulus-response associations in conjunction with decreased processing demands [234]. Here we observed repetition-related effects on neural activation and propagation that were most consistent with the predictive coding model, though requiring some modification. As a result, we suggest a revised model in which back-propagation of neural activity leads to repetition suppression in two cortical areas (VOTC and inferior frontal gyrus). More specifically, repetition suppression in VOTC results from enhanced neural feedback from downstream cortical areas. Subsequent repetition suppression in inferior frontal gyrus may result from enhanced predictive encoding of phonological and syllable representations (seen as enhanced activation) in posterior STG and frontal areas, but it may also result from decreased bottom-up flows from VOTC. Additional studies with more patients may be needed to verify our findings and test this modified model in greater detail.

Chapter 6

Multi-Scale Decoding of Elements of Speech using Connectivity Features

6.1 Abstract

The neurophysiological representation of speech production is broadly distributed over temporal, parietal, frontal, and peri-Rolandic regions of cortex, but highly organized, dense maps of articulators have been found in speech sensorimotor cortex. We therefore used multi-scale electrocorticography recordings to explore the utility of measures of macro- and micro-scale cortical connectivity for a brain-machine interface to decode speech. We constructed classifiers for articulatory features to compare

classification accuracy when using power spectral features and connectivity features across both scales. We found that connectivity at the macro and micro scale contributed to a statistically significant increase in decoding accuracy, with an average increase from 67% accuracy using power spectral features to 72% accuracy using connectivity features. Cross-scale connectivity was also informative for decoding, improving three-class decoding an average of 12% (23% in one subject) and two-class decoding an average of 4% (12% for vowel height in one subject). The decoding value of connectivity across macro- and micro-scales is a novel finding that points to the interactions of global cortical circuits with local processing. These results suggest that multi-scale neural recordings and cortical connectivity information should be used in creating a high-performance speech BMI.

6.2 Introduction

Brain-machine interfaces (BMI) aim to reduce disability and promote functional recovery in patients suffering from stroke, traumatic brain injury, paralysis, ALS, and other disorders by directly decoding movement [42, 52] or speech [8, 9, 58, 59, 235–237] from neural signals. It is possible to decode information about overt (fully articulated) or covert (imagined) speech from neural signals [237], but in part due to the broad distribution of cortical networks required for speech [16] and the high density of the articulatory map in speech sensorimotor cortex [60], these efforts have achieved

modest accuracy. We propose to integrate information from both distributed cortical networks and dense local processing areas to decode fundamental elements of speech.

The electrocorticographic (ECoG) signal, recorded from electrodes on the surface of the brain, has high resolution on a temporal scale (on the order of milliseconds) and spatial scale (traditionally on the order of centimeters, and more recently on the order of millimeters). The power in low and high frequency bands of the ECoG signal has been shown to contain information that can be used to control a BMI [44], and power in the high gamma frequency band (>70 Hz) has been shown to reflect population firing rates [29, 30, 238]. These features make ECoG a promising modality for high-fidelity, multi-dimensional BMIs.

Vowels have been decoded from the human ECoG in a two-class classification either distinguishing between two overt or covert vowels or between an overt or covert vowel and rest (at least 69% accuracy by end of testing, with 50% chance accuracy) [8]. Broadly distributed activation was observed in this study during the task, but interactions between cortical areas involved in production were not explicitly used for decoding. Another study classified both vowels and consonants during overt and covert speech, with 41% accuracy in a four-class classification [235]. Others have classified a subset of words using the ECoG signal [58] and have distinguished between spoken sentences [236]. Significant progress must be made in decoding accuracy before these building-blocks of speech can be combined to create a clinically relevant tool for the disabled.

The speech network is highly distributed and involves cascades of cortical processing that lead to a flow of information through frontal, temporal, and parietal lobes [16]. Information about higher-level motivation and intent must be propagated to lexical, sensorimotor, and auditory sites to accomplish articulation. Methods of mapping cortical connectivity [55] that estimate this flow of information may provide features that a BMI can use to more accurately decode speech. Time-varying dynamic Bayesian networks [161] are a computationally efficient approach to estimating single-trial, directional, weighted connectivity with high temporal resolution, making this approach ideal for extracting connectivity information for a real-time BMI.

High-density ECoG (approximately 4 mm inter-electrode spacing) has been used to map 18-19 consonants paired with 3 vowels to speech sensorimotor areas [60]. A highly structured sensorimotor map organized according to speech-articulator representations has been found, in part due to the novel application of high-density ECoG to functional mapping. Building upon this finding of a highly specific, dense map of phonetic features, we have made use of high-density microECoG grids (approximately 1 mm inter-electrode spacing) located in sensorimotor, frontal, and temporal cortices, to decode articulatory features (place of articulation, vowel height, and voicing). We hypothesize that integrating this micro-scale information with the large-scale network flows during speech recorded with 1-cm spaced ECoG grids will lead to improved decoding accuracy. This result would indicate that both connectivity information and multi-scale neural data are valuable components of a clinically viable speech BMI.

6.3 Methods

6.3.1 Subjects and Experimental Paradigm

Two human subjects (one female, ages 25 and 32) underwent craniotomies and received ECoG grids (Ad-Tech, Racine, Wisconsin) over the left hemisphere (Fig. 6.1) in preparation for resection surgery for the treatment of epilepsy. Registration of the post-operative CT to pre-operative MRI for reconstruction of electrode placement on the cortical service was done using Bioimage [239]. Between 64 ECoG electrodes and 16 or 48 microECoG electrodes (one or three grommets of 16 microECoG electrodes each) were recorded for each patient. Placement of the electrodes was determined solely based on clinical considerations, and patients gave consent to participate in language tasks. The protocol was approved by the Johns Hopkins University Institutional Review Board.

Stimuli were consonant-vowel pairs (Table 6.1) presented 10-15 times in pseudo-random order using a computer monitor. Subjects were instructed to read each syllable as it appeared on the screen. During the intertrial interval, a fixation cross was displayed. Six consonants and two vowels were included in the stimuli set. The consonants varied by place of articulation, or the location in the vocal tract at which air was obstructed, and voicing, or whether the vocal cords vibrated during consonant production. The vowels varied by height, or the position of the tongue.

All syllables were presented to subject A. Due to reduced time for experimental

participation, only syllables with voiced consonants were presented to subject B.

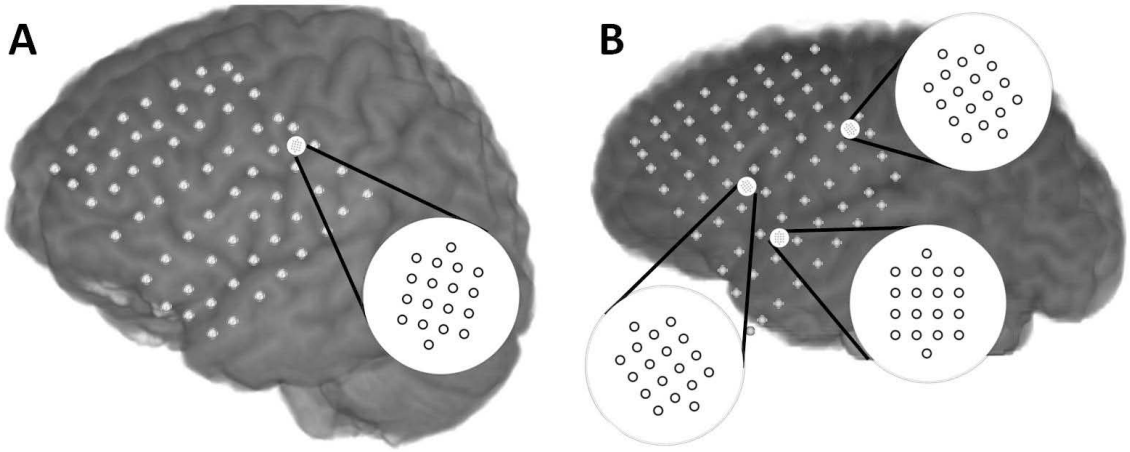

Figure 6.1: Placement of ECoG and microECoG electrodes for both subjects participating in the study. Subject A had coverage of frontal lobe and some coverage of parietal and temporal lobe, with one microECoG grommet in sensorimotor cortex. Subject B had similar ECoG coverage of frontal, parietal, and temporal lobes, with three microECoG grommets in sensorimotor cortex, inferior frontal gyrus, and temporal lobe.

	Labial		Coronal		Gutteral	
	Voiced	**Voiceless**	**Voiced**	**Voiceless**	**Voiced**	**Voiceless**
Low	Bah	Pah	Dah	Tah	Gah	Kah
High	Bee	Pee	Dee	Tee	Ghee	Kee

Table 6.1: Syllable Stimuli

6.3.2 Data Collection and Pre-Processing

The ECoG and microECoG signals were recorded with a NeuroPort amplifier (Blackrock Microsystems, Salt Lake City, Utah) at 10 kHz with an analog anti-

aliasing filter. ECoG signals were referenced to an electrode on the ECoG grid, and microECoG signals were referenced to a reference electrode provided on the microECoG grommet. A photodiode analog input to the amplifier was used to record the onset of each stimulus presentation. A Zoom H2 microphone (Samson Technologies, Hauppauge, New York) was used to record the subjects' speech at 10 kHz through an analog input to the amplifier.

Electrodes with noise or artifacts, identified by visual inspection of unfiltered ECoG and spectrograms, were excluded from analysis. The remaining electrodes were spatially filtered with a common average reference; bandpass filtered at 1-8 Hz, 8-25 Hz, and 70-120 Hz; and downsampled to 500 Hz. Trials in which the subject failed to correctly read the stimulus were excluded from analysis.

6.3.3 Feature Extraction and Selection

Power spectral features were computed using Welch's power spectral density estimate on 256 ms sliding windows, implemented in MATLAB (Mathworks). The power was log transformed and averaged in each frequency band of interest (1-8 Hz, 8-25 Hz, and 70-120 Hz). Next a z-score was computed for each power sample compared to the baseline power in the trial. Finally the power spectral feature was downsampled to five samples per channel and frequency band per trial.

Connectivity features were computing using time-varying dynamic Bayesian networks. For details on the method, see [161, 240]. Briefly, the model uses the concept

of a first-order Markov model:

$$X^T = A^t X^{t-1} + \varepsilon \tag{6.1}$$

where X^t is a vector of filtered ECoG samples across all channels used in the model at time t, A^t is the matrix of directed, weighted connectivity estimates at time t from the ith to the jth channel, and ε is a noise term. To enable estimation of A^t and encourage smoothness of the connectivity in time, a Gaussian RBF kernel was used to integrate data from the past in X^{t-1}. The A^t term was then estimated with:

$$\hat{A}_i^t = \text{argmin}_{A_i^t \in \mathbb{R}^{1\times N}} \frac{1}{T} \sum_{\tau=1}^{t-1} w^t(\tau) x_i^{t^*} - A_i^t X^{\tau-1} + \lambda \left\| A_i^t \right\| \tag{6.2}$$

where N is the number of ECoG channels used in the network model; λ is the ridge regression parameter, for which we used 100 [240]; and the Gaussian RBF kernel used for $w^t(\tau)$ is:

$$w^t(\tau) = \frac{K_h(\tau - t)}{\sum_{\tau=1}^{t-1} K_h(\tau - t)} \tag{6.3}$$

$$K_h(\cdot) = e^{-t^2/h} \tag{6.4}$$

We used 500 for the kernel width, h, to create a smoothing similar to that used in estimating power spectral features. Then the connectivity features were z-scored and downsampled in the same way as the power spectral features.

6.3.4 Classification

Linear discriminant analysis (LDA) as implemented in MATLAB was used to classify syllable type by place of articulation (both subjects), vowel height (both subjects), and voicing (subject A). To directly compare power features with connectivity features, pairs of task-activated electrodes were added to the decoder sequentially until peak decoding accuracy was reached. A single feature in the power-based decoder was the power in each of the electrodes in the pair, and a single feature in the connectivity-based decoder was the reciprocal connections between the two electrodes in the pair. In this way, the total number of features remained the same for both the power- and connectivity-based decoders.

Separate LDA classifiers were built for each of the three frequency bands (1-8 Hz, 8-25 Hz, or 70-120 Hz) and each of the electrode types (ECoG, microECoG, or both). Five-fold cross-validation was used, and the total analysis was repeated 100 times to generate sufficient data for statistical testing.

6.4 Results

6.4.1 Contributions of Connectivity to Classification

The use of connectivity features improved the classification of place of articulation in both subjects, and improved classification of consonant voicing and vowel height in subject A (Table 6.2). The improvement in decoding accuracy with connectivity features was much more prominent for subject A than for subject B. As an example, the classification accuracy for vowel height using power features and connectivity features in different frequency bands is shown in Fig. 6.2. In most frequency bands, connectivity features improved classification accuracy. However, for subject B, connectivity features decreased classification accuracy in the 70-120 Hz (high gamma) band.

Subject	Decoding Accuracy Increase (%): Place of Articulation	Decoding Accuracy Increase (%): Vowel Height	Decoding Accuracy Increase (%): Consonant Voicing
A	9.0 ± 0.3	5.7 ± 0.3	3.6 ± 0.3
B	0.48 ± 0.04	-2 ± 0.4	

Table 6.2: Change in classification accuracy (%) with 95% confidence interval when using connectivity features as opposed to power features. Positive numbers represent an increase in classification accuracy as a result of using connectivity features.

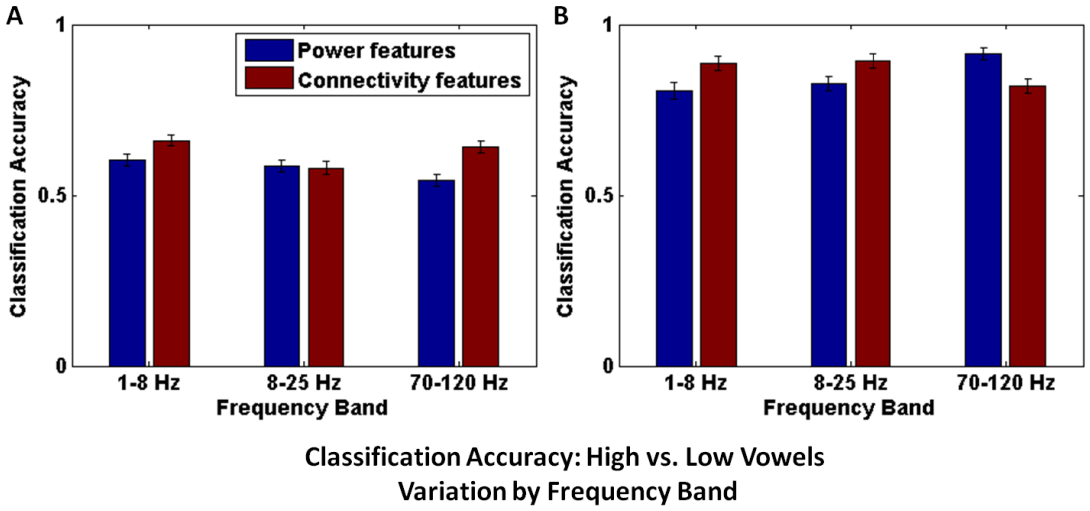

Figure 6.2: Classification accuracy for high vs. low vowels, compared by frequency band. Error bars are 95% confidence intervals. Decoding accuracy was maximized across electrode type. Chance classification accuracy is 0.5. In two frequency bands per subject, connectivity features statistically significantly improved decoding accuracy over power features. In one frequency band for subject B, however, there was a statistically significant decrease in decoding accuracy using connectivity features in the 70-120 Hz band.

6.4.2 Contributions of High-Density Neural Information to Classification

The connectivity information contained in high-density microECoG arrays, and in the connections between ECoG and microECoG arrays, was informative for decoding articulatory features (Table 6.3). For subject A, decoding accuracy was similar for both ECoG and microECoG when classifying place of articulation (chance accuracy 33%) and vowel height (chance accuracy 50%). However, incorporating cross-scale connectivity features (both ECoG and microECoG in the same connectivity network) dramatically improved classification accuracy. Information about consonant voicing (chance accuracy 50%) was almost entirely contained within the microECoG network. For subject B, the microECoG network also contained much more information about vowel height than the ECoG network.

An example of the comparison between power features and connectivity features is shown for decoding high vs. low vowels in Fig. 6.3. In subject A, ECoG and microECoG features individually had relatively little utility for decoding vowel height. However, using cross-scale features improved decoding accuracy, and notably, led to an increase in the value of connectivity features over power features for decoding. In subject B, decoding vowel height is much more effective with microECoG and with cross-scale features than with ECoG.

The five most informative electrode connections in the multi-scale networks for

Subject	Peak Decoding Accuracy (% Correct): Place of Articulation			Peak Decoding Accuracy (% Correct): Vowel Height			Peak Decoding Accuracy (% Correct): Consonant Voicing		
	Macro ECoG	Micro ECoG	Both	Macro ECoG	Micro ECoG	Both	Macro ECoG	Micro ECoG	Both
A	38 ± 2	39 ± 2	62 ± 1	54 ± 2	52 ± 2	66 ± 2	52 ± 2	67 ± 2	69 ± 2
B	71 ± 3		72 ± 2	64 ± 3	89 ± 2	88 ± 2			

Table 6.3: Peak connectivity-based classification accuracy across frequency bands (% correctly classified trials) with 95% confidence interval for all manners of articulation tested.

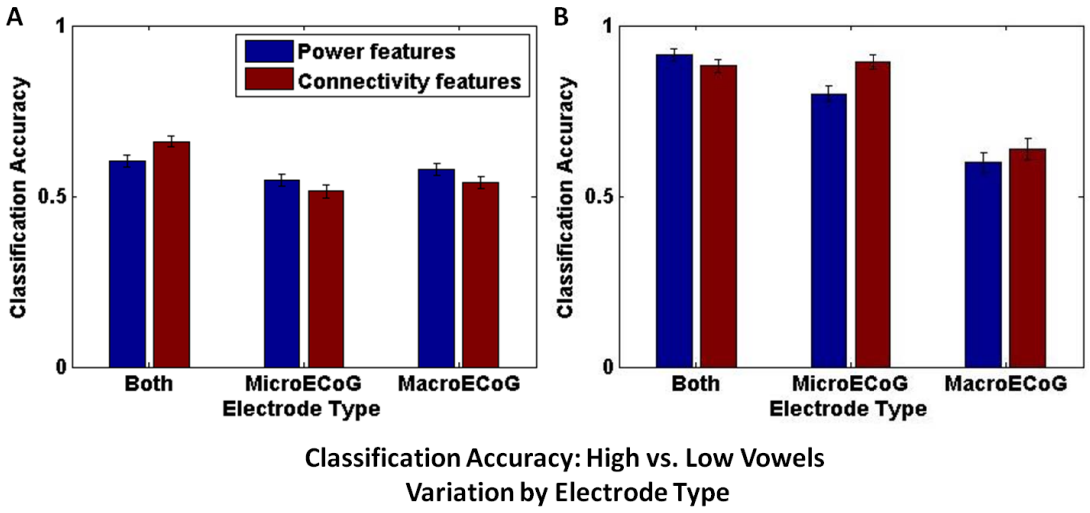

Figure 6.3: Classification accuracy for high vs. low vowels, compared by electrode type. Error bars are 95% confidence intervals. Decoding accuracy was maximized across frequency bands. In subject A, including both ECoG and microECoG connectivity features improved decoding accuracy. Cross-scale connectivity, in particular, was more accurate than power features. In subject B, microECoG connectivity features were notably more valuable than ECoG connectivity features.

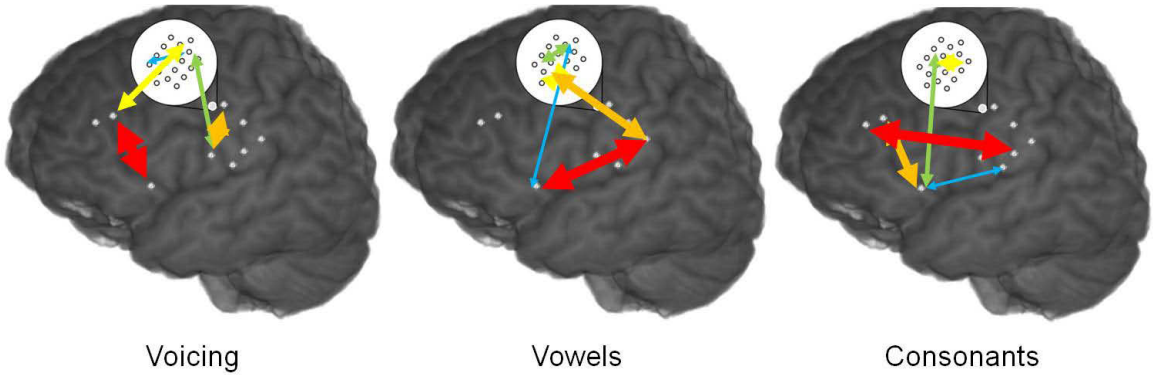

Figure 6.4: The five most informative connectivity features for each articulatory feature in subject A during preliminary feature screening. Intra-ECoG, intra-microECoG, and cross-scale connectivity features are all informative for decoding all manners of articulation.

each of the manners of articulation decoded, according to a preliminary screening analysis without cross-validation in subject A, are shown in Fig. 6.4. ECoG, microECoG, and cross-scale connections are all represented, confirming that multiple network scales contain information about articulatory features.

6.5 Discussion and Conclusions

6.5.1 Summary and Recommendations

We have found evidence that dynamic connectivity models of human ECoG data capture information about articulatory features during speech. This information improves the accuracy of classifiers for location of articulation, consonant voicing, and vowel height over classifiers that use power spectral features. We also computed con-

nectivity models that incorporated microECoG networks in cortical areas involved in speech processing, including temporal lobe, inferior frontal gyrus, and speech motor cortex. These models contained additional information about articulatory features over connectivity models without microECoG. Multi-scale connectivity between ECoG and microECoG sites was particularly informative in one subject for decoding place of articulation and vowel height. These results suggest that multi-scale connectivity features should be incorporated in BMIs for decoding speach.

We considered power spectral features and connectivity features in three frequency bands (1-8 Hz, 8-25 Hz, and 70-120 Hz). In most frequency bands, a connectivity-based classifier outperformed a power-based classifier for vowel height. However, for one subject the power-based classifier was significantly better in the 70-120 Hz frequency band. It has been demonstrated that lower frequencies modulate population firing in the neocortex [132].

6.5.2 Limitations and Extensions

The subjects who participated in this research were patients undergoing treatment for epilepsy, and the locations of the ECoG and microECoG grids were dependent upon clinical and surgical considerations. To some extent, this uncontrolled variability may have accounted for differences in classification accuracy observed in subjects A and B.

Because the purpose of this study was to determine the value of connectivity and

multi-scale connectivity features for decoding, the classifiers for articulatory features were not optimized for maximal classification accuracy. An optimal decoder would include both power and connectivity features, in addition to relevant features from all frequency bands, improvements that we did not explore.

In order to be useful for a patient population, a speech decoder will need to be functional during covert, or imagined, speech in addition to the overt, or fully articulated, speech investigated here. It has been demonstrated previously that neural activity during covert speech is similar to that during overt speech [235], so this extension, while nontrivial, is feasible.

Chapter 7

General Discussion

7.1 Summary and Significance of Results

The work presented here has demonstrated that effective connectivity models of the ECoG signal contain information about neural processing that can inform movement and speech mapping and decoding. We first showed that effective connectivity features were a promising feature for decoding dexterous movement, and then verified their utility in a decoder for joint angle during grasp. Next we demonstrated that effective connectivity maps capture information about speech processing that can be used to test models of the neural mechanisms underlying behavioral priming. Finally, we tested multi-scale effective connectivity features in ECoG and microECoG data, and found that in some cases they improved accuracy for classifiers of articulatory features during speech. These results suggest that brain-machine interface (BMI)

design should incorporate task-related cortical connectivity.

7.1.1 Variation in Connectivity during Movement

7.1.1.1 Change in connectivity coefficients preceding and during movement

Connectivity features of the local motor potential (LMP), a low frequency band (12-30 Hz), and a high frequency band (75-150 Hz) varied consistently across trials preceding and during grasp in three of four subjects. In the fourth subject, neither connectivity nor power spectral features mapped well to movement, possibly indicating that ECoG sites were not localized to task-relevant areas.

Connectivity features in canonical, smaller frequency bands (delta, theta, mu, beta, gamma, and high gamma) and connectivity of the LMP also varied consistently before and during individual finger movement. Because the number of possible connectivity features far exceeds the number of possible power spectral and temporal features ($N^2 - N$ compared to N for any given channel), connectivity features may contain additional information useful for decoding movement kinematics from neural signals.

7.1.1.2 Principal components of connectivity reflect task-related processing

Principal component analysis was used to extract subsets of connections that covaried during grasp for one subject. Consistent with predictions of current models [69, 190–195], widespread cortical areas related to movement developed connections preceding movement. A limited network involving a site in or near primary motor cortex was active during movement onset. A more widespread network potentially related to feedback continued to interact throughout the movement.

7.1.2 Connectivity-Based Movement Decoding

We decoded continuous joint angles during palmar grasps for four subjects using general regression neural networks constructed with both power spectral features and connectivity features computed with the LMP, the low frequency band, and the high frequency band. In all cases, the correlation coefficient between the actual and predicted joint angles was higher for the connectivity-based decoders compared to the power-based decoders. In part, this improvement in accuracy may have been due to the increased number of connectivity features available compared to power and temporal features. In subsequent sections, when testing speech classification with connectivity features, we specifically limited the number of connectivity features to be equal to the power spectral features, in order to confirm that additional information

was present without an increased feature set.

7.1.3 Mapping of Dynamic Connectivity during Speech

Following these demonstrations that connectivity mapping was useful in motor applications, we applied these methods to two speech applications in mapping and decoding. In addition to relevance for BMI applications, the measures of dynamic effective connectivity that are made possible by the high temporal resolution of the ECoG signal may be useful for testing hypotheses about neural processing mechanisms. As an example, we mapped connectivity changes during behavioral priming of speech to test models of neural repetition suppression, the decrease in neural activation that accompanies decreased reaction time.

When subjects were asked to name novel and repeated pictures, we found evidence of cortical flows that was consistent with a "predictive coding" model of the changes in neural activity underlying behavioral priming and repetition suppression during the repeated picture naming. Briefly, top-down inflows from cortical areas related to speech production (including sensorimotor areas, inferior frontal gyrus, and posterior superior temporal gyrus) increased to cortical areas related to stimulus processing and pre-lexical object representation. After these top-down inflows, outflows from the sites with repetition suppression were decreased. These findings suggest that

following early initial propagation of stimulus processing, top-down predictive models from speech processing areas extinguish the need for additional stimulus processing. This result demonstrates the utility of mapping dynamic effective connectivity for testing models of the neurophysiology underlying behavior.

7.1.4 Connectivity-Based Speech Decoding

After mapping connectivity during speech to test hypotheses about the neural mechanisms underlying priming and repetition suppression, we explored the utility of connectivity features for a speech BMI. Specifically, we compared several classifiers for articulatory features using power features and connectivity features in three frequency bands (1-8 Hz, 8-25 Hz, and 70-120 Hz) from two different recording scales (clinical ECoG and high-density microECoG). We found that in many bands the connectivity-based classifiers were more accurate than the power-based classifiers. We also showed that connectivity features from the microECoG signals were often more informative than connectivity features from the standard clinical ECoG signals. In some cases, however, the most effective classifiers used connectivity features from networks that included both ECoG and microECoG sites. These results suggest that the effective connectivity metrics used here captured both global synchronization and local networks responsible for fine processing of articulatory features. Multi-scale connectivity features therefore improve decoding accuracy for a speech BMI.

7.2 Future Directions

7.2.1 Dynamic Connectivity Mapping for Identification of Critical Processing Nodes

While we have demonstrated that connectivity mapping captures important elements of motor and speech networks, and that as a result connectivity features can improve the ability to decode movement and speech, there are additional applications for models of cortical connectivity that should be explored. One clinically relevant application is the use of connectivity to identify "eloquent cortex," or cortical areas critical for movement and speech processing, preceding surgical brain resections for the treatment of epilepsy and tumors. Most mapping of the eloquent cortex relies on electrocortical stimulation mapping (ESM, [22–24], and recent research has made use of fMRI [27] or ECoG signals [28]. Because connectivity mapping is informative about the neural activity underlying movement and speech, a natural extension is its use in this context. It is possible that connectivity mapping may identify important "hub" nodes that critically coordinate interactions between local processing sites, which could provide valuable information about the likely effect of removing such sites.

7.2.2 Integrated Decoders using Power Spectral and Connectivity Features

Because our aim was to characterize the value of connectivity features for BMI, we did not optimize the movement and speech decoders in all possible ways. In particular, the combination of standard power and temporal features with connectivity features would create the opportunity for a variety of approaches to BMI design. An important next step is the assessment of decoding accuracy when connectivity features are integrated with traditional features. If some complementary information is present in connectivity and power features, for example, feature selection should be optimized.

It is possible that some of the increased decoding accuracy we observed when using connectivity features arose from the ability to implicitly detect sequences of activation related to movement or speech. For example, in a speech task, effective connectivity could model the activation of posterior superior temporal gyrus (pSTG) during phonological coding, followed by the activation of inferior frontal gyrus (IFG) during syllabification. When a connection from pSTG to IFG increases, a classifier could anticipate the onset of speech. There are a variety of approaches to detecting such sequential activation, such as template matching or a series of gated decoders, but effective connectivity provides an elegant solution by modeling the sequential activation as a single Granger causal feature. This sequence detection should be

considered in BMI design.

7.2.3 State-Based Decoding with Connectivity Features

We observed consistent changes in connectivity preceding and during movement and speech, which suggests connectivity features may be useful for a classifier of cognitive state or progression through a task. Because connectivity often changes before movement and speech onset, its utility for decoding stimulus processing, movement and speech planning, movement and speech onset, and movement and speech duration should be assessed. As BMI design begins to incorporate more practical clinical considerations, synchronous decoding, or decoding of a task with reference to a specific cue, is less desirable than asynchronous decoding, or decoding that does not require a cue-based task. Using connectivity features to decode cognitive state could enable an asynchronous BMI.

In the context of movement, interactions between visual or auditory areas and motor areas could indicate stimulus processing as a step in movement preparation. Interactions between premotor and primary motor areas, or anterior parietal cortex and primary motor areas, could indicate imminent speech and signal a kinematic decoder to initiate movement. Such pre-movement detection could decrease the lag inherent in a BMI system, which must process neural data and fit it to a model

before actuating a limb. A decrease in lag time from the neural activity expressing intent to move and the limb actuation could yield substantial benefits in visual and proprioceptive feedback that matches forward models in the brain, and increased sense of embodiment of the BMI limb [241].

In the context of speech, interactions between auditory cortex and pSTG may be used to detect speech processing, a potential early indicator of an upcoming intent to speak. Interactions between pSTG and IFG, followed by interactions between these areas and primary speech motor areas, could be a cue for the initiation of speech in a BMI. Such an early detection system would have similar benefits as those for the motor system. Because connectivity features provide new information about the neural activity underlying movement and speech, they create a variety of opportunities for improving BMI design and accuracy.

Bibliography

[1] C. T. Nordhausen, E. M. Maynard, and R. A. Normann, "Single unit recording capabilities of a 100 microelectrode array." *Brain Research*, vol. 726, no. 1-2, pp. 129–40, Jul. 1996. [Online]. Available: http://www.ncbi.nlm.nih.gov/pubmed/8836553

[2] W. Wang, A. D. Degenhart, J. L. Collinger, R. Vinjamuri, G. P. Sudre, P. D. Adelson, D. L. Holder, E. C. Leuthardt, D. W. Moran, M. L. Boninger, A. B. Schwartz, D. J. Crammond, E. C. Tyler-Kabara, and D. J. Weber, "Human motor cortical activity recorded with Micro-ECoG electrodes, during individual finger movements." *Conference Proceedings of the Annual International Conference of the IEEE Engineering in Medicine and Biology Society.*, vol. 2009, pp. 586–9, Jan. 2009. [Online]. Available: http://www.ncbi.nlm.nih.gov/pmc/articles/PMC3142578/

[3] J. Viventi, D.-H. Kim, L. Vigeland, E. S. Frechette, J. A. Blanco, Y.-S. Kim, A. E. Avrin, V. R. Tiruvadi, S.-W. Hwang, A. C. Vanleer, D. F. Wulsin,

K. Davis, C. E. Gelber, L. Palmer, J. Van der Spiegel, J. Wu, J. Xiao, Y. Huang, D. Contreras, J. A. Rogers, and B. Litt, "Flexible, foldable, actively multiplexed, high-density electrode array for mapping brain activity in vivo." *Nature Neuroscience*, vol. 14, no. 12, pp. 1599–605, Dec. 2011. [Online]. Available: http://www.ncbi.nlm.nih.gov/pmc/articles/PMC3235709/

[4] M. D. Serruya, N. G. Hatsopoulos, L. Paninski, M. R. Fellows, and J. P. Donoghue, "Instant neural control of a movement signal." *Nature*, vol. 416, no. 6877, pp. 141–2, Mar. 2002. [Online]. Available: http://www.ncbi.nlm.nih.gov/pubmed/11894084

[5] L. Paninski, M. R. Fellows, N. G. Hatsopoulos, and J. P. Donoghue, "Spatiotemporal tuning of motor cortical neurons for hand position and velocity." *Journal of Neurophysiology*, vol. 91, no. 1, pp. 515–32, Jan. 2004. [Online]. Available: http://www.ncbi.nlm.nih.gov/pubmed/13679402

[6] W. Truccolo, G. M. Friehs, J. P. Donoghue, and L. R. Hochberg, "Primary motor cortex tuning to intended movement kinematics in humans with tetraplegia." *Journal of Neuroscience*, vol. 28, no. 5, pp. 1163–78, Jan. 2008. [Online]. Available: http://www.ncbi.nlm.nih.gov/pubmed/18234894

[7] J. S. Brumberg, E. J. Wright, D. S. Andreasen, F. H. Guenther, and P. R. Kennedy, "Classification of intended phoneme production from chronic intracortical microelectrode recordings in speech-motor cortex."

Frontiers in Neuroscience, vol. 5, p. 65, Jan. 2011. [Online]. Available: http://www.ncbi.nlm.nih.gov/pmc/articles/PMC3096823/

[8] E. C. Leuthardt, C. Gaona, M. Sharma, N. Szrama, J. Roland, Z. Freudenberg, J. Solis, J. Breshears, and G. Schalk, "Using the electrocorticographic speech network to control a brain-computer interface in humans." *Journal of Neural Engineering*, vol. 8, no. 3, p. 036004, Jun. 2011. [Online]. Available: http://www.ncbi.nlm.nih.gov/pmc/articles/PMC3701859/

[9] E. M. Mugler, J. L. Patton, R. D. Flint, Z. A. Wright, S. U. Schuele, J. Rosenow, J. J. Shih, D. J. Krusienski, and M. W. Slutzky, "Direct classification of all American English phonemes using signals from functional speech motor cortex." *Journal of Neural Engineering*, vol. 11, no. 3, p. 035015, Jun. 2014. [Online]. Available: http://www.ncbi.nlm.nih.gov/pubmed/24836588

[10] G. Toyoda, E. C. Brown, N. Matsuzaki, K. Kojima, M. Nishida, and E. Asano, "Electrocorticographic correlates of overt articulation of 44 English phonemes: Intracranial recording in children with focal epilepsy," *Clinical Neurophysiology*, 2013. [Online]. Available: http://www.ncbi.nlm.nih.gov/pubmed/24315545

[11] J. Engel, R. Rausch, J. P. Lieb, D. E. Kuhl, and P. H. Crandall, "Correlation of criteria used for localizing epileptic foci in patients considered for surgical therapy of epilepsy." *Annals of Neurology*, vol. 9, no. 3, pp. 215–24, Mar. 1981. [Online]. Available: http://www.ncbi.nlm.nih.gov/pubmed/7013652

[12] M. S. Berger, J. Kincaid, G. A. Ojemann, and E. Lettich, "Brain mapping techniques to maximize resection, safety, and seizure control in children with brain tumors." *Neurosurgery*, vol. 25, no. 5, pp. 786–92, Nov. 1989. [Online]. Available: http://www.ncbi.nlm.nih.gov/pubmed/2586730

[13] P. G. Matz, C. Cobbs, and M. S. Berger, "Intraoperative cortical mapping as a guide to the surgical resection of gliomas." *Journal of Neuro-Oncology*, vol. 42, no. 3, pp. 233–45, May 1999. [Online]. Available: http://www.ncbi.nlm.nih.gov/pubmed/10433107

[14] N. Sanai, Z. Mirzadeh, and M. S. Berger, "Functional outcome after language mapping for glioma resection." *The New England Journal of Medicine*, vol. 358, no. 1, pp. 18–27, Jan. 2008. [Online]. Available: http://www.ncbi.nlm.nih.gov/pubmed/18172171

[15] N. J. Hill, D. Gupta, P. Brunner, A. Gunduz, M. A. Adamo, A. Ritaccio, and G. Schalk, "Recording human electrocorticographic (ECoG) signals for neuroscientific research and real-time functional cortical mapping." *Journal of Visualized Experiments*, no. 64, Jan. 2012. [Online]. Available: http://www.ncbi.nlm.nih.gov/pmc/articles/PMC3471287/

[16] P. Indefrey and W. J. M. Levelt, "The spatial and temporal signatures of word production components." *Cognition*, vol. 92, no. 1-2, pp. 101–44, 2004. [Online]. Available: http://www.ncbi.nlm.nih.gov/pubmed/15037128

[17] P. Kwan and M. J. Brodie, "Early identification of refractory epilepsy." *The New England Journal of Medicine*, vol. 342, no. 5, pp. 314–9, Feb. 2000. [Online]. Available: http://www.ncbi.nlm.nih.gov/pubmed/10660394

[18] J. P. Lachaux, D. Rudrauf, and P. Kahane, "Intracranial EEG and human brain mapping." *Journal of Physiology, Paris*, vol. 97, no. 4-6, pp. 613–28, 2003. [Online]. Available: http://www.ncbi.nlm.nih.gov/pubmed/15242670

[19] E. Behrens, J. Zentner, D. van Roost, A. Hufnagel, C. E. Elger, and J. Schramm, "Subdural and depth electrodes in the presurgical evaluation of epilepsy." *Acta Neurochirurgica*, vol. 128, no. 1-4, pp. 84–7, Jan. 1994. [Online]. Available: http://www.ncbi.nlm.nih.gov/pubmed/7847148

[20] E. Wyllie, H. Lüders, H. H. Morris, R. P. Lesser, D. S. Dinner, A. D. Rothner, G. Erenberg, R. Cruse, D. Friedman, and J. Hahn, "Subdural electrodes in the evaluation for epilepsy surgery in children and adults." *Neuropediatrics*, vol. 19, no. 2, pp. 80–6, May 1988. [Online]. Available: http://www.ncbi.nlm.nih.gov/pubmed/3374766

[21] S. Goldring and E. M. Gregorie, "Surgical management of epilepsy using epidural recordings to localize the seizure focus. Review of 100 cases." *Journal of Neurosurgery*, vol. 60, no. 3, pp. 457–66, Mar. 1984. [Online]. Available: http://www.ncbi.nlm.nih.gov/pubmed/6699689

[22] G. Ojemann, J. Ojemann, E. Lettich, and M. Berger, "Cortical language

localization in left, dominant hemisphere. An electrical stimulation mapping investigation in 117 patients." *Journal of Neurosurgery*, vol. 71, no. 3, pp. 316–26, Sep. 1989. [Online]. Available: http://www.ncbi.nlm.nih.gov/pubmed/2769383

[23] S. Y. Bookheimer, T. A. Zeffiro, T. Blaxton, B. A. Malow, W. D. Gaillard, S. Sato, C. Kufta, P. Fedio, and W. H. Theodore, "A direct comparison of PET activation and electrocortical stimulation mapping for language localization." *Neurology*, vol. 48, no. 4, pp. 1056–65, Apr. 1997. [Online]. Available: http://www.ncbi.nlm.nih.gov/pubmed/9109900

[24] D. B. FitzGerald, G. R. Cosgrove, S. Ronner, H. Jiang, B. R. Buchbinder, J. W. Belliveau, B. R. Rosen, and R. R. Benson, "Location of language in the cortex: a comparison between functional MR imaging and electrocortical stimulation." *American Journal of Neuroradiology*, vol. 18, no. 8, pp. 1529–39, Sep. 1997. [Online]. Available: http://www.ncbi.nlm.nih.gov/pubmed/9296196

[25] W. T. Blume, D. C. Jones, and P. Pathak, "Properties of after-discharges from cortical electrical stimulation in focal epilepsies." *Clinical Neurophysiology*, vol. 115, no. 4, pp. 982–9, Apr. 2004. [Online]. Available: http://www.ncbi.nlm.nih.gov/pubmed/15003782

[26] A. Sinai, C. W. Bowers, C. M. Crainiceanu, D. Boatman, B. Gordon, R. P. Lesser, F. A. Lenz, and N. E. Crone, "Electrocorticographic high gamma activity versus electrical cortical stimulation mapping of naming."

Brain, vol. 128, no. Pt 7, pp. 1556–70, Jul. 2005. [Online]. Available: http://www.ncbi.nlm.nih.gov/pubmed/15817517

[27] D. S. Sabsevitz, S. J. Swanson, T. A. Hammeke, M. V. Spanaki, E. T. Possing, G. L. Morris, W. M. Mueller, and J. R. Binder, "Use of preoperative functional neuroimaging to predict language deficits from epilepsy surgery." *Neurology*, vol. 60, no. 11, pp. 1788–92, Jun. 2003. [Online]. Available: http://www.ncbi.nlm.nih.gov/pubmed/12796532

[28] P. Brunner, A. L. Ritaccio, T. M. Lynch, J. F. Emrich, J. A. Wilson, J. C. Williams, E. J. Aarnoutse, N. F. Ramsey, E. C. Leuthardt, H. Bischof, and G. Schalk, "A practical procedure for real-time functional mapping of eloquent cortex using electrocorticographic signals in humans." *Epilepsy & Behavior*, vol. 15, no. 3, pp. 278–86, Jul. 2009. [Online]. Available: http://www.ncbi.nlm.nih.gov/pmc/articles/PMC2754703/

[29] N. E. Crone, A. Korzeniewska, and P. J. Franaszczuk, "Cortical γ responses: searching high and low." *International Journal of Psychophysiology*, vol. 79, no. 1, pp. 9–15, Jan. 2011. [Online]. Available: http://www.ncbi.nlm.nih.gov/pmc/articles/PMC3958992/

[30] J.-P. Lachaux, N. Axmacher, F. Mormann, E. Halgren, and N. E. Crone, "High-frequency neural activity and human cognition: past, present and possible future of intracranial EEG research." *Progress in*

Neurobiology, vol. 98, no. 3, pp. 279–301, Sep. 2012. [Online]. Available: http://www.ncbi.nlm.nih.gov/pmc/articles/PMC3980670/

[31] N. V. Thakor, "Translating the Brain-Machine Interface." *Science Translational Medicine*, vol. 5, no. 210, p. 210ps17, Nov. 2013. [Online]. Available: http://www.ncbi.nlm.nih.gov/pubmed/24197734

[32] A. Cahill, H. Fredine, and L. Zilberman, "Initial Briefing Prevalence of Paralysis Including Spinal Cord Injuries in the United States, 2008," Christopher and Dana Reeve Foundation, Paralysis Resource Foundation, The University of New Mexico, School of Medicine, Tech. Rep., 2009.

[33] L. G. Stansbury, S. J. Lalliss, J. G. Branstetter, M. R. Bagg, and J. B. Holcomb, "Amputations in U.S. military personnel in the current conflicts in Afghanistan and Iraq." *Journal of Orthopaedic Trauma*, vol. 22, no. 1, pp. 43–6, Jan. 2008. [Online]. Available: http://www.ncbi.nlm.nih.gov/pubmed/18176164

[34] J. Adamson, A. Beswick, and S. Ebrahim, "Is stroke the most common cause of disability?" *Journal of Stroke and Cerebrovascular Diseases*, vol. 13, no. 4, pp. 171–7. [Online]. Available: http://www.ncbi.nlm.nih.gov/pubmed/17903971

[35] E. Smith and M. Delargy, "Locked-in syndrome." *BMJ (Clinical research ed.)*, vol. 330, no. 7488, pp. 406–9, Feb. 2005. [Online]. Available: http://www.ncbi.nlm.nih.gov/pmc/articles/PMC549115/

[36] J. R. Wolpaw, D. J. McFarland, G. W. Neat, and C. A. Forneris, "An EEG-based brain-computer interface for cursor control." *Electroencephalography and Clinical Neurophysiology*, vol. 78, no. 3, pp. 252–9, Mar. 1991. [Online]. Available: http://www.ncbi.nlm.nih.gov/pubmed/1707798

[37] F. Lotte, M. Congedo, A. Lécuyer, F. Lamarche, and B. Arnaldi, "A review of classification algorithms for EEG-based brain-computer interfaces." *Journal of Neural Engineering*, vol. 4, no. 2, pp. R1–R13, Jun. 2007. [Online]. Available: http://www.ncbi.nlm.nih.gov/pubmed/17409472

[38] J. Mellinger, G. Schalk, C. Braun, H. Preissl, W. Rosenstiel, N. Birbaumer, and A. Kübler, "An MEG-based brain-computer interface (BCI)." *NeuroImage*, vol. 36, no. 3, pp. 581–93, Jul. 2007. [Online]. Available: http://www.ncbi.nlm.nih.gov/pmc/articles/PMC2017111/

[39] N. Weiskopf, K. Mathiak, S. W. Bock, F. Scharnowski, R. Veit, W. Grodd, R. Goebel, and N. Birbaumer, "Principles of a brain-computer interface (BCI) based on real-time functional magnetic resonance imaging (fMRI)." *IEEE Transactions on Biomedical Engineering*, vol. 51, no. 6, pp. 966–70, Jun. 2004. [Online]. Available: http://www.ncbi.nlm.nih.gov/pubmed/15188865

[40] S.-S. Yoo, T. Fairneny, N.-K. Chen, S.-E. Choo, L. P. Panych, H. Park, S.-Y. Lee, and F. A. Jolesz, "Brain-computer interface using fMRI: spatial

navigation by thoughts." *Neuroreport*, vol. 15, no. 10, pp. 1591–5, Jul. 2004. [Online]. Available: http://www.ncbi.nlm.nih.gov/pubmed/15232289

[41] S. M. Coyle, T. E. Ward, and C. M. Markham, "Brain-computer interface using a simplified functional near-infrared spectroscopy system." *Journal of Neural Engineering*, vol. 4, no. 3, pp. 219–26, Sep. 2007. [Online]. Available: http://www.ncbi.nlm.nih.gov/pubmed/17873424

[42] L. R. Hochberg, M. D. Serruya, G. M. Friehs, J. A. Mukand, M. Saleh, A. H. Caplan, A. Branner, D. Chen, R. D. Penn, and J. P. Donoghue, "Neuronal ensemble control of prosthetic devices by a human with tetraplegia." *Nature*, vol. 442, no. 7099, pp. 164–71, Jul. 2006. [Online]. Available: http://www.ncbi.nlm.nih.gov/pubmed/16838014

[43] D. A. Heldman, W. Wang, S. S. Chan, and D. W. Moran, "Local field potential spectral tuning in motor cortex during reaching." *IEEE Transactions on Neural Systems and Rehabilitation Engineering*, vol. 14, no. 2, pp. 180–3, Jun. 2006. [Online]. Available: http://www.ncbi.nlm.nih.gov/pubmed/16792288

[44] E. C. Leuthardt, G. Schalk, J. R. Wolpaw, J. G. Ojemann, and D. W. Moran, "A brain computer interface using electrocorticographic signals in humans," *Journal of Neural Engineering*, vol. 1, pp. 63–71, 2004. [Online]. Available: http://www.ncbi.nlm.nih.gov/pubmed/15876624

[45] L. J. Trejo, R. Rosipal, and B. Matthews, "Brain-computer interfaces for

1-D and 2-D cursor control: designs using volitional control of the EEG spectrum or steady-state visual evoked potentials." *IEEE Transactions on Neural Systems and Rehabilitation Engineering*, vol. 14, no. 2, pp. 225–9, Jun. 2006. [Online]. Available: http://www.ncbi.nlm.nih.gov/pubmed/16792300

[46] F. Galán, M. Nuttin, E. Lew, P. Ferrez, G. Vanacker, J. Philips, and J. d. R. Millán, "A brain-actuated wheelchair: Asynchronous and non-invasive Braincomputer interfaces for continuous control of robots." *Clinical Neurophysiology*, vol. 119, no. 9, pp. 2159–69, Sep. 2008. [Online]. Available: http://www.ncbi.nlm.nih.gov/pubmed/18621580

[47] G. R. Müller-Putz and G. Pfurtscheller, "Control of an electrical prosthesis with an SSVEP-based BCI." *IEEE Transactions on Biomedical Engineering*, vol. 55, no. 1, pp. 361–4, Jan. 2008. [Online]. Available: http://www.ncbi.nlm.nih.gov/pubmed/18232384

[48] N. Naseer, M. J. Hong, and K.-S. Hong, "Online binary decision decoding using functional near-infrared spectroscopy for the development of brain-computer interface." *Experimental Brain Research*, vol. 232, no. 2, pp. 555–64, Feb. 2014. [Online]. Available: http://www.ncbi.nlm.nih.gov/pubmed/24258529

[49] J. L. Collinger, B. Wodlinger, J. E. Downey, W. Wang, E. C. Tyler-Kabara, D. J. Weber, A. J. C. McMorland, M. Velliste, M. L. Boninger, and A. B. Schwartz, "High-performance neuroprosthetic control by an individual with

tetraplegia." *Lancet*, vol. 381, no. 9866, pp. 557–64, Feb. 2013. [Online]. Available: http://www.ncbi.nlm.nih.gov/pmc/articles/PMC3641862/

[50] R. Biran, D. C. Martin, and P. A. Tresco, "Neuronal cell loss accompanies the brain tissue response to chronically implanted silicon microelectrode arrays." *Experimental Neurology*, vol. 195, no. 1, pp. 115–26, Sep. 2005. [Online]. Available: http://www.ncbi.nlm.nih.gov/pubmed/16045910

[51] V. S. Polikov, P. A. Tresco, and W. M. Reichert, "Response of brain tissue to chronically implanted neural electrodes." *Journal of Neuroscience Methods*, vol. 148, no. 1, pp. 1–18, Oct. 2005. [Online]. Available: http://www.ncbi.nlm.nih.gov/pubmed/16198003

[52] W. Wang, J. L. Collinger, A. D. Degenhart, E. C. Tyler-Kabara, A. B. Schwartz, D. W. Moran, D. J. Weber, B. Wodlinger, R. K. Vinjamuri, R. C. Ashmore, J. W. Kelly, and M. L. Boninger, "An electrocorticographic brain interface in an individual with tetraplegia." *PloS One*, vol. 8, no. 2, p. e55344, Jan. 2013. [Online]. Available: http://www.ncbi.nlm.nih.gov/pmc/articles/PMC3566209/

[53] J. Richiardi, H. Eryilmaz, S. Schwartz, P. Vuilleumier, and D. Van De Ville, "Decoding brain states from fMRI connectivity graphs." *NeuroImage*, vol. 56, no. 2, pp. 616–26, May 2011. [Online]. Available: http://www.ncbi.nlm.nih.gov/pubmed/20541019

[54] W. R. Shirer, S. Ryali, E. Rykhlevskaia, V. Menon, and M. D. Greicius,

"Decoding subject-driven cognitive states with whole-brain connectivity patterns." *Cerebral Cortex*, vol. 22, no. 1, pp. 158–65, Jan. 2012. [Online]. Available: http://www.ncbi.nlm.nih.gov/pmc/articles/PMC3236795/

[55] M. Billinger, C. Brunner, and G. R. Müller-Putz, "Single-trial connectivity estimation for classification of motor imagery data." *Journal of Neural Engineering*, vol. 10, no. 4, p. 046006, Aug. 2013. [Online]. Available: http://www.ncbi.nlm.nih.gov/pubmed/23751454

[56] D. J. Krusienski, E. W. Sellers, F. Cabestaing, S. Bayoudh, D. J. McFarland, T. M. Vaughan, and J. R. Wolpaw, "A comparison of classification techniques for the P300 Speller." *Journal of Neural Engineering*, vol. 3, no. 4, pp. 299–305, Dec. 2006. [Online]. Available: http://www.ncbi.nlm.nih.gov/pubmed/17124334

[57] F. Nijboer, E. W. Sellers, J. Mellinger, M. A. Jordan, T. Matuz, A. Furdea, S. Halder, U. Mochty, D. J. Krusienski, T. M. Vaughan, J. R. Wolpaw, N. Birbaumer, and A. Kübler, "A P300-based brain-computer interface for people with amyotrophic lateral sclerosis." *Clinical Neurophysiology*, vol. 119, no. 8, pp. 1909–16, Aug. 2008. [Online]. Available: http://www.ncbi.nlm.nih.gov/pmc/articles/PMC2853977/

[58] S. Kellis, K. Miller, K. Thomson, R. Brown, P. House, and B. Greger, "Decoding spoken words using local field potentials recorded from the cortical

surface." *Journal of Neural Engineering*, vol. 7, no. 5, p. 056007, Oct. 2010. [Online]. Available: http://www.ncbi.nlm.nih.gov/pmc/articles/PMC2970568/

[59] S. Ikeda, T. Shibata, N. Nakano, R. Okada, N. Tsuyuguchi, K. Ikeda, and A. Kato, "Neural decoding of single vowels during covert articulation using electrocorticography." *Frontiers in Human Neuroscience*, vol. 8, p. 125, Jan. 2014. [Online]. Available: http://www.pubmedcentral.nih.gov/articlerender.fcgi?artid=3945950

[60] K. E. Bouchard, N. Mesgarani, K. Johnson, and E. F. Chang, "Functional organization of human sensorimotor cortex for speech articulation." *Nature*, vol. 495, no. 7441, pp. 327–32, Mar. 2013. [Online]. Available: http://www.ncbi.nlm.nih.gov/pmc/articles/PMC3606666/

[61] W. M. Mueller, F. Z. Yetkin, T. A. Hammeke, G. L. Morris, S. J. Swanson, K. Reichert, R. Cox, and V. M. Haughton, "Functional magnetic resonance imaging mapping of the motor cortex in patients with cerebral tumors." *Neurosurgery*, vol. 39, no. 3, pp. 515–20; discussion 520–1, Sep. 1996. [Online]. Available: http://www.ncbi.nlm.nih.gov/pubmed/8875481

[62] K. Roessler, M. Donat, R. Lanzenberger, K. Novak, A. Geissler, A. Gartus, A. R. Tahamtan, D. Milakara, T. Czech, M. Barth, E. Knosp, and R. Beisteiner, "Evaluation of preoperative high magnetic field motor functional MRI (3 Tesla) in glioma patients by navigated electrocortical stimulation

and postoperative outcome." *Journal of Neurology, Neurosurgery, and Psychiatry*, vol. 76, no. 8, pp. 1152–7, Aug. 2005. [Online]. Available: http://www.ncbi.nlm.nih.gov/pmc/articles/PMC1739751/

[63] O. Suess, S. Suess, M. Brock, and T. Kombos, "Intraoperative electrocortical stimulation of Brodman area 4: a 10-year analysis of 255 cases." *Head & Face Medicine*, vol. 2, p. 20, Jan. 2006. [Online]. Available: http://www.ncbi.nlm.nih.gov/pmc/articles/PMC1524941/

[64] M. Lebedev, "Brain-machine interfaces: an overview," *Translational Neuroscience*, vol. 5, no. 1, pp. 99–110, Mar. 2014. [Online]. Available: http://link.springer.com/article/10.2478/s13380-014-0212-z

[65] G. Rizzolatti, L. Fogassi, and V. Gallese, "Motor and cognitive functions of the ventral premotor cortex." *Current Opinion in Neurobiology*, vol. 12, no. 2, pp. 149–54, Apr. 2002. [Online]. Available: http://www.ncbi.nlm.nih.gov/pubmed/12015230

[66] P. Cisek and J. F. Kalaska, "Neural correlates of mental rehearsal in dorsal premotor cortex." *Nature*, vol. 431, no. 7011, pp. 993–6, Oct. 2004. [Online]. Available: http://www.ncbi.nlm.nih.gov/pubmed/15496925

[67] ——, "Neural correlates of reaching decisions in dorsal premotor cortex: specification of multiple direction choices and final selection of action."

Neuron, vol. 45, no. 5, pp. 801–14, Mar. 2005. [Online]. Available: http://www.ncbi.nlm.nih.gov/pubmed/15748854

[68] M. Davare, M. Andres, G. Cosnard, J.-L. Thonnard, and E. Olivier, "Dissociating the role of ventral and dorsal premotor cortex in precision grasping." *The Journal of Neuroscience*, vol. 26, no. 8, pp. 2260–8, Feb. 2006. [Online]. Available: http://www.ncbi.nlm.nih.gov/pubmed/16495453

[69] J. Tanji and K. Shima, "Role for supplementary motor area cells in planning several movements ahead." *Nature*, vol. 371, no. 6496, pp. 413–6, Oct. 1994. [Online]. Available: http://www.ncbi.nlm.nih.gov/pubmed/8090219

[70] S.-J. Blakemore and A. Sirigu, "Action prediction in the cerebellum and in the parietal lobe." *Experimental Brain Research*, vol. 153, no. 2, pp. 239–45, Nov. 2003. [Online]. Available: http://www.ncbi.nlm.nih.gov/pubmed/12955381

[71] M. Fabri and H. Burton, "Ipsilateral cortical connections of primary somatic sensory cortex in rats." *The Journal of Comparative Neurology*, vol. 311, no. 3, pp. 405–24, Sep. 1991. [Online]. Available: http://www.ncbi.nlm.nih.gov/pubmed/1720147

[72] U. Halsband, N. Ito, J. Tanji, and H. J. Freund, "The role of premotor cortex and the supplementary motor area in the temporal control of movement in man." *Brain*, vol. 116 (Pt 1), pp. 243–66, Feb. 1993. [Online]. Available: http://www.ncbi.nlm.nih.gov/pubmed/8453461

[73] F. Binkofski, C. Dohle, S. Posse, K. M. Stephan, H. Hefter, R. J. Seitz, and H. J. Freund, "Human anterior intraparietal area subserves prehension: a combined lesion and functional MRI activation study." *Neurology*, vol. 50, no. 5, pp. 1253–9, May 1998. [Online]. Available: http://www.ncbi.nlm.nih.gov/pubmed/9595971

[74] A. P. Batista and R. A. Andersen, "The parietal reach region codes the next planned movement in a sequential reach task." *Journal of Neurophysiology*, vol. 85, no. 2, pp. 539–44, Feb. 2001. [Online]. Available: http://www.ncbi.nlm.nih.gov/pubmed/11160491

[75] D. J. Serrien, L. H. A. Strens, A. Oliviero, and P. Brown, "Repetitive transcranial magnetic stimulation of the supplementary motor area (SMA) degrades bimanual movement control in humans." *Neuroscience Letters*, vol. 328, no. 2, pp. 89–92, Aug. 2002. [Online]. Available: http://www.ncbi.nlm.nih.gov/pubmed/12133562

[76] J. D. Connolly, R. A. Andersen, and M. A. Goodale, "FMRI evidence for a 'parietal reach region' in the human brain." *Experimental Brain Research*, vol. 153, no. 2, pp. 140–5, Nov. 2003. [Online]. Available: http://www.ncbi.nlm.nih.gov/pubmed/12955383

[77] M. Guye, G. J. M. Parker, M. Symms, P. Boulby, C. A. M. Wheeler-Kingshott, A. Salek-Haddadi, G. J. Barker, and J. S. Duncan, "Combined functional

MRI and tractography to demonstrate the connectivity of the human primary motor cortex in vivo." *NeuroImage*, vol. 19, no. 4, pp. 1349–60, Aug. 2003. [Online]. Available: http://www.ncbi.nlm.nih.gov/pubmed/12948693

[78] E. Tunik, S. H. Frey, and S. T. Grafton, "Virtual lesions of the anterior intraparietal area disrupt goal-dependent on-line adjustments of grasp." *Nature Neuroscience*, vol. 8, no. 4, pp. 505–11, Apr. 2005. [Online]. Available: http://www.ncbi.nlm.nih.gov/pubmed/15778711

[79] J. Fernandez-Ruiz, H. C. Goltz, J. F. X. DeSouza, T. Vilis, and J. D. Crawford, "Human parietal "reach region" primarily encodes intrinsic visual direction, not extrinsic movement direction, in a visual motor dissociation task." *Cerebral Cortex*, vol. 17, no. 10, pp. 2283–92, Oct. 2007. [Online]. Available: http://www.ncbi.nlm.nih.gov/pubmed/17215478

[80] M. A. Maier, J. Armand, P. A. Kirkwood, H.-W. Yang, J. N. Davis, and R. N. Lemon, "Differences in the corticospinal projection from primary motor cortex and supplementary motor area to macaque upper limb motoneurons: an anatomical and electrophysiological study." *Cerebral Cortex*, vol. 12, no. 3, pp. 281–96, Mar. 2002. [Online]. Available: http://www.ncbi.nlm.nih.gov/pubmed/11839602

[81] S. Kakei, D. S. Hoffman, and P. L. Strick, "Muscle and movement representa-

tions in the primary motor cortex." *Science*, vol. 285, no. 5436, pp. 2136–9, Sep. 1999. [Online]. Available: http://www.ncbi.nlm.nih.gov/pubmed/10497133

[82] D. W. Moran and A. B. Schwartz, "Motor cortical representation of speed and direction during reaching." *Journal of Neurophysiology*, vol. 82, no. 5, pp. 2676–92, Nov. 1999. [Online]. Available: http://www.ncbi.nlm.nih.gov/pubmed/10561437

[83] S. H. Scott and J. F. Kalaska, "Reaching movements with similar hand paths but different arm orientations. I. Activity of individual cells in motor cortex." *Journal of Neurophysiology*, vol. 77, no. 2, pp. 826–52, Feb. 1997. [Online]. Available: http://www.ncbi.nlm.nih.gov/pubmed/9065853

[84] C. E. Vargas-Irwin, G. Shakhnarovich, P. Yadollahpour, J. M. K. Mislow, M. J. Black, and J. P. Donoghue, "Decoding complete reach and grasp actions from local primary motor cortex populations." *The Journal of Neuroscience*, vol. 30, no. 29, pp. 9659–69, Jul. 2010. [Online]. Available: http://www.ncbi.nlm.nih.gov/pmc/articles/PMC2921895/

[85] R. N. Holdefer and L. E. Miller, "Primary motor cortical neurons encode functional muscle synergies." *Experimental Brain Research*, vol. 146, no. 2, pp. 233–43, Sep. 2002. [Online]. Available: http://www.ncbi.nlm.nih.gov/pubmed/12195525

[86] M. S. A. Graziano, C. S. R. Taylor, and T. Moore, "Complex

movements evoked by microstimulation of precentral cortex." *Neuron*, vol. 34, no. 5, pp. 841–51, May 2002. [Online]. Available: http://www.ncbi.nlm.nih.gov/pubmed/12062029

[87] J. D. Meier, T. N. Aflalo, S. Kastner, and M. S. A. Graziano, "Complex organization of human primary motor cortex: a high-resolution fMRI study." *Journal of Neurophysiology*, vol. 100, no. 4, pp. 1800–12, Oct. 2008. [Online]. Available: http://www.ncbi.nlm.nih.gov/pmc/articles/PMC2576195/

[88] S. Dehaene, G. Le Clec'H, J.-B. Poline, D. Le Bihan, and L. Cohen, "The visual word form area: a prelexical representation of visual words in the fusiform gyrus." *Neuroreport*, vol. 13, no. 3, pp. 321–5, Mar. 2002. [Online]. Available: http://www.ncbi.nlm.nih.gov/pubmed/11930131

[89] D. Howard, K. Patterson, R. Wise, W. D. Brown, K. Friston, C. Weiller, and R. Frackowiak, "The cortical localization of the lexicons. Positron emission tomography evidence." *Brain*, vol. 115 (Pt 6), pp. 1769–82, Dec. 1992. [Online]. Available: http://www.ncbi.nlm.nih.gov/pubmed/1486460

[90] L. H. Tan, A. R. Laird, K. Li, and P. T. Fox, "Neuroanatomical correlates of phonological processing of Chinese characters and alphabetic words: a meta-analysis." *Human Brain Mapping*, vol. 25, no. 1, pp. 83–91, May 2005. [Online]. Available: http://www.ncbi.nlm.nih.gov/pubmed/15846817

[91] M. Papoutsi, J. A. de Zwart, J. M. Jansma, M. J. Pickering, J. A.

Bednar, and B. Horwitz, "From phonemes to articulatory codes: an fMRI study of the role of Broca's area in speech production." *Cerebral Cortex*, vol. 19, no. 9, pp. 2156–65, Sep. 2009. [Online]. Available: http://www.ncbi.nlm.nih.gov/pmc/articles/PMC2722428/

[92] D. Wildgruber, H. Ackermann, U. Klose, B. Kardatzki, and W. Grodd, "Functional lateralization of speech production at primary motor cortex: a fMRI study." *Neuroreport*, vol. 7, no. 15-17, pp. 2791–5, Nov. 1996. [Online]. Available: http://www.ncbi.nlm.nih.gov/pubmed/8981469

[93] A. Postma, "Detection of errors during speech production: a review of speech monitoring models." *Cognition*, vol. 77, no. 2, pp. 97–132, Nov. 2000. [Online]. Available: http://www.ncbi.nlm.nih.gov/pubmed/10986364

[94] Y. Hashimoto and K. L. Sakai, "Brain activations during conscious self-monitoring of speech production with delayed auditory feedback: an fMRI study." *Human Brain Mapping*, vol. 20, no. 1, pp. 22–8, Sep. 2003. [Online]. Available: http://www.ncbi.nlm.nih.gov/pubmed/12953303

[95] G. Pfurtscheller, B. Graimann, J. E. Huggins, S. P. Levine, and L. A. Schuh, "Spatiotemporal patterns of beta desynchronization and gamma synchronization in corticographic data during self-paced movement." *Clinical Neurophysiology*, vol. 114, no. 7, pp. 1226–36, Jul. 2003. [Online]. Available: http://www.ncbi.nlm.nih.gov/pubmed/12842719

[96] J. A. Wilson, E. a. Felton, P. C. Garell, G. Schalk, and J. C. Williams, "ECoG factors underlying multimodal control of a brain-computer interface." *IEEE Transactions on Neural Systems and Rehabilitation Engineering*, vol. 14, no. 2, pp. 246–50, Jun. 2006. [Online]. Available: http://www.ncbi.nlm.nih.gov/pubmed/16792305

[97] E. A. Felton, J. A. Wilson, J. C. Williams, and P. C. Garell, "Electrocorticographically controlled brain-computer interfaces using motor and sensory imagery in patients with temporary subdural electrode implants. Report of four cases." *Journal of Neurosurgery*, vol. 106, no. 3, pp. 495–500, Mar. 2007. [Online]. Available: http://www.ncbi.nlm.nih.gov/pubmed/17367076

[98] G. Schalk, J. Kubánek, K. J. Miller, N. R. Anderson, E. C. Leuthardt, J. G. Ojemann, D. Limbrick, D. W. Moran, L. A. Gerhardt, and J. R. Wolpaw, "Decoding two-dimensional movement trajectories using electrocorticographic signals in humans." *Journal of Neural Engineering*, vol. 4, no. 3, pp. 264–75, Sep. 2007. [Online]. Available: http://stacks.iop.org/1741-2552/4/i=3/a=012

[99] T. Blakely, K. J. Miller, S. P. Zanos, R. P. N. Rao, and J. G. Ojemann, "Robust, long-term control of an electrocorticographic brain-computer interface with fixed parameters." *Neurosurgical Focus*, vol. 27, no. 1, p. E13, Jul. 2009. [Online]. Available: http://www.ncbi.nlm.nih.gov/pubmed/19569888

[100] E. A. Felton, R. G. Radwin, J. A. Wilson, and J. C. Williams,

"Evaluation of a modified Fitts law brain-computer interface target acquisition task in able and motor disabled individuals." *Journal of Neural Engineering*, vol. 6, no. 5, p. 056002, Oct. 2009. [Online]. Available: http://www.ncbi.nlm.nih.gov/pubmed/19700814

[101] J. Kubánek, K. J. Miller, J. G. Ojemann, J. R. Wolpaw, and G. Schalk, "Decoding flexion of individual fingers using electrocorticographic signals in humans." *Journal of Neural Engineering*, vol. 6, no. 6, p. 066001, Dec. 2009. [Online]. Available: http://www.ncbi.nlm.nih.gov/pubmed/19794237

[102] R. Scherer, S. P. Zanos, K. J. Miller, R. P. N. Rao, and J. G. Ojemann, "Classification of contralateral and ipsilateral finger movements for electrocorticographic brain-computer interfaces." *Neurosurgical Focus*, vol. 27, no. 1, p. E12, Jul. 2009. [Online]. Available: http://www.ncbi.nlm.nih.gov/pubmed/19569887

[103] M. J. Vansteensel, D. Hermes, E. J. Aarnoutse, M. G. Bleichner, G. Schalk, P. C. van Rijen, F. S. S. Leijten, and N. F. Ramsey, "Brain-computer interfacing based on cognitive control." *Annals of Neurology*, vol. 67, no. 6, pp. 809–16, Jun. 2010. [Online]. Available: http://www.ncbi.nlm.nih.gov/pubmed/20517943

[104] K. J. Miller, G. Schalk, E. E. Fetz, M. den Nijs, J. G. Ojemann, and R. P. N. Rao, "Cortical activity during motor execution, motor imagery, and imagery-based online feedback." *Proceedings of the National Academy of*

Sciences of the United States of America, vol. 107, no. 9, pp. 4430–5, Mar. 2010. [Online]. Available: http://www.ncbi.nlm.nih.gov/pubmed/20160084

[105] S. Acharya, M. S. Fifer, H. L. Benz, N. E. Crone, and N. V. Thakor, "Electrocorticographic amplitude predicts finger positions during slow grasping motions of the hand." *Journal of Neural Engineering*, vol. 7, no. 4, p. 046002, May 2010. [Online]. Available: http://www.ncbi.nlm.nih.gov/pubmed/20489239

[106] K. J. Friston and C. Buchel, "Functional connectivity," *Human Brain Function*, vol. 2, pp. 999–1018, 2003.

[107] B. P. Rogers, V. L. Morgan, A. T. Newton, and J. C. Gore, "Assessing functional connectivity in the human brain by fMRI." *Magnetic Resonance Imaging*, vol. 25, no. 10, pp. 1347–57, Dec. 2007. [Online]. Available: http://www.ncbi.nlm.nih.gov/pmc/articles/PMC2169499/

[108] K. J. Friston, "Functional and effective connectivity: a review." *Brain Connectivity*, vol. 1, no. 1, pp. 13–36, Jan. 2011. [Online]. Available: http://www.ncbi.nlm.nih.gov/pubmed/22432952

[109] L. A. Baccalá, M. Y. Alvarenga, K. Sameshima, C. L. Jorge, and L. H. Castro, "Graph theoretical characterization and tracking of the effective neural connectivity during episodes of mesial temporal epileptic seizure." *Journal of Integrative Neuroscience*, vol. 3, no. 4, pp. 379–95, Dec. 2004. [Online]. Available: http://www.ncbi.nlm.nih.gov/pubmed/15657975

[110] K. J. Friston, L. Harrison, and W. Penny, "Dynamic causal modelling." *NeuroImage*, vol. 19, no. 4, pp. 1273–302, Aug. 2003. [Online]. Available: http://www.ncbi.nlm.nih.gov/pubmed/12948688

[111] J.-P. Lachaux, A. Lutz, D. Rudrauf, D. Cosmelli, M. Le Van Quyen, J. Martinerie, and F. Varela, "Estimating the time-course of coherence between single-trial brain signals: an introduction to wavelet coherence." *Clinical Neurophysiology*, vol. 32, no. 3, pp. 157–74, Jun. 2002. [Online]. Available: http://www.ncbi.nlm.nih.gov/pubmed/12162182

[112] D. R. Cox and P. A. Lewis, "The statistical analysis of series of events," in *Monographs on Applied Probability and Statistics*. London: Chapman and Hall, 1966.

[113] T. H. Bullock, M. C. McClune, J. Z. Achimowicz, V. J. Iragui-Madoz, R. B. Duckrow, and S. S. Spencer, "Temporal fluctuations in coherence of brain waves." *Proceedings of the National Academy of Sciences of the United States of America*, vol. 92, no. 25, pp. 11 568–72, Dec. 1995. [Online]. Available: http://www.ncbi.nlm.nih.gov/pmc/articles/PMC40443/

[114] C. Andrew and G. Pfurtscheller, "Event-related coherence as a tool for studying dynamic interaction of brain regions." *Electroencephalography and Clinical Neurophysiology*, vol. 98, no. 2, pp. 144–8, Feb. 1996. [Online]. Available: http://www.ncbi.nlm.nih.gov/pubmed/8598174

[115] L. Leocani, C. Toro, P. Manganotti, P. Zhuang, and M. Hallett, "Event-related coherence and event-related desynchronization/synchronization in the 10 Hz and 20 Hz EEG during self-paced movements." *Electroencephalography and Clinical Neurophysiology*, vol. 104, no. 3, pp. 199–206, May 1997. [Online]. Available: http://www.ncbi.nlm.nih.gov/pubmed/9186234

[116] W. H. Miltner, C. Braun, M. Arnold, H. Witte, and E. Taub, "Coherence of gamma-band EEG activity as a basis for associative learning." *Nature*, vol. 397, no. 6718, pp. 434–6, Feb. 1999. [Online]. Available: http://www.ncbi.nlm.nih.gov/pubmed/9989409

[117] V. L. Towle, R. K. Carder, L. Khorasani, and D. Lindberg, "Electrocorticographic coherence patterns." *Journal of Clinical Neurophysiology*, vol. 16, no. 6, pp. 528–47, Nov. 1999. [Online]. Available: http://www.ncbi.nlm.nih.gov/pubmed/10600021

[118] F. Aoki, E. E. Fetz, L. Shupe, E. Lettich, and G. A. Ojemann, "Changes in power and coherence of brain activity in human sensorimotor cortex during performance of visuomotor tasks." *Bio Systems*, vol. 63, no. 1-3, pp. 89–99. [Online]. Available: http://www.ncbi.nlm.nih.gov/pubmed/11595332

[119] K. J. Meador, P. G. Ray, J. R. Echauz, D. W. Loring, and G. J. Vachtsevanos, "Gamma coherence and conscious perception." *Neurol-*

ogy, vol. 59, no. 6, pp. 847–54, Sep. 2002. [Online]. Available: http://www.ncbi.nlm.nih.gov/pubmed/12297565

[120] P. Sauseng, W. Klimesch, M. Schabus, and M. Doppelmayr, "Fronto-parietal EEG coherence in theta and upper alpha reflect central executive functions of working memory." *International Journal of Psychophysiology*, vol. 57, no. 2, pp. 97–103, Aug. 2005. [Online]. Available: http://www.ncbi.nlm.nih.gov/pubmed/15967528

[121] R. W. Thatcher, D. North, and C. Biver, "EEG and intelligence: relations between EEG coherence, EEG phase delay and power." *Clinical Neurophysiology*, vol. 116, no. 9, pp. 2129–41, Sep. 2005. [Online]. Available: http://www.ncbi.nlm.nih.gov/pubmed/16043403

[122] M. Murias, S. J. Webb, J. Greenson, and G. Dawson, "Resting state cortical connectivity reflected in EEG coherence in individuals with autism." *Biological Psychiatry*, vol. 62, no. 3, pp. 270–3, Aug. 2007. [Online]. Available: http://www.ncbi.nlm.nih.gov/pmc/articles/PMC2001237/

[123] J. P. Lachaux, E. Rodriguez, J. Martinerie, and F. J. Varela, "Measuring phase synchrony in brain signals." *Human Brain Mapping*, vol. 8, no. 4, pp. 194–208, Jan. 1999. [Online]. Available: http://www.ncbi.nlm.nih.gov/pubmed/10619414

[124] W. Singer, "Neuronal synchrony: a versatile code for the definition of

relations?" *Neuron*, vol. 24, no. 1, pp. 49–65, 111–25, Sep. 1999. [Online]. Available: http://www.ncbi.nlm.nih.gov/pubmed/10677026

[125] J. M. Palva, S. Palva, and K. Kaila, "Phase synchrony among neuronal oscillations in the human cortex." *The Journal of Neuroscience*, vol. 25, no. 15, pp. 3962–72, Apr. 2005. [Online]. Available: http://www.ncbi.nlm.nih.gov/pubmed/15829648

[126] E. Pereda, R. Q. Quiroga, and J. Bhattacharya, "Nonlinear multivariate analysis of neurophysiological signals." *Progress in Neurobiology*, vol. 77, no. 1-2, pp. 1–37, 2005. [Online]. Available: http://www.ncbi.nlm.nih.gov/pubmed/16289760

[127] W. J. Freeman and L. J. Rogers, "Fine temporal resolution of analytic phase reveals episodic synchronization by state transitions in gamma EEGs." *Journal of Neurophysiology*, vol. 87, no. 2, pp. 937–45, Feb. 2002. [Online]. Available: http://www.ncbi.nlm.nih.gov/pubmed/11826058

[128] ——, "A neurobiological theory of meaning in perception part V: Multicortical patterns of phase modulation in gamma EEG." *International Journal of Bifurcation and Chaos*, vol. 13, no. 10, pp. 2867–2887, 2003.

[129] R. Kozma and W. J. Freeman, "Intermittent spatio-temporal desynchronization and sequenced synchrony in ECoG signals." *Chaos*,

vol. 18, no. 3, p. 037131, Sep. 2008. [Online]. Available: http://www.ncbi.nlm.nih.gov/pubmed/19045505

[130] E. Rodriguez, N. George, J. P. Lachaux, J. Martinerie, B. Renault, and F. J. Varela, "Perception's shadow: long-distance synchronization of human brain activity." *Nature*, vol. 397, no. 6718, pp. 430–3, Feb. 1999. [Online]. Available: http://www.ncbi.nlm.nih.gov/pubmed/9989408

[131] M. Breakspear, L. M. Williams, and C. J. Stam, "A novel method for the topographic analysis of neural activity reveals formation and dissolution of 'Dynamic Cell Assemblies'." *Journal of Computational Neuroscience*, vol. 16, no. 1, pp. 49–68, 2004. [Online]. Available: http://www.ncbi.nlm.nih.gov/pubmed/14707544

[132] R. T. Canolty, E. Edwards, S. S. Dalal, M. Soltani, S. S. Nagarajan, H. E. Kirsch, M. S. Berger, N. M. Barbaro, and R. T. Knight, "High gamma power is phase-locked to theta oscillations in human neocortex." *Science*, vol. 313, no. 5793, pp. 1626–8, Sep. 2006. [Online]. Available: http://www.ncbi.nlm.nih.gov/pmc/articles/PMC2628289/

[133] R. W. Thatcher, D. M. North, and C. J. Biver, "Development of cortical connections as measured by EEG coherence and phase delays." *Human Brain Mapping*, vol. 29, no. 12, pp. 1400–15, Dec. 2008. [Online]. Available: http://www.ncbi.nlm.nih.gov/pubmed/17957703

[134] M. Chávez, M. Le Van Quyen, V. Navarro, M. Baulac, and J. Martinerie, "Spatio-temporal dynamics prior to neocortical seizures: amplitude versus phase couplings." *IEEE Transactions on Biomedical Engineering*, vol. 50, no. 5, pp. 571–83, May 2003. [Online]. Available: http://www.ncbi.nlm.nih.gov/pubmed/12769433

[135] F. Mormann, K. Lehnertz, P. David, and C. E. Elger, "Mean phase coherence as a measure for phase synchronization and its application to the EEG of epilepsy patients." *Physica D: Nonlinear Phenomena*, vol. 144, no. 3, pp. 358–369, 2000.

[136] C. J. Stam, G. Nolte, and A. Daffertshofer, "Phase lag index: assessment of functional connectivity from multi channel EEG and MEG with diminished bias from common sources." *Human Brain Mapping*, vol. 28, no. 11, pp. 1178–93, Nov. 2007. [Online]. Available: http://www.ncbi.nlm.nih.gov/pubmed/17266107

[137] M. Breakspear, "Nonlinear phase desynchronization in human electroencephalographic data." *Human Brain Mapping*, vol. 15, no. 3, pp. 175–98, Mar. 2002. [Online]. Available: http://www.ncbi.nlm.nih.gov/pubmed/11835608

[138] K. Sameshima and L. A. Baccalá, "Using partial directed coherence to describe neuronal ensemble interactions." *Journal of Neuroscience Methods*, vol. 94, no. 1, pp. 93–103, Dec. 1999. [Online]. Available: http://www.ncbi.nlm.nih.gov/pubmed/10638818

[139] L. A. Baccalá and K. Sameshima, "Partial directed coherence: a new concept in neural structure determination." *Biological Cybernetics*, vol. 84, no. 6, pp. 463–74, Jun. 2001. [Online]. Available: http://www.ncbi.nlm.nih.gov/pubmed/11417058

[140] M. J. Kamiski and K. J. Blinowska, "A new method of the description of the information flow in the brain structures." *Biological Cybernetics*, vol. 65, no. 3, pp. 203–10, Jan. 1991. [Online]. Available: http://www.ncbi.nlm.nih.gov/pubmed/1912013

[141] R. Kuś, M. Kamiski, and K. J. Blinowska, "Determination of EEG activity propagation: pair-wise versus multichannel estimate." *IEEE Transactions on Biomedical Engineering*, vol. 51, no. 9, pp. 1501–10, Sep. 2004. [Online]. Available: http://www.ncbi.nlm.nih.gov/pubmed/15376498

[142] A. Korzeniewska, M. Maczak, M. Kamiski, K. J. Blinowska, and S. Kasicki, "Determination of information flow direction among brain structures by a modified directed transfer function (dDTF) method," *Journal of Neuroscience Methods*, vol. 125, no. 1, pp. 195–207, 2003. [Online]. Available: http://www.ncbi.nlm.nih.gov/pubmed/12763246

[143] M. Ding, S. L. Bressler, W. Yang, and H. Liang, "Short-window spectral analysis of cortical event-related potentials by adaptive multivariate autoregressive modeling: data preprocessing, model validation, and variability

assessment." *Biological Cybernetics*, vol. 83, no. 1, pp. 35–45, Jul. 2000. [Online]. Available: http://www.ncbi.nlm.nih.gov/pubmed/10933236

[144] A. Korzeniewska, C. M. Crainiceanu, R. Kuś, P. J. Franaszczuk, and N. E. Crone, "Dynamics of event-related causality in brain electrical activity." *Human Brain Mapping*, vol. 29, no. 10, pp. 1170–92, Oct. 2008. [Online]. Available: http://www.ncbi.nlm.nih.gov/pubmed/17712784

[145] M. G. Philiastides and P. Sajda, "Causal influences in the human brain during face discrimination: a short-window directed transfer function approach." *IEEE Transactions on Biomedical Engineering*, vol. 53, no. 12 Pt 2, pp. 2602–5, Dec. 2006. [Online]. Available: http://www.ncbi.nlm.nih.gov/pubmed/17152440

[146] M. Brázdil, C. Babiloni, R. Roman, P. Daniel, M. Bares, I. Rektor, F. Eusebi, P. M. Rossini, and F. Vecchio, "Directional functional coupling of cerebral rhythms between anterior cingulate and dorsolateral prefrontal areas during rare stimuli: a directed transfer function analysis of human depth EEG signal." *Human Brain Mapping*, vol. 30, no. 1, pp. 138–46, Jan. 2009. [Online]. Available: http://www.ncbi.nlm.nih.gov/pubmed/17999400

[147] G. G. Supp, A. Schlögl, N. Trujillo-Barreto, M. M. Müller, and T. Gruber, "Directed cortical information flow during human object recognition: analyzing induced EEG gamma-band responses in brain's source

space." *PloS One*, vol. 2, no. 8, p. e684, Jan. 2007. [Online]. Available: http://www.ncbi.nlm.nih.gov/pmc/articles/PMC1925146/

[148] M. Bertini, M. Ferrara, L. De Gennaro, G. Curcio, F. Moroni, C. Babiloni, F. Infarinato, P. M. Rossini, and F. Vecchio, "Directional information flows between brain hemispheres across waking, non-REM and REM sleep states: an EEG study." *Brain Research Bulletin*, vol. 78, no. 6, pp. 270–5, Mar. 2009. [Online]. Available: http://www.ncbi.nlm.nih.gov/pubmed/19121373

[149] A. Korzeniewska, P. J. Franaszczuk, C. M. Crainiceanu, R. Kuś, and N. E. Crone, "Dynamics of large-scale cortical interactions at high gamma frequencies during word production: event related causality (ERC) analysis of human electrocorticography (ECoG)." *NeuroImage*, vol. 56, pp. 2218–2237, Jun. 2011. [Online]. Available: http://www.ncbi.nlm.nih.gov/pubmed/21419227

[150] C. Wilke, L. Ding, and B. He, "Estimation of time-varying connectivity patterns through the use of an adaptive directed transfer function." *IEEE Transactions on Biomedical Engineering*, vol. 55, no. 11, pp. 2557–64, Nov. 2008. [Online]. Available: http://www.ncbi.nlm.nih.gov/pmc/articles/PMC2597483/

[151] J. S. Kim, C. H. Im, Y. J. Jung, E. Y. Kim, S. K. Lee, and C. K. Chung, "Localization and propagation analysis of ictal source rhythm by electrocorticography." *NeuroImage*, vol. 52, no. 4, pp. 1279–88, Oct. 2010. [Online]. Available: http://www.ncbi.nlm.nih.gov/pubmed/20420923

[152] C. Wilke, W. van Drongelen, M. Kohrman, and B. He, "Neocortical seizure foci localization by means of a directed transfer function method." *Epilepsia*, vol. 51, no. 4, pp. 564–72, Apr. 2010. [Online]. Available: http://www.ncbi.nlm.nih.gov/pmc/articles/PMC2855748/

[153] Y.-J. Jung, H.-C. Kang, K.-O. Choi, J. S. Lee, D.-S. Kim, J.-H. Cho, S.-H. Kim, C.-H. Im, and H. D. Kim, "Localization of ictal onset zones in Lennox-Gastaut syndrome using directional connectivity analysis of intracranial electroencephalography." *Seizure*, vol. 20, no. 6, pp. 449–57, Jul. 2011. [Online]. Available: http://www.ncbi.nlm.nih.gov/pubmed/21515079

[154] G. Varotto, L. Tassi, S. Franceschetti, R. Spreafico, and F. Panzica, "Epileptogenic networks of type II focal cortical dysplasia: a stereo-EEG study." *NeuroImage*, vol. 61, no. 3, pp. 591–8, Jul. 2012. [Online]. Available: http://www.ncbi.nlm.nih.gov/pubmed/22510255

[155] A. Graef, M. Hartmann, C. Flamm, C. Baumgartner, M. Deistler, and T. Kluge, "A novel method for the identification of synchronization effects in multichannel ECoG with an application to epilepsy." *Biological Cybernetics*, vol. 107, no. 3, pp. 321–35, Jun. 2013. [Online]. Available: http://www.ncbi.nlm.nih.gov/pmc/articles/PMC3661083/

[156] A. Korzeniewska, M. C. Cervenka, C. C. Jouny, J. R. Perilla, J. Harezlak, G. K. Bergey, P. J. Franaszczuk, and N. E. Crone, "Ictal propagation of

high frequency activity is recapitulated in interictal recordings: Effective connectivity of epileptogenic networks recorded with intracranial EEG." *NeuroImage*, vol. 101C, pp. 96–113, Jul. 2014. [Online]. Available: http://www.ncbi.nlm.nih.gov/pubmed/25003814

[157] C. Babiloni, G. B. Frisoni, M. Pievani, F. Vecchio, F. Infarinato, C. Geroldi, S. Salinari, R. Ferri, C. Fracassi, F. Eusebi, and P. M. Rossini, "White matter vascular lesions are related to parietal-to-frontal coupling of EEG rhythms in mild cognitive impairment." *Human Brain Mapping*, vol. 29, no. 12, pp. 1355–67, Dec. 2008. [Online]. Available: http://www.ncbi.nlm.nih.gov/pubmed/17979121

[158] C. Babiloni, R. Ferri, G. Binetti, F. Vecchio, G. B. Frisoni, B. Lanuzza, C. Miniussi, F. Nobili, G. Rodriguez, F. Rundo, A. Cassarino, F. Infarinato, E. Cassetta, S. Salinari, F. Eusebi, and P. M. Rossini, "Directionality of EEG synchronization in Alzheimer's disease subjects." *Neurobiology of Aging*, vol. 30, no. 1, pp. 93–102, Jan. 2009. [Online]. Available: http://www.ncbi.nlm.nih.gov/pubmed/17573161

[159] C. Babiloni, G. Albertini, P. Onorati, F. Vecchio, P. Buffo, M. Sarà, C. Condoluci, F. Pistoia, F. Carducci, and P. M. Rossini, "Inter-hemispheric functional coupling of eyes-closed resting EEG rhythms in adolescents with

Down syndrome." *Clinical Neurophysiology*, vol. 120, no. 9, pp. 1619–27, Sep. 2009. [Online]. Available: http://www.ncbi.nlm.nih.gov/pubmed/19643663

[160] J. Chiang, Z. J. Wang, and M. J. McKeown, "A multiblock PLS model of cortico-cortical and corticomuscular interactions in Parkinson's disease." *NeuroImage*, vol. 63, no. 3, pp. 1498–509, Nov. 2012. [Online]. Available: http://www.ncbi.nlm.nih.gov/pubmed/22982102

[161] L. Song, M. Kolar, and E. Xing, "Time-Varying Dynamic Bayesian Networks," pp. 1732–1740, 2009.

[162] D. Ruppert, M. P. Wand, and R. J. Carroll, *Semiparametric regression*. Cambridge University Press, 2003.

[163] A. K. Engel and W. Singer, "Temporal binding and the neural correlates of sensory awareness." *Trends in Cognitive Sciences*, vol. 5, no. 1, pp. 16–25, Jan. 2001. [Online]. Available: http://www.ncbi.nlm.nih.gov/pubmed/11164732

[164] E. Salinas and T. J. Sejnowski, "Correlated neuronal activity and the flow of neural information." *Nature Reviews. Neuroscience*, vol. 2, no. 8, pp. 539–50, Aug. 2001. [Online]. Available: http://www.ncbi.nlm.nih.gov/pmc/articles/PMC2868968/

[165] D. C. Krawczyk, "Contributions of the prefrontal cortex to the neural basis of human decision making." *Neuroscience and Biobehavioral*

Reviews, vol. 26, no. 6, pp. 631–64, Oct. 2002. [Online]. Available: http://www.ncbi.nlm.nih.gov/pubmed/12479840

[166] T. Yanagawa, Z. C. Chao, N. Hasegawa, and N. Fujii, "Large-scale information flow in conscious and unconscious states: an ECoG study in monkeys." *PloS One*, vol. 8, no. 11, p. e80845, Jan. 2013. [Online]. Available: http://www.ncbi.nlm.nih.gov/pmc/articles/PMC3829858/

[167] W. Klimesch, "EEG alpha and theta oscillations reflect cognitive and memory performance: a review and analysis." *Brain Research*, vol. 29, no. 2-3, pp. 169–95, Apr. 1999. [Online]. Available: http://www.ncbi.nlm.nih.gov/pubmed/10209231

[168] C. Tallon-Baudry, O. Bertrand, C. Delpuech, and J. Pernier, "Stimulus specificity of phase-locked and non-phase-locked 40 Hz visual responses in human." *The Journal of Neuroscience*, vol. 16, no. 13, pp. 4240–9, Jul. 1996. [Online]. Available: http://www.ncbi.nlm.nih.gov/pubmed/8753885

[169] H. Mizuhara, L.-Q. Wang, K. Kobayashi, and Y. Yamaguchi, "Long-range EEG phase synchronization during an arithmetic task indexes a coherent cortical network simultaneously measured by fMRI." *NeuroImage*, vol. 27, no. 3, pp. 553–63, Sep. 2005. [Online]. Available: http://www.ncbi.nlm.nih.gov/pubmed/15921932

[170] H. Mizuhara and Y. Yamaguchi, "Human cortical circuits for cen-

tral executive function emerge by theta phase synchronization." *NeuroImage*, vol. 36, no. 1, pp. 232–44, May 2007. [Online]. Available: http://www.ncbi.nlm.nih.gov/pubmed/17433880

[171] N. R. Anderson, K. Wisneski, L. Eisenman, D. W. Moran, E. C. Leuthardt, and D. J. Krusienski, "An offline evaluation of the autoregressive spectrum for electrocorticography." *IEEE Transactions on Biomedical Engineering*, vol. 56, no. 3, pp. 913–6, Mar. 2009. [Online]. Available: http://www.ncbi.nlm.nih.gov/pubmed/19389689

[172] H. Zhang, H. L. Benz, A. Bezerianos, S. Acharya, N. E. Crone, A. Maybhate, X. Zheng, and N. V. Thakor, "Connectivity mapping of the human ECoG during a motor task with a time-varying dynamic Bayesian network." *Conference proceedings of the Annual International Conference of the IEEE Engineering in Medicine and Biology Society.*, vol. 1, pp. 130–3, Jan. 2010. [Online]. Available: http://www.ncbi.nlm.nih.gov/pubmed/21096524

[173] N. Friedman, M. Linial, I. Nachman, and D. Pe'er, "Using Bayesian networks to analyze expression data." *Journal of Computational Biology*, vol. 7, no. 3-4, pp. 601–20, Jan. 2000. [Online]. Available: http://www.ncbi.nlm.nih.gov/pubmed/11108481

[174] N. M. Luscombe, M. M. Babu, H. Yu, M. Snyder, S. a. Teichmann, and M. Gerstein, "Genomic analysis of regulatory network dynamics reveals large

topological changes." *Nature*, vol. 431, no. 7006, pp. 308–12, Sep. 2004. [Online]. Available: http://www.ncbi.nlm.nih.gov/pubmed/15372033

[175] N. Dobigeon, J.-Y. Tourneret, and M. Davy, "Joint Segmentation of Piecewise Constant Autoregressive Processes by Using a Hierarchical Model and a Bayesian Sampling Approach," *IEEE Transactions on Signal Processing*, vol. 55, no. 4, pp. 1251–1263, Apr. 2007. [Online]. Available: http://ieeexplore.ieee.org/lpdocs/epic03/wrapper.htm?arnumber=4133027

[176] J. O'Keefe and M. L. Recce, "Phase relationship between hippocampal place units and the EEG theta rhythm." *Hippocampus*, vol. 3, no. 3, pp. 317–30, Jul. 1993. [Online]. Available: http://www.ncbi.nlm.nih.gov/pubmed/8353611

[177] P. Nunez, "EEG coherency I: statistics, reference electrode, volume conduction, Laplacians, cortical imaging, and interpretation at multiple scales," *Electroencephalography and Clinical Neurophysiology*, vol. 103, no. 5, pp. 499–515, Nov. 1997. [Online]. Available: http://dx.doi.org/10.1016/S0013-4694(97)00066-7

[178] P. L. Nunez, R. B. Silberstein, Z. Shi, M. R. Carpenter, R. Srinivasan, D. M. Tucker, S. M. Doran, P. J. Cadusch, and R. S. Wijesinghe, "EEG coherency II: experimental comparisons of multiple measures." *Clinical Neurophysiology*, vol. 110, no. 3, pp. 469–86, Mar. 1999. [Online]. Available: http://www.ncbi.nlm.nih.gov/pubmed/10363771

[179] B. Schack, P. Rappelsberger, S. Weiss, and E. Möller, "Adaptive phase estimation and its application in EEG analysis of word processing." *Journal of Neuroscience Methods*, vol. 93, no. 1, pp. 49–59, Oct. 1999. [Online]. Available: http://www.ncbi.nlm.nih.gov/pubmed/10598864

[180] B. Schack, "Phase-coupling of thetagamma EEG rhythms during short-term memory processing," *International Journal of Psychophysiology*, vol. 44, no. 2, pp. 143–163, May 2002. [Online]. Available: http://dx.doi.org/10.1016/S0167-8760(01)00199-4

[181] G. Nolte, O. Bai, L. Wheaton, Z. Mari, S. Vorbach, and M. Hallett, "Identifying true brain interaction from EEG data using the imaginary part of coherency." *Clinical Neurophysiology*, vol. 115, no. 10, pp. 2292–307, Oct. 2004. [Online]. Available: http://www.ncbi.nlm.nih.gov/pubmed/15351371

[182] C. Zou, K. J. Denby, and J. Feng, "Granger causality vs. dynamic Bayesian network inference: a comparative study." *BMC Bioinformatics*, vol. 10, p. 122, Jan. 2009. [Online]. Available: http://www.ncbi.nlm.nih.gov/pubmed/19393071

[183] D. Goldman, "The clinical use of the "average" reference electrode in monopolar recording." *Electroencephalography and Clinical Neurophysiology*, vol. 2, no. 2, pp. 209–12, May 1950. [Online]. Available: http://www.ncbi.nlm.nih.gov/pubmed/15421286

[184] M. Hauschild, R. Davoodi, and G. E. Loeb, "A virtual reality environment for

designing and fitting neural prosthetic limbs." *IEEE Transactions on Neural Systems and Rehabilitation Engineering*, vol. 15, no. 1, pp. 9–15, Mar. 2007. [Online]. Available: http://www.ncbi.nlm.nih.gov/pubmed/17436870

[185] N. E. Crone, D. L. Miglioretti, B. Gordon, J. M. Sieracki, M. T. Wilson, S. Uematsu, and R. P. Lesser, "Functional mapping of human sensorimotor cortex with electrocorticographic spectral analysis. I. Alpha and beta event-related desynchronization." *Brain*, vol. 121 (Pt 1, pp. 2271–99, Dec. 1998. [Online]. Available: http://www.ncbi.nlm.nih.gov/pubmed/9874480

[186] N. E. Crone, D. L. Miglioretti, B. Gordon, and R. P. Lesser, "Functional mapping of human sensorimotor cortex with electrocorticographic spectral analysis. II. Event-related synchronization in the gamma band," *Brain*, vol. 121, no. 12, pp. 2301–2315, Dec. 1998. [Online]. Available: http://brain.oxfordjournals.org/cgi/content/abstract/121/12/2301

[187] R. N. Bracewell, "The Fourier transform." *Scientific American*, vol. 260, no. 6, pp. 86–9, 92–5, Jun. 1989. [Online]. Available: http://www.ncbi.nlm.nih.gov/pubmed/2727659

[188] M. W. Slutzky, L. R. Jordan, T. Krieg, M. Chen, D. J. Mogul, and L. E. Miller, "Optimal spacing of surface electrode arrays for brain-machine interface applications." *Journal of Neural Engi-*

neering, vol. 7, no. 2, p. 26004, Apr. 2010. [Online]. Available: http://www.pubmedcentral.nih.gov/articlerender.fcgi?artid=2844916

[189] K. J. Miller, E. C. Leuthardt, G. Schalk, R. P. N. Rao, N. R. Anderson, D. W. Moran, J. W. Miller, and J. G. Ojemann, "Spectral changes in cortical surface potentials during motor movement." *The Journal of Neuroscience*, vol. 27, no. 9, pp. 2424–32, Feb. 2007. [Online]. Available: http://www.ncbi.nlm.nih.gov/pubmed/17329441

[190] P. E. Roland, B. Larsen, N. A. Lassen, and E. Skinhø j, "Supplementary motor area and other cortical areas in organization of voluntary movements in man." *Journal of Neurophysiology*, vol. 43, no. 1, pp. 118–36, Jan. 1980. [Online]. Available: http://www.ncbi.nlm.nih.gov/pubmed/7351547

[191] G. Goldberg, "Supplementary motor area structure and function: Review and hypotheses," *Behavioral and Brain Sciences*, vol. 8, no. 04, pp. 567–588, Dec. 1985. [Online]. Available: http://journals.cambridge.org/abstract_S0140525X00045167

[192] S. P. Wise, D. Boussaoud, P. B. Johnson, and R. Caminiti, "Premotor and parietal cortex: corticocortical connectivity and combinatorial computations." *Annual Review of Neuroscience*, vol. 20, pp. 25–42, Jan. 1997. [Online]. Available: http://www.annualreviews.org/doi/abs/10.1146/annurev.neuro.20.1.25

[193] M. T. Kaufman, M. M. Churchland, G. Santhanam, B. M. Yu,

A. Afshar, S. I. Ryu, and K. V. Shenoy, "Roles of monkey premotor neuron classes in movement preparation and execution." *Journal of Neurophysiology*, vol. 104, no. 2, pp. 799–810, Aug. 2010. [Online]. Available: http://jn.physiology.org/cgi/content/abstract/104/2/799

[194] H. Shibasaki, N. Sadato, H. Lyshkow, Y. Yonekura, M. Honda, T. Nagamine, S. Suwazono, Y. Magata, A. Ikeda, M. Miyazaki, H. Fukuyama, R. Asato, and J. Konishi, "Both primary motor cortex and supplementary motor area play an important role in complex finger movement," *Brain*, vol. 116, no. 6, pp. 1387–1398, Dec. 1993. [Online]. Available: http://brain.oxfordjournals.org/cgi/content/abstract/116/6/1387

[195] L. Shen and G. E. Alexander, "Neural Correlates of a Spatial Sensory-To-Motor Transformation in Primary Motor Cortex," *Journal of Neurophysiology*, vol. 77, no. 3, pp. 1171–1194, 1997. [Online]. Available: http://jn.physiology.org/cgi/content/abstract/77/3/1171

[196] J. Ginter, K. J. Blinowska, M. Kamiski, and P. J. Durka, "Phase and amplitude analysis in time-frequency space–application to voluntary finger movement." *Journal of Neuroscience Methods*, vol. 110, no. 1-2, pp. 113–24, Sep. 2001. [Online]. Available: http://www.ncbi.nlm.nih.gov/pubmed/11564531

[197] K. J. Blinowska, R. Kuś, and M. Kamiski, "Granger causality and information flow in multivariate processes," *Physical Re-*

view E, vol. 70, no. 5, pp. 1–4, Nov. 2004. [Online]. Available: http://link.aps.org/doi/10.1103/PhysRevE.70.050902

[198] J. Ginter, K. J. Blinowska, M. Kamiski, P. J. Durka, G. Pfurtscheller, and C. Neuper, "Propagation of EEG activity in the beta and gamma band during movement imagery in humans." *Methods of Information in Medicine*, vol. 44, no. 1, pp. 106–13, Jan. 2005. [Online]. Available: http://www.ncbi.nlm.nih.gov/pubmed/15778801

[199] G. Buzsáki and A. Draguhn, "Neuronal oscillations in cortical networks." *Science*, vol. 304, no. 5679, pp. 1926–9, Jun. 2004. [Online]. Available: http://www.sciencemag.org/content/304/5679/1926.abstract

[200] L. Melloni, C. Molina, M. Pena, D. Torres, W. Singer, and E. Rodriguez, "Synchronization of neural activity across cortical areas correlates with conscious perception." *The Journal of Neuroscience*, vol. 27, no. 11, pp. 2858–65, Mar. 2007. [Online]. Available: http://www.jneurosci.org/cgi/content/abstract/27/11/2858

[201] J. A. Doeringer and N. Hogan, "Performance of above elbow body-powered prostheses in visually guided unconstrained motion tasks." *IEEE Transactions on Biomedical Engineering*, vol. 42, no. 6, pp. 621–31, Jun. 1995. [Online]. Available: http://www.ncbi.nlm.nih.gov/pubmed/7790019

[202] M. S. Fifer, M. Mollazadeh, S. Acharya, N. V. Thakor, and N. E.

Crone, "Asynchronous decoding of grasp aperture from human ECoG during a reach-to-grasp task." *Conference Proceedings of the Annual International Conference of the IEEE Engineering in Medicine and Biology Society*, vol. 2011, pp. 4584–7, Jan. 2011. [Online]. Available: http://www.pubmedcentral.nih.gov/articlerender.fcgi?artid=3324943

[203] T. Yanagisawa, M. Hirata, Y. Saitoh, T. Goto, H. Kishima, R. Fukuma, H. Yokoi, Y. Kamitani, and T. Yoshimine, "Real-time control of a prosthetic hand using human electrocorticography signals." *Journal of Neurosurgery*, Feb. 2011. [Online]. Available: http://www.ncbi.nlm.nih.gov/pubmed/21314273

[204] D. F. Specht, "A general regression neural network." *IEEE Transactions on Neural Networks*, vol. 2, no. 6, pp. 568–76, Jan. 1991. [Online]. Available: http://www.ncbi.nlm.nih.gov/pubmed/18282872

[205] G. S. Wig, S. T. Grafton, K. E. Demos, and W. M. Kelley, "Reductions in neural activity underlie behavioral components of repetition priming." *Nature Neuroscience*, vol. 8, no. 9, pp. 1228–33, Sep. 2005. [Online]. Available: http://www.ncbi.nlm.nih.gov/pubmed/16056222

[206] P. A. Chouinard, B. F. Morrissey, S. Köhler, and M. A. Goodale, "Repetition suppression in occipital-temporal visual areas is modulated by physical rather than semantic features of objects." *NeuroImage*, vol. 41, no. 1, pp. 130–44, May 2008. [Online]. Available: http://www.ncbi.nlm.nih.gov/pubmed/18375148

[207] A. Rodriguez Merzagora, T. J. Coffey, M. R. Sperling, A. Sharan, B. Litt, G. Baltuch, and J. Jacobs, "Repeated stimuli elicit diminished high-gamma electrocorticographic responses." *NeuroImage*, Jul. 2013. [Online]. Available: http://www.ncbi.nlm.nih.gov/pubmed/23867555

[208] J. Larsson and A. T. Smith, "fMRI repetition suppression: neuronal adaptation or stimulus expectation?" *Cerebral Cortex*, vol. 22, no. 3, pp. 567–76, Mar. 2012. [Online]. Available: http://www.pubmedcentral.nih.gov/articlerender.fcgi?artid=3278317

[209] J. R. Gilbert, S. J. Gotts, F. W. Carver, and A. Martin, "Object repetition leads to local increases in the temporal coordination of neural responses." *Frontiers in Human Neuroscience*, vol. 4, no. April, p. 30, Jan. 2010. [Online]. Available: http://www.pubmedcentral.nih.gov/articlerender.fcgi?artid=2868300

[210] S. J. Gotts, C. C. Chow, and A. Martin, "Repetition Priming and Repetition Suppression: A Case for Enhanced Efficiency Through Neural Synchronization." *Cognitive Neuroscience*, vol. 3, no. 3-4, pp. 227–237, Jan. 2012. [Online]. Available: http://www.pubmedcentral.nih.gov/articlerender.fcgi?artid=3491809

[211] M. S. Mellem, R. B. Friedman, and A. V. Medvedev, "Gamma- and theta-band synchronization during semantic priming reflect local and long-range lexical-

semantic networks." *Brain and Language*, vol. 127, no. 3, pp. 440–451, Oct. 2013. [Online]. Available: http://www.ncbi.nlm.nih.gov/pubmed/24135132

[212] A. Martin and S. J. Gotts, "Making the causal link: frontal cortex activity and repetition priming." *Nature Neuroscience*, vol. 8, no. 9, pp. 1134–5, Sep. 2005. [Online]. Available: http://www.ncbi.nlm.nih.gov/pubmed/16127445

[213] K. Grill-Spector, R. Henson, and A. Martin, "Repetition and the brain: neural models of stimulus-specific effects." *Trends in Cognitive Sciences*, vol. 10, no. 1, pp. 14–23, Jan. 2006. [Online]. Available: http://www.ncbi.nlm.nih.gov/pubmed/16321563

[214] X. Papademetris, M. Jackowski, N. Rajeevan, H. Okuda, R. Constable, and L. Staib, "BioImage Suite: An integrated medical image analysis suite." [Online]. Available: http://www.bioimagesuite.org

[215] M. C. Cervenka, J. Corines, D. F. Boatman-Reich, A. Eloyan, X. Sheng, P. J. Franaszczuk, and N. E. Crone, "Electrocorticographic functional mapping identifies human cortex critical for auditory and visual naming." *NeuroImage*, vol. 69, pp. 267–76, Apr. 2013. [Online]. Available: http://www.pubmedcentral.nih.gov/articlerender.fcgi?artid=3612948

[216] P. Mitra and H. Bokil, *Observed Brain Dynamics*. Oxford University Press, 2007, vol. 5. [Online]. Available: http://books.google.com/books?hl=en&lr=&id=0t3oOEFeyY8C&pgis=1

[217] Y. Benjamini and Y. Hochberg, "Controlling the false discovery rate: a practical and powerful approach to multiple testing," *Journal of the Royal Statistical Society. Series B (Methodological)*, pp. 289–300, 1995.

[218] P. J. Franaszczuk and C. C. Jouny, "Software system for data management and distributed processing of multichannel biomedical signals." *Conference proceedings of the Annual International Conference of the IEEE Engineering in Medicine and Biology Society.*, vol. 2, pp. 983–5, Jan. 2004. [Online]. Available: http://www.ncbi.nlm.nih.gov/pubmed/17271845

[219] K. P. Burnham and D. R. Anderson, *Model Selection and Multimodel Inference: A Practical Information-Theoretic Approach.* Springer Science & Business Media, 2002. [Online]. Available: http://books.google.com/books?hl=en&lr=&id=fT1Iu-h6E-oC&pgis=1

[220] G. Yule, "On a method of investigating periodicities in disturbed series, with special reference to Wolfer's sunspot numbers," *Philosophical Transactions of the Royal Society of London. Series A, Containing Papers of a Mathematical or Physical Character*, vol. 226, no. 636-646, pp. 267–298, 1927.

[221] G. Walker, "On periodicity in series of related terms," *Proceedings of the Royal Society of London. Series A*, vol. 131, no. 818, pp. 518–532, 1931.

[222] T. W. James and I. Gauthier, "Repetition-induced changes in BOLD response

reflect accumulation of neural activity," *Human Brain Mapping*, vol. 27, pp. 37–46, 2006.

[223] T. Allison, G. McCarthy, A. Nobre, A. Puce, and A. Belger, "Human extrastriate visual cortex and the perception of faces, words, numbers, and colors." *Cerebral Cortex*, vol. 4, no. 5, pp. 544–54, 1994. [Online]. Available: http://www.ncbi.nlm.nih.gov/pubmed/7833655

[224] X. Jiang, E. Bradley, R. A. Rini, T. Zeffiro, J. Vanmeter, and M. Riesenhuber, "Categorization training results in shape- and category-selective human neural plasticity." *Neuron*, vol. 53, no. 6, pp. 891–903, Mar. 2007. [Online]. Available: http://www.pubmedcentral.nih.gov/articlerender.fcgi?artid=1989663

[225] K. Friston, "A theory of cortical responses." *Philosophical transactions of the Royal Society of London. Series B, Biological sciences*, vol. 360, no. 1456, pp. 815–36, Apr. 2005. [Online]. Available: http://rstb.royalsocietypublishing.org/content/360/1456/815.short

[226] W. J. Levelt, "Models of word production," *Trends in Cognitive Sciences*, vol. 3, no. 6, pp. 223–232, Jun. 1999. [Online]. Available: http://www.sciencedirect.com/science/article/pii/S1364661399013194

[227] G. Glosser, A. E. Salvucci, and N. D. Chiaravalloti, "Naming and recognizing famous faces in temporal lobe epilepsy." *Neurology*, vol. 61, no. 1, pp. 81–6, Jul. 2003. [Online]. Available: http://www.ncbi.nlm.nih.gov/pubmed/12847161

[228] D. L. Drane, G. A. Ojemann, E. Aylward, J. G. Ojemann, L. C. Johnson, D. L. Silbergeld, J. W. Miller, and D. Tranel, "Category-specific naming and recognition deficits in temporal lobe epilepsy surgical patients." *Neuropsychologia*, vol. 46, no. 5, pp. 1242–55, Apr. 2008. [Online]. Available: http://www.pubmedcentral.nih.gov/articlerender.fcgi?artid=2474808

[229] M. J. Hamberger, "Cortical language mapping in epilepsy: a critical review." *Neuropsychology Review*, vol. 17, no. 4, pp. 477–89, Dec. 2007. [Online]. Available: http://www.ncbi.nlm.nih.gov/pubmed/18004662

[230] M. J. Hamberger, A. C. Williams, and C. A. Schevon, "Extraoperative neurostimulation mapping: results from an international survey of epilepsy surgery programs." *Epilepsia*, vol. 55, no. 6, pp. 933–9, Jun. 2014. [Online]. Available: http://www.ncbi.nlm.nih.gov/pubmed/24816083

[231] P. Indefrey, "The spatial and temporal signatures of word production components: a critical update." *Frontiers in Psychology*, vol. 2, p. 255, Jan. 2011. [Online]. Available: http://www.pubmedcentral.nih.gov/articlerender.fcgi?artid=3191502

[232] L. L. Chao, J. V. Haxby, and A. Martin, "Attribute-based neural substrates in temporal cortex for perceiving and knowing about objects." *Nature Neuroscience*, vol. 2, no. 10, pp. 913–9, Oct. 1999. [Online]. Available: http://www.ncbi.nlm.nih.gov/pubmed/10491613

[233] A. J. Horner and R. N. Henson, "Priming, response learning and repetition suppression." *Neuropsychologia*, vol. 46, no. 7, pp. 1979–91, Jan. 2008. [Online]. Available: http://www.pubmedcentral.nih.gov/articlerender.fcgi?artid=2430995

[234] E. A. Race, S. Shanker, and A. D. Wagner, "Neural priming in human frontal cortex: multiple forms of learning reduce demands on the prefrontal executive system." *Journal of Cognitive Neuroscience*, vol. 21, no. 9, pp. 1766–81, Sep. 2009. [Online]. Available: http://www.pubmedcentral.nih.gov/articlerender.fcgi?artid=2788302

[235] X. Pei, D. L. Barbour, E. C. Leuthardt, and G. Schalk, "Decoding vowels and consonants in spoken and imagined words using electrocorticographic signals in humans." *Journal of Neural Engineering*, vol. 8, no. 4, p. 046028, Aug. 2011. [Online]. Available: http://www.pubmedcentral.nih.gov/articlerender.fcgi?artid=3772685

[236] D. Zhang, E. Gong, W. Wu, J. Lin, W. Zhou, and B. Hong, "Spoken sentences decoding based on intracranial high gamma response using dynamic time warping." *Conference proceedings of the Annual International Conference of the IEEE Engineering in Medicine and Biology Society.*, vol. 2012, pp. 3292–5, Jan. 2012. [Online]. Available: http://www.ncbi.nlm.nih.gov/pubmed/23366629

[237] S. Martin, P. Brunner, C. Holdgraf, H.-J. Heinze, N. E. Crone, J. Rieger,

G. Schalk, R. T. Knight, and B. N. Pasley, "Decoding spectrotemporal features of overt and covert speech from the human cortex." *Frontiers in Neuroengineering*, vol. 7, p. 14, Jan. 2014. [Online]. Available: http://www.pubmedcentral.nih.gov/articlerender.fcgi?artid=4034498

[238] S. Ray, N. E. Crone, E. Niebur, P. J. Franaszczuk, and S. S. Hsiao, "Neural correlates of high-gamma oscillations (60-200 Hz) in macaque local field potentials and their potential implications in electrocorticography." *The Journal of Neuroscience*, vol. 28, no. 45, pp. 11 526–36, Nov. 2008. [Online]. Available: http://www.pubmedcentral.nih.gov/articlerender.fcgi?artid=2715840

[239] J. S. Duncan, X. Papademetris, J. Yang, M. Jackowski, X. Zeng, and L. H. Staib, "Geometric strategies for neuroanatomic analysis from MRI." *NeuroImage*, vol. 23 Suppl 1, pp. S34–45, Jan. 2004. [Online]. Available: http://www.pubmedcentral.nih.gov/articlerender.fcgi?artid=2832750

[240] H. L. Benz, H. Zhang, A. Bezerianos, S. Acharya, N. E. Crone, X. Zheng, and N. V. Thakor, "Connectivity analysis as a novel approach to motor decoding for prosthesis control." *IEEE Transactions on Neural Systems and Rehabilitation Engineering*, vol. 20, no. 2, pp. 143–52, Mar. 2012. [Online]. Available: http://ieeexplore.ieee.org/articleDetails.jsp?arnumber=6072267

[241] F. Filimon, J. D. Nelson, R.-S. Huang, and M. I. Sereno, "Multiple parietal reach regions in humans: cortical representations for visual

and proprioceptive feedback during on-line reaching." *The Journal of Neuroscience*, vol. 29, no. 9, pp. 2961–71, Mar. 2009. [Online]. Available: http://www.ncbi.nlm.nih.gov/pubmed/19261891

Vita

Heather L. Benz was born July 19, 1985 in Washington, D.C. She received a B.S. degree in Biomedical Engineering from Case Western Reserve University in 2007, and was awarded the Robert and Joyce Shaefer Prize for major contributions to campus publications. She subsequently enrolled in the Biomedical Engineering Ph.D. program at Johns Hopkins University. Her research focuses on analyzing human neural connectivity to improve mapping and decoding of movement and speech with cortical signals. Her paper introducing cortical connectivity as a novel signal for decoding grasp was a finalist at the 2010 IEEE International Conference of the Engineering in Medicine and Biology Society.

In September 2014, Heather will join the US Food & Drug Administration in Silver Spring, MD as an ORISE Fellow, where she will work on the DARPA Hand Propriception & Touch Interfaces (HAPTIX) project.